Volume 11, N ILLEGIB

May, 1962

ILLEGIB

THE SOVIET JOURNAL OF

ATOMIC ENERGY

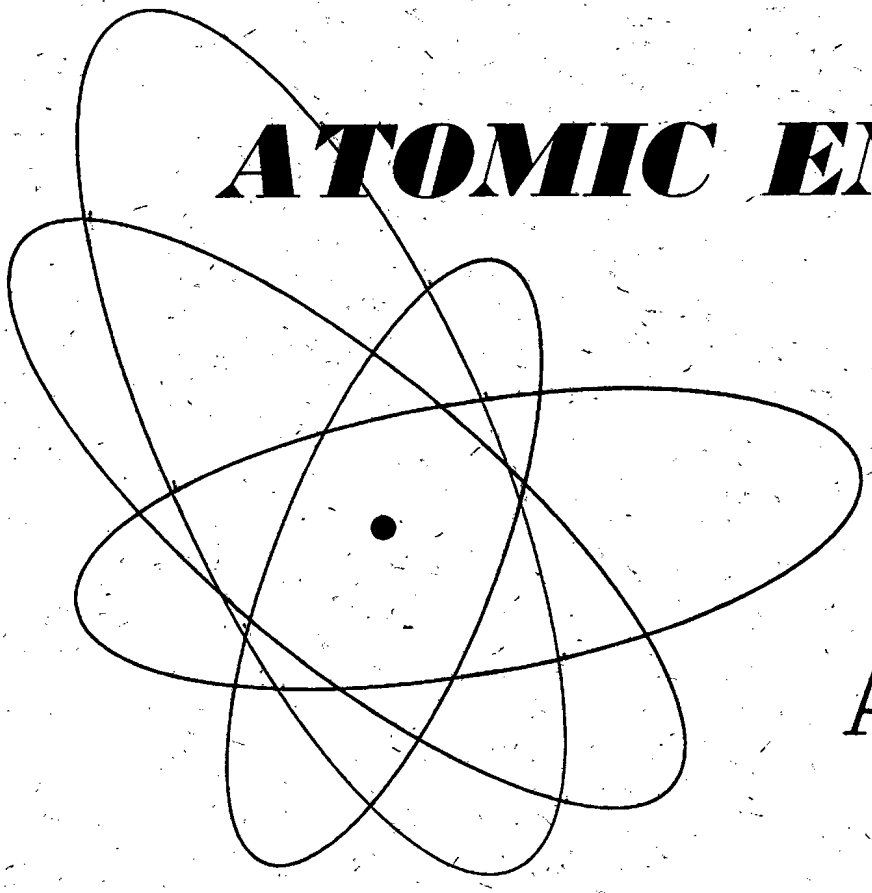

Атомная энергия

TRANSLATED FROM RUSSIAN

CONSULTANTS BUREAU

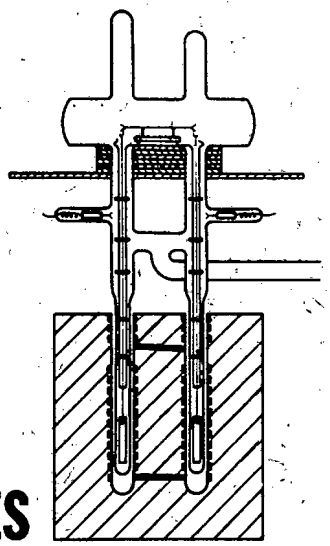

VOLUME I

VACUUM MICROBALANCE TECHNIQUES

Proceedings of the 1960 Conference Sponsored by
The Institute for Exploratory Research
U. S. Army Signal Research and Development Laboratory

Edited by
M. J. KATZ
U. S. Army Signal Research and Development Laboratory
Fort Monmouth, New Jersey

Introduction by
Thor N. Rhodin
Cornell University

The proceedings of this conference provide an authoritative introduction to the rapidly widening scope of microbalance methods which is not available elsewhere in a single publication.

The usefulness of microbalance techniques in the study of the properties of materials lies in their extreme sensitivity and versatility. This renders them particularly important in studies of properties of condensed systems. In addition to the historical use of microbalance techniques as a tool of microchemistry, they have, in recent years, found extensive application in the fields of metallurgy, physics, and chemistry. The uniqueness of the method results from the facility it provides in making a series of precise measurements of high sensitivity under carefully controlled conditions over a wide range of temperature and pressure.

This significant new volume contains papers in three major categories. The first group of reports deals with the general structural features and measuring capabilities of microbalances. In the second group, a sophisticated consideration and much needed evaluation of sources of spurious mass changes associated with microbalances is presented. The third group describes some of the most recent extensions in microbalance work to new research areas such as semiconductors, ultra-high vacuum, and high temperatures. These papers provide an interesting account of advances in the application of the microgravimetric method to three new and important fields of research on the behavior of materials.

170 pages **$6.50**

PLENUM PRESS, INC. 227 West 17th St., New York 11, N. Y.

THE SOVIET JOURNAL OF

ATOMIC ENERGY

A translation of ATOMNAYA ÉNERGIYA,
a publication of the Academy of Sciences of the USSR

(Russian Original Dated December, 1961)

Vol. 11, No. 6 May, 1962

CONTENTS

Annual subscription $ 75.00
Single issue 20.00
Single article 12.50

CONTENTS (continued)

Note. The Table of Contents lists all materials that appears in Atomnaya Energiya. Those items that originated in the English language are not included in the translation and are shown enclosed in brackets. Whenever possible, the English-language source containing the omitted reports will be given. Consultants Bureau Enterprises, Inc.

INTERACTION OF INTENSE ELECTRON BEAMS WITH A PLASMA

A. K. Berezin, Ya. B. Fainberg, G. P. Berezin,

L. I. Bolotin and V. G. Stupak

Translated from Atomnaya Énergiya, Vol. 11, No. 6, pp. 493-497,
December, 1961
Original article submitted June 17, 1961

In this work an experimental determination has been made of the energy losses of an initially unmodulated electron beam passing through a plasma (with no magnetic field). These losses amount to 12% of the beam energy for a beam current of 8 amp, a beam voltage of 26 kev and a plasma density of $7\text{-}9 \cdot 10^{10}$ cm^{-3}.

It is shown that these high losses are due to the coherent interaction of the beam with the plasma.

INTRODUCTION

The interaction of an electron beam with a plasma has been studied by a number of authors [1-9]. It has been shown theoretically [1-5, 8, 9] that a beam of charged particles passing through a plasma excites density waves in the plasma and that the resulting interaction between the beam and plasma results in the transfer of energy from the beam to the wave with a consequent reduction in the energy of the electron beam.

This effect has been investigated experimentally by several workers [6, 7]. In this work the energy losses of pulsed electron beams were studied of beam currents of 1 amp at 80 kev; both modulated and unmodulated beams were used. The energy losses were found to increase with increasing beam current and diminishing beam energy. For this reason, in the present work the beam energy has been reduced to 26 kev while the beam current has been increased to 8 amp. The energy lost by the beam in passing through a plasma with an electron density of $7\text{-}9 \cdot 10^{10}$ cm^{-3} has been studied with no magnetic field. The dependence of loss on beam current was also investigated.

Description of the Apparatus and Method of Measurement

A diagram of the apparatus used in these experiments is shown in Fig. 1. The pressure differential between the plasma chamber and the electron beam chamber, in which a high vacuum is needed, is achieved by means of a copper tube 150 mm long with an inner diameter of 12 mm. The plasma chamber itself is a quartz tube with an inner diameter of 40 mm and an over-all length of either 64 cm or 32 cm. The pressure in the tube is maintained at $3 \cdot 10^{-4}$ to $4 \cdot 10^{-3}$ mm Hg by means of a mechanical valve. These experiments use air as the working gas. The electron gun and the pressure-differential tube are located in a uniform region of the magnetic focusing field. The maximum value of this field is 2000 oe. The magnetic field cuts off sharply beyond the tube and it may be assumed that there is essentially no magnetic field in most of the plasma chamber (Fig. 2B).

The cathode of the electron gun is a disc of lanthanum boride 10 mm in diameter oriented perpendicularly to the magnetic field. Pulsed voltages up to 30 kev are applied to the gun [pulse lengths, 3.5 μsec and repetition rate, 50 cps (Fig. 3a)]. The electron gun provides pulsed currents up to 9 amp with a focusing field of 1200 oe at the entrance to the plasma chamber. The current is measured with a Faraday cup with an aperture 25 mm in diameter; the Faraday cup is 80 mm long. The current distribution along the axis of the plasma chamber is shown in Fig. 2C. It is evident from this curve that the beam current falls off as the electrons traverse greater and greater distances in the chamber. This behavior is understandable because the beam moves in a region with no magnetic focusing field in which it suffers Coulomb scattering; as a result some of the electrons strike the walls of the quartz chamber before the beam reaches the end of the chamber.

In passing through the plasma chamber the electron beam ionizes the residual gas, forming a plasma whose density is proportional to the beam current and the pressure of the residual gas. The plasma density is measured in

a cylindrical cavity 300 mm in diameter and 100 mm high. This cavity is excited in the TM_{030} mode by means of a klystron. The plasma density is determined by the shift of the resonance frequency. As is well-known, there is an upper limit to the electron density that can be measured by this technique. In the present case this limit is $4 \cdot 10^{10}$ cm^{-3}. Since the plasma density is higher than this value during the beam traversal time it is necessary to determine the density by the following technique. It is known that the plasma decays exponentially [10, 11], in accordance with the relation(when diffusion losses are much greater than the recombination losses)

$$n = n_0 \exp(-t/\tau),$$

where n is the plasma density at time t; τ is the mean plasma decay time; n_0 is the initial plasma density, corresponding to t = 0. In the present work, at least three values of the density, n_1, n_2 and n_3, are measured at three corresponding values of the time t_1, t_2 and t_3, after the current pulse is terminated. These density values are then plotted as a function of time on a semilogarithmic curve (the quantity ln n is plotted along the ordinate axis with t as the abscissa). This curve is a straight line that can be extrapolated to t = 0, thereby making it possible to obtain the initial density of the plasma during the beam traversal time. The distribution of plasma electron density along the axis of the system with a current of 6 amp into the plasma chamber (pressure $4 \cdot 10^{-3}$ mm Hg) is shown in Fig. 2D.

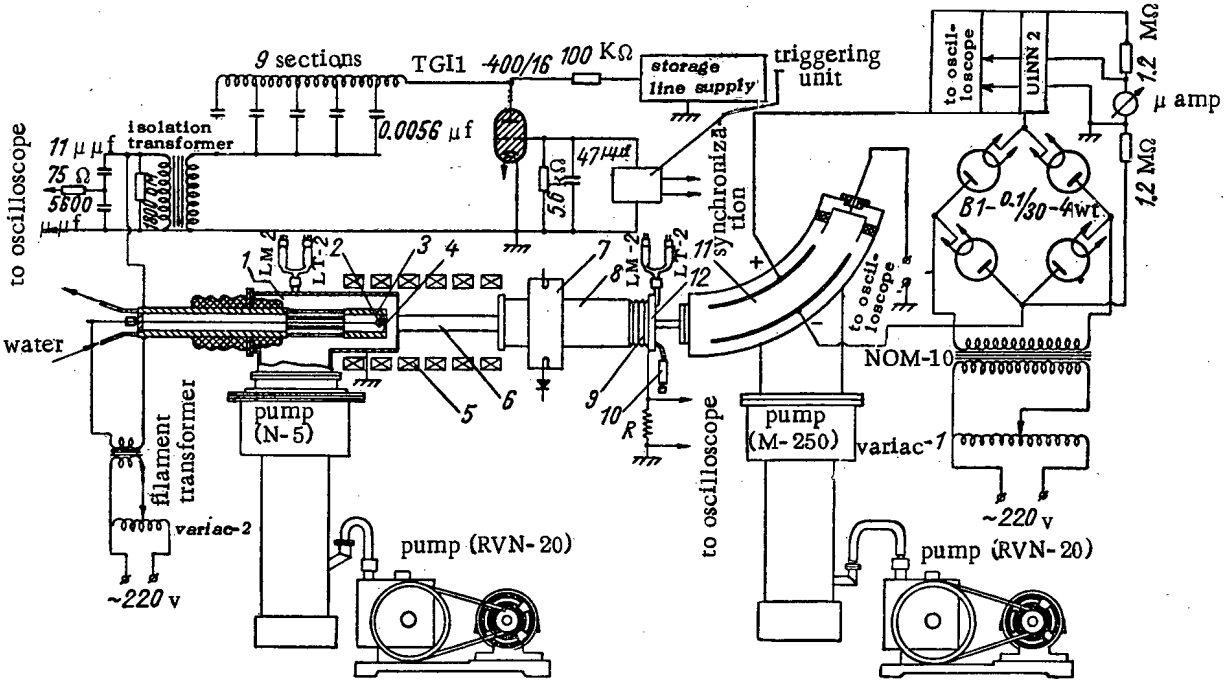

Fig. 1. General diagram of the experiment: 1) electron beam chamber; 2) incandescent cathode; 3) cathode cooling jacket; 4) cathode; 5) magnetic focusing field; 6) tube for producing a pressure differential; 7) microwave cavity; 8) plasma chamber; 9) sylphon bellows; 10) mechanical valve; 11) electrostatic analyzer; 12) collector for measuring current.

The maximum electron density is $7 \cdot 10^{10}$ cm^{-3}. Measurements of the electron density under these conditions with a microwave interfermometer at 3.2 cm give a maximum plasma density of $9 \cdot 10^{10}$ cm^{-3}. At currents of the order of 8 amp the maximum plasma density measured with the microwave cavity is $8.3 \cdot 10^{10}$ cm^{-3} (pressure $4 \cdot 10^{-3}$ mm Hg).

In passing through the plasma chamber, most of the current reaches the collector (see Fig. 2A) which has a central aperture 3 mm in diameter. An oscillogram of the current pulse is shown in Fig. 3b. Part of the electron beam that passes through the central aperture of the collector reaches an electrostatic analyzer and then the Faraday cylinder. The angle subtended by the aperture in the electrostatic analyzer is approximately 4°. The resolving power is 1%. The voltage from the Faraday cylinder is fed to an integrating circuit and then to the vertical amplifier of the oscilloscope. A voltage proportional to the analyzer voltage is applied to the horizontal plates. Thus, the oscilloscope presentation shows the number of electrons as a function of energy, i.e., the electron energy spectrum.

The collector is fastened to the plasma chamber through a sylphon bellows so that the electrostatic analyzer can be moved with respect to the axis of the plasma chamber. In this way the energy spectrum of the electrons at the axis of the chamber and at the periphery can be measured separately.

Results of the Measurements and Discussion

In all the experiments reported here the pulsed voltage applied to the electron gun was 26 kev. The electron energy spectra were measured (at pressures of $3 \cdot 10^{-4}$ and $4 \cdot 10^{-3}$ mm Hg) at the entrance to the 64 cm plasma chamber and at exit from the chamber. The entrance electron spectra for these pressures are shown in Fig. 4 (curve 1).

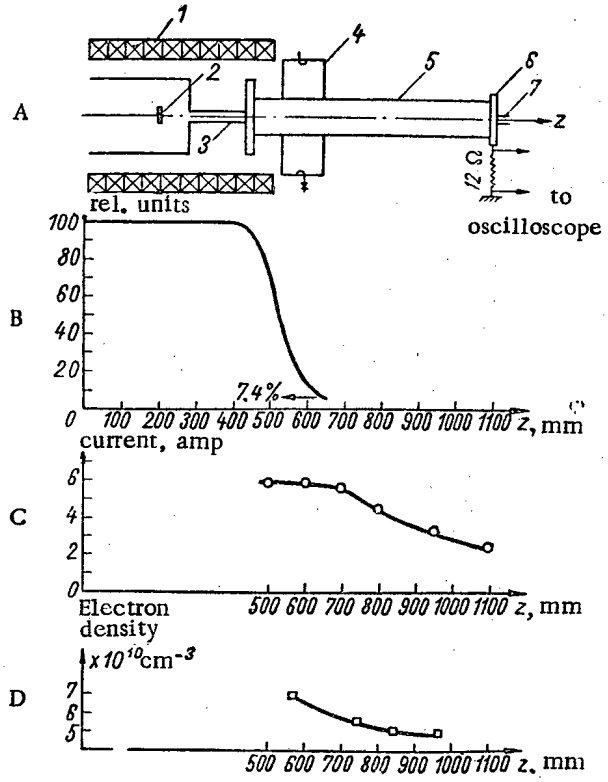

Fig. 2. Basic physical parameters of the experiment. A) Diagram of the apparatus (to scale): 1) solonoid for magnetic focusing field; 2) cathode; 3) copper tube to produce pressure differential; 4) microwave cavity; 5) plasma chamber; 6) current measurement collector; 7) input to electrostatic analyzer; B) distribution of longitudinal magnetic field along the system axis; C) distribution of electron current along the system axis; D) distribution of plasma electron density along the axis (pressure in the plasma chamber, $4 \cdot 10^{-3}$ mm Hg).

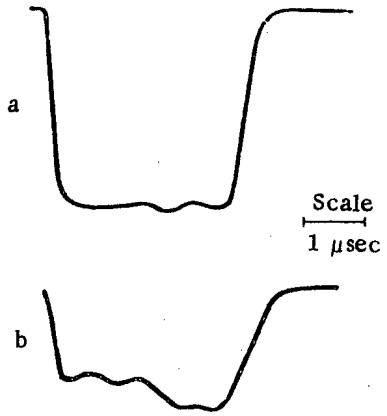

Fig. 3. Oscillogram of the voltage pulse applied to the electron gun (a) and oscillogram of the current pulse at the collector (b).

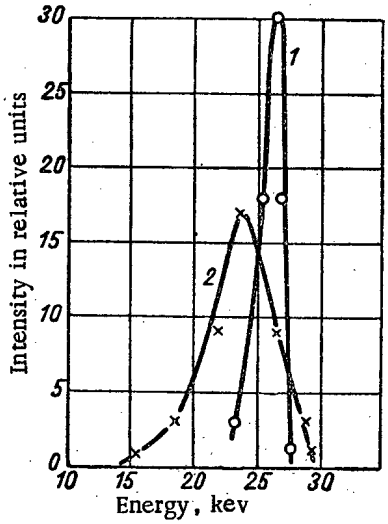

Fig. 4. Electron spectra: 1) at entrance to the plasma chamber at pressures of $3 \cdot 10^{-4}$ and $4 \cdot 10^{-3}$ mm Hg; 2) spectrum of electrons that have traversed the axis of the plasma chamber at a pressure of $4 \cdot 10^{-3}$ mm Hg.

The exit energy spectrum is essentially the same (within the limits of accuracy of the measurements) for a pressure of $3 \cdot 10^{-4}$ mm Hg. Curve 2 of Fig. 4 shows the exit energy spectrum at a pressure of $4 \cdot 10^{-3}$ mm Hg with an entrance current of 6 amp. It is evident from these curves that at $3 \cdot 10^{-4}$ mm Hg the beam energy loss is less than 1% of the initial beam energy; on the other hand, at $4 \cdot 10^{-3}$ mm Hg (corresponding to an initial plasma density

of $7 \cdot 10^{10}$ cm^{-3}) the spectrum half-width (Fig. 4, curve 2) is increased appreciably and the energy loss of the electrons in the beam is 2.7 kev or 11% of the initial energy. Thus, the energy losses of the electron beam increase with increasing plasma density.*

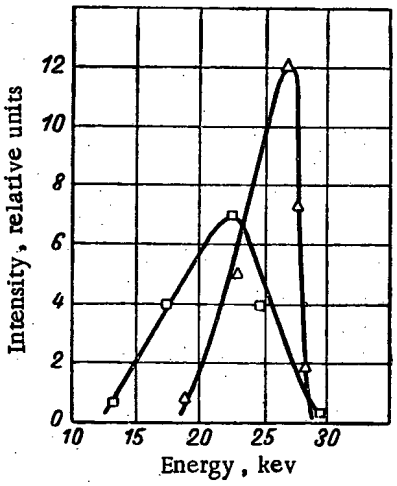

Fig. 5. Electron spectrum for peripheral electrons (10 mm from the axis) at a residual gas pressure of $3 \cdot 10^{-4}$ mm Hg (△) and $4 \cdot 10^{-3}$ mm Hg (□).

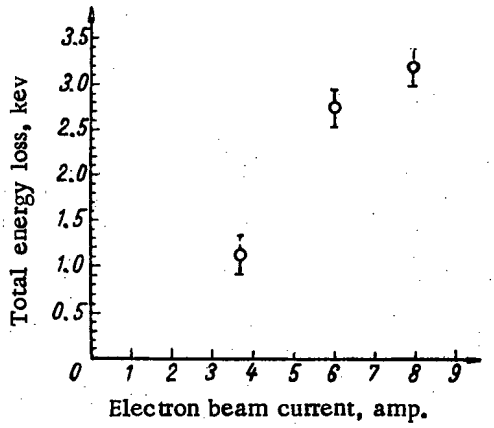

Fig. 6. Energy loss as a function of beam current (residual gas pressure $4 \cdot 10^{-3}$ mm Hg, initial beam energy 26 kev).

The spectra of the peripheral electrons in the beam (10 mm from the axis) are shown in Fig. 5 for the same values of the residual gas pressure in the plasma chamber. The energy loss is 3.2 kev. The half-width of the spectrum is also increased appreciably compared with the half-width at $3 \cdot 10^{-4}$ mm Hg.

In Fig. 6 we show the electron energy losses as a function of beam current. As expected, the losses increase with increasing current.

When the interaction length is increased from 32 to 64 mm, i.e., when the beam-plasma interaction length is doubled, the energy losses also are doubled. It follows that the electron beam loses energy over the whole length of the beam-plasma interaction path, rather than in a localized region. An electron beam passing through a plasma can lose energy via the following mechanisms: elastic electron collisions, inelastic collisions of electrons with molecules of the residual gas, and excitation of longitudinal density waves, leading to the coherent interaction of the beam with the plasma.

We now estimate the energy loss due to each of these mechanisms. The energy loss due to elastic collisions is

$$\delta E_1 \simeq n_1 \sigma v \frac{m}{M} E \frac{L}{v}.$$

where n_1 is the number of neutral particles per cubic centimeter, m is the electron mass, M is the mass of the residual gas molecule, v is the electron velocity, σ is the cross section for the collision process, E is the electron energy, L is the electron path length. Substituting a residual gas pressure of $4 \cdot 10^{-3}$ mm Hg, a plasma chamber length of 64 cm and energy of 26 kev, we have

$$\delta E_1 \simeq 0.04 \text{ ev}.$$

* It has been shown in later experiments that a magnetic field can cause a substantial increase in these losses. Furthermore, one observes electrons with energies appreciably greater than the initial beam energy (1.5-2 times).

The losses due to inelastic collisions are given by

$$\delta E_2 \simeq \varepsilon(V)\, pLk.$$

where $\epsilon(V)$ is the specific ionization (the number of electron-ion pairs formed by a particle per centimeter of path length at a gas pressure of 1 mm Hg), p is the pressure of the residual gas (mm Hg), k is the specific energy loss due to the formation of an electron-ion pair. Taking $v \simeq 10^{10}$ cm/sec; $\epsilon(V) \simeq 0.3$ [12]; $p = 4 \cdot 10^{-3}$ mm Hg; $L = 64$ cm and $k = 32$ ev [12], we find $\delta E_2 \simeq 3$ ev.

Finally, the interaction of the beam with the plasma causes self-modulation of the beam, as a result the initially unmodulated beam becomes bunched [1, 3, 8]. Under these conditions a coherent interaction can occur [5]. If the conditions for a coherent interaction are satisfied the specific energy loss of a single particle in a bunch is given by [5, 7, 8]

$$\left|\frac{dE}{dx}\right| = \frac{eN\omega_0^2}{2v^2} \ln\left(1 + \frac{v^2}{\omega_0^2 b_\perp^2}\right).$$

where e is the electron charge, ω_0 is the plasma frequency; v is the velocity of the electron beam; N is the number of particles in a bunch; $b_\perp$ is the transverse dimension of a bunch.

The field produced by a coherent bunch can be amplified if the coherence conditions are satisfied for a series of such bunches [9, 13]; however, these conditions are not satisfied in the present experiments. With $n \simeq 7 \cdot 10^{10}$ cm^{-3}; $v \simeq 9 \cdot 10^9$ cm/sec; $N \simeq 6 \cdot 10^9$ cm^{-3}; $b_\perp \simeq 2$ cm and 40% modulation the energy lost by the beam should be 3.2 kev for a plasma interaction length of 64 cm; this value is in satisfactory agreement with the present experimental data.

Thus, it may be assumed that in the present experiment the principal energy losses of the electron beam passing through the plasma are due to a coherent interaction.

LITERATURE CITED

1. A. I. Akhiezer and Ya. B. Fainberg, Dokl. AN SSSR 69, 555 (1949).
2. A. I. Akhiezer and Ya. B. Fainberg, Zh. éksperim. i teor. fiz. 21, 1262 (1951).
3. D. Bohm and E. Gross, Phys. Rev. 75, 1851, 1864 (1949).
4. D. Bohm and E. Gross, Phys. Rev. 79, 992 (1950).
5. V. I. Veksler, Proc. Symp. CERN 1, 80 (1956).
6. I. F. Kharchenko et al., Second International Conference on the Peaceful Uses of Atomic Energy (Geneva, 1958). Reports of Soviet scientists, Vol. 1 (Moscow, Atomizdat, 1959), p. 110.
7. I. F. Kharchenko et al., Zh. éksperim. i teor. fiz. 38, 685 (1960).
8. Ya. B. Fainberg, Dissertation, FIAN (1960).
9. B. M. Bolotovskii, Dissertation, FIAN (1954).
10. M. Biondi and S. Brown, Phys. Rev. 75, 1700 (1949).
11. M. D. Raizer and I. S. Shpigel', Usp. fiz. nauk 64, 641 (1958).
12. A. Éngel', Ionized Gases [in Russian] (Moscow, Fizmatgis, 1959), p. 67.
13. V. L. Ginzburg and I. M. Frank, Dokl. AN SSSR 56, 699 (1947).

All abbreviations of periodicals in the above bibliography are letter-by-letter transliterations of the abbreviations as given in the original Russian journal. *Some or all of this periodical literature may well be available in English translation.* A complete list of the cover-to-cover English translations appears at the back of this issue.

INVESTIGATION OF THE BR-5 FAST REACTOR (SPACE-ENERGY NEUTRON DISTRIBUTIONS)

A. I. Leipunskii, A. I. Abramov, Yu. A. Aleksandrov,
G. V. Anikin, I. I. Bondarenko, A. G. Guseinov,
V. I. Ivanov, O. D. Kazachkovskii, V. F. Kuznetsov,
B. D. Kuz'minov, V. N. Morozov, M. N. Nikolaev,
O. A. Sal'nikov, G. N. Smirenkin, A. S. Soldatov,
L. N. Usachev and M. G. Yutkin

Translated from Atomnaya Énergiya, Vol. 11, No. 6, pp. 498-505,
December, 1961
Original article submitted August 17, 1961

The present article provides a brief description of a fast reactor which is in operation and of its basic experimental equipment. The reactor is designed for studying various materials and for technological and physical investigations. Its over-all rated power level is 5000 kw. The article also provides the characteristics which illustrate the experimental possibilities of the device as a source of fast and slow neutrons and also the results obtained in investigating the spectrum of neutrons in the reactor core, the reflector, and the experimental devices (beams, channels, and the thermal column). The obtained data are compared with the calculated values.

The BR-5 fast reactor is designed for research purposes. The heat output of the reactor is 5000 kw; the reactor is designed for the accumulation of experience and for producing data necessary for constructing fast power reactors with increased breeding of fissionable material. Plutonium oxide serves as the fuel in the reactor. Sodium is used as the coolant. The reactor's reflector consists of two layers: a thin layer of natural uranium and a thick nickel layer. The design of this reactor was described in detail in a report to the Second International Conference on the Peaceful Uses of Atomic Energy [1].

The reactor is provided with a large number of experimental devices, which are designed for the investigation of various materials and for performing technological and physical experiments with fast, slow, and thermal neutrons. High-power neutron beams, the experimental channels, and the thermal column offer great possibilities for measuring the nuclear constants, which are necessary in designing reactors and in experiments on nuclear physics. The vertical and horizontal cross sections of the reactor are shown in Figs. 1 and 2.

A channel, which is intended for the performance of loop experiments with experimental fuel elements, passes along the vertical axis of the reactor core. The OK-70 vertical channel, which has a diameter of 70 mm, passes through the nickel reflector at a distance of 40 cm from the center of the reactor. Two horizontal channels for the extraction of fast-neutron beams (channels B-1 and B-3) pass from the reactor core surface through the reflector and the reactor's shield. The P-2 horizontal channel, which serves for extracting the beam of intermediate neutrons, emerges from the nickel reflector. Moreover, there is a wide channel, B-2, which is designed for experiments on radiation protection. The reactor has a graphite thermal column with a number of vertical channels, the diameter of which is equal to 20 mm, with the exception of the OK-3 and AK channels, the diameter of which is 70 and 100 mm, respectively.

The present article provides the results obtained in measuring the space-energy distribution of neutrons and also certain characteristics of the experimental devices.

The neutron-energy spectra are different in different sections of the BR-5 reactor. In the reactor core, the neutron spectrum is rather hard, and a considerable portion of it lies in the region above 100 kev. While passing

through the nickel reflector of the reactor, the neutrons quickly lose their energy due to inelastic and subsequently also elastic collisions, so that the average energy of neutron spectra amounts to only a few tens of electron volts in the external layers of the screen.

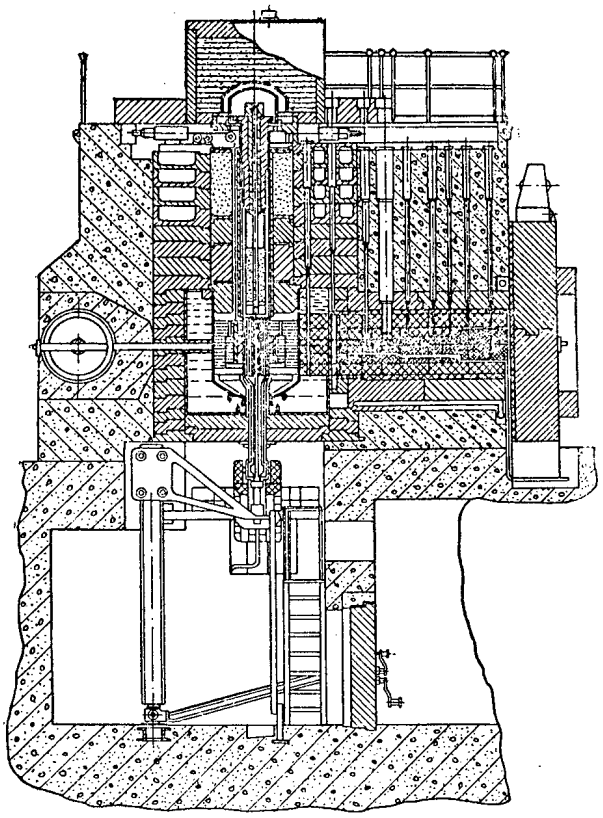

Fig. 1. Vertical cross section of the BR-5 reactor.

The measurement of neutron spectra, especially in the kiloelectron volt region, constitutes a very complex experimental problem. Because of this, detailed spectral measurements were performed only in the region of comparatively fast neutrons (E_n > 50 kev) for the most important neutron beams and channels. In other cases, the

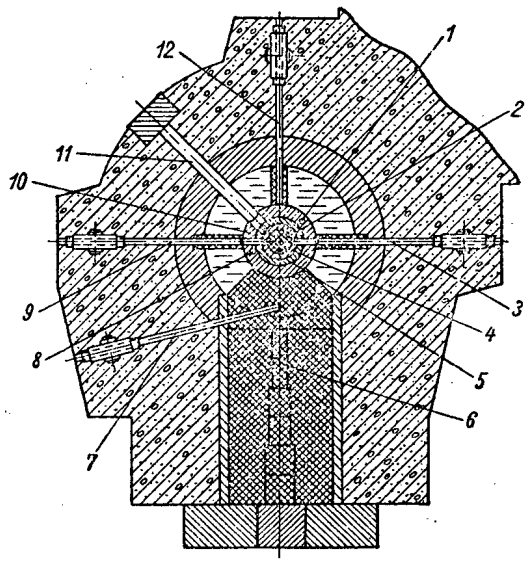

Fig. 2. Horizontal cross section of the BR-5 reactor. 1) OK-50 channel; 2) reactor core; 3) B-1 channel; 4) compensating cylinder; 5) screen compensator; 6) removable part of the thermal column; 7) T-4 channel; 8) OK-70 channel; 9) B-3 channel; 10) fixed nickel screen; 11) B-2 channel; 12) P-2 channel.

cross sections of reactions with a known energy distribution, which were averaged with respect to the energy spectrum under investigation, were used as the spectral characteristics. Among such reactions were the U^{238} (n, f), Th^{232} (n, f), and Al^{27} (n, α) Na^{24} fission reactions, whose effective thresholds were in the vicinity of 1, 4, and 5 Mev, respectively, and whose cross sections were approximately constant in the energy region above the threshold, the Pu^{239} (n, f) reaction, the cross section of which was almost constant in the energy region from 50 kev to 6 Mev, and the Na^{23} (n, γ), Cu^{63} (n, γ) and Au^{197} (n, γ) reactions, which served mainly as indicators of slow neutrons. The distribution of U^{235} fissions was also measured. In order to obtain more detailed information on the soft portion of the spectrum in the reactor's reflector, investigations of the spatial distributions of neutrons with $E_n \simeq 5$ ev were also performed by means of gold indicators by using the method of resonance blocking [2].

The irradiation of these indicators was performed in the vertical experimental channel, which was located at a distance of 5 cm from the reactor's axis. Small-size fission chambers, which contained thin layers of fissionable materials, served as fission detectors. The chambers were filled with pure argon to a pressure of 10 atm. The conditions under which the filling was performed were such that the sensitivity of the chamber was independent of time and temperature up to 400° C with an accuracy of 2%, which was quite satisfactory, since the reactor core's temperature during measurements did not exceed 250° C. The activation detectors consisted of aluminum, copper, and gold foils and NaF pellets. The beta-activity of specimens was measured by means of an end-type Geiger counter.

The total flux of neutrons of all energies was measured only in those places of the reactor where the basic portion of the neutron spectrum lies in the region of constant Pu^{239} fission cross sections. In this case, the fission

chamber with a Pu^{239} layer served as an all-wave detector. The amount of matter in the fissionable layer was determined with respect to α-activity. The flux of fast neutrons was measured in a similar manner by means of a fission chamber with natural and impoverished uranium. The amount of matter in the chambers was determined by comparing the counting rates of these chambers with the counting rate of the fission chamber with Pu^{239} after they were irradiated with equal thermal-neutron fluxes.

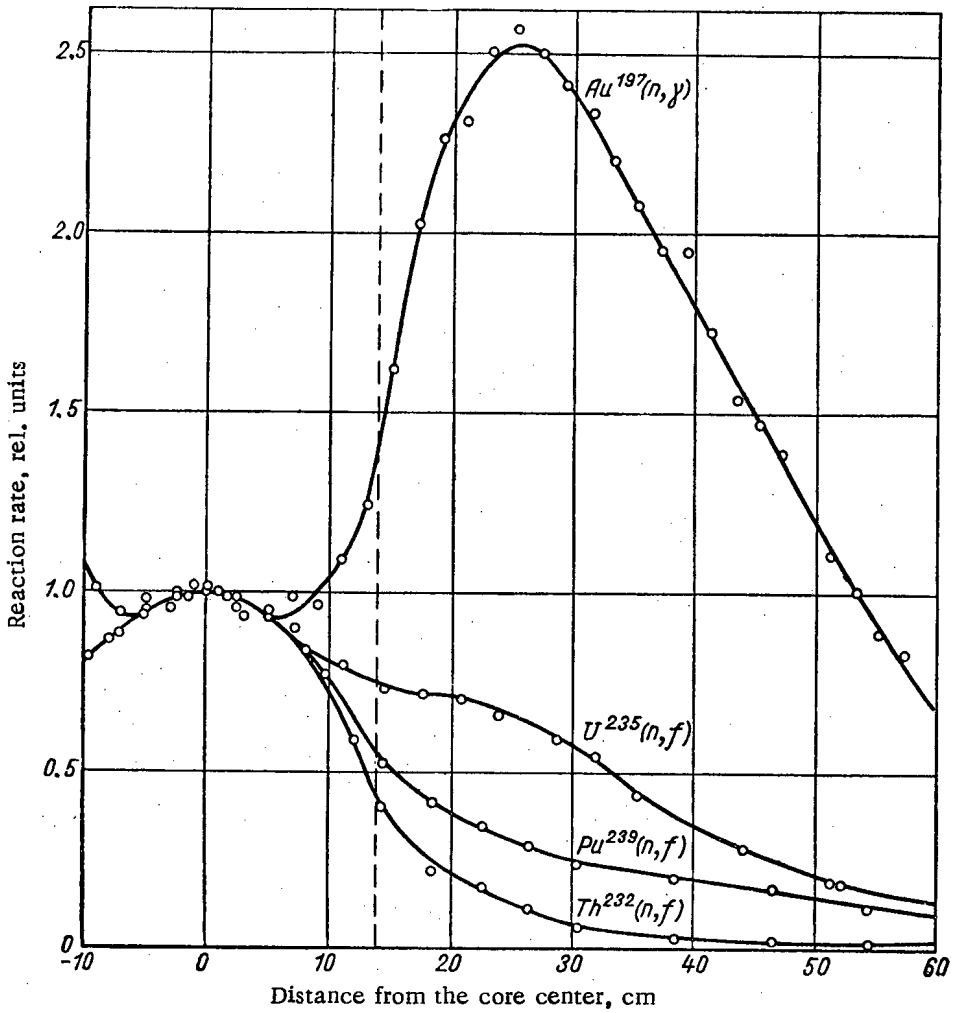

Fig. 3. Distribution of the rates of various reactions along the BR-5 reactor's central channel. The rates of all reactions at the reactor core's center were assumed to be equal to unity.

The direct measurements of neutron spectra were performed in the vertical OK-70 channel and in the horizontal B-3 channel (see Figs. 1 and 2). In the OK-70 channel, the neutron spectrum was measured by means of an ionization chamber which was filled with a mixture of He^3 and argon, while the spectrum in the B-3 channel was measured by using the method of transmission through a hydrogenous substance (n-hexane) in a "good" geometry. A boron counter was used as the detector. The inverse Laplace transformation was performed on the transmission curve (image). After the energy sensitivity of the detector and the energy curves of the total cross sections of hydrogen and carbon, which were present in the diffuser, were taken into account, the obtained original made it possible to determine the neutron spectrum. The neutron spectrum in the B-3 channel was also measured by using the photoemulsion method.

The results of all the measurements performed are given below. Figure 3 shows the distributions of the counting rates of different detectors along the reactor's vertical axis. The reactor core's boundary is marked by a dotted line. In the central portion of the reactor core, all distributions, including the distributions of Th^{232} fission and captures in

Au^{197}, which have totally different energy dependences of the cross sections, obey the same law. This indicates that the reactor core dimensions are sufficiently large, and that a steady neutron-energy spectrum is established in those regions of the core which are far removed from the boundaries. The reflector effect is not pronounced in these regions. In the peripheral layers of the reactor core, the admixture of slow neutrons incoming from the reflector becomes noticeable. As a result of this, the distributions plotted by means of detectors with different energy sensitivities are different at the boundary between the reactor core and the reflector. This difference is most strongly pronounced in the reactor's screen, where the neutrons quickly lose their energy as a result of inelastic scattering, after which they are further slowed down as a result of elastic collisions. Due to the intensive blocking of resonance capture by resonance scattering, the probability that resonance capture in elastic moderation in nickel will be avoided is rather high. Therefore, the greater portion of neutrons, while being slowed down, passes through the resonance region of nickel avoiding capture, after which they continue to be slowed down without noticeable absorption to an energy of the order of 10 ev, where the 1/v law begins to take effect. The described qualitative pattern indicates that the density of neutron capture in gold increases almost threefold in comparison with the neutron capture density at the reactor core's center, regardless of the fact that the lower resonances in the gold foils used are heavily blocked. The sharp increase in the cross section in transition from the reactor core to the reflector also affects the distribution of U^{235} fission and, to a lesser degree, the distribution of Pu^{239} fission. The latter fact is caused by the weaker dependence of the Pu^{239} fission cross section on energy.

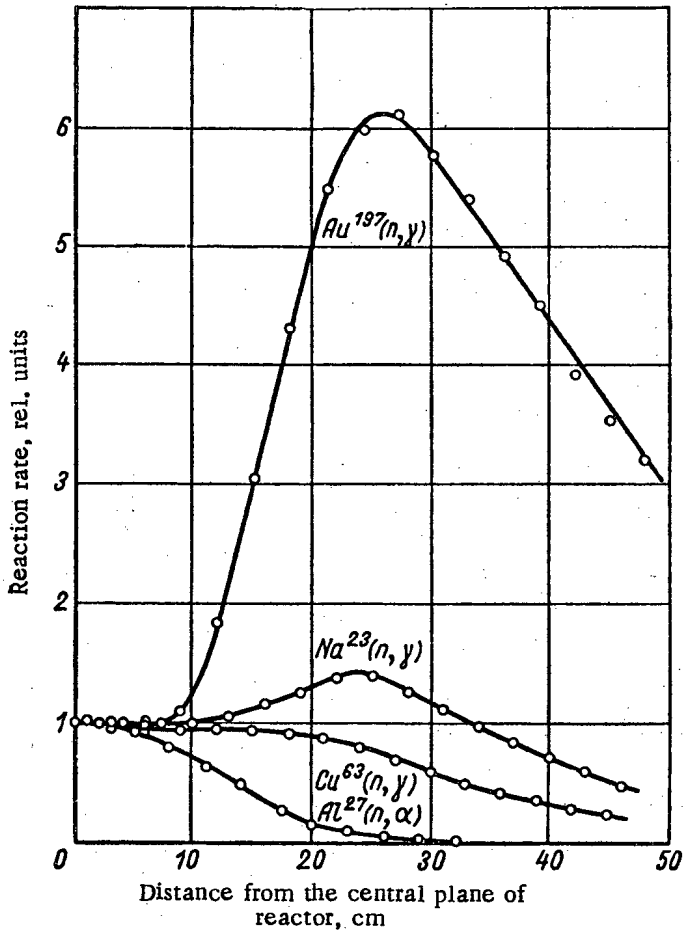

Fig. 4. Distributions of the number of Al(n, α) reactions and of captures in Na^{23}, Cu^{63}, and Au^{197} (thin indicator), which were measured in the vertical channel that was located at a distance of 5 cm from the reactor's axis. The number of reactions in the central plane of the reactor core was assumed to be equal to unity.

Figure 4 shows the distributions of the rates of Al^{27} (n, α) reactions and of captures in Na^{23}, Cu^{63} and Au^{197} (thin indicators), which were measured in the vertical experimental channel that was located at a distance of 5 cm from the reactor's axis. These results confirm the conclusions drawn on the basis of the data obtained in the central channel of the reactor. The distributions of the specific activities of gold foils, which were screened on both sides by means of gold filters with different thicknesses, confirm the intensive moderation of neutrons in the nickel reflector in a most obvious manner. By extrapolating these data for the "zero" thickness of the indicator foil and the "infinite" thickness of the filter, it is possible to determine the activity that is caused almost exclusively by neutrons with the energy E_n = 4.9 ev in the resonance region. Figure 5 shows the spatial distribution of the neutron flux with E = 4.9 ev along the experimental channel's height, which was calculated by using the difference between the extrapolated activities for the rated power level of the reactor.

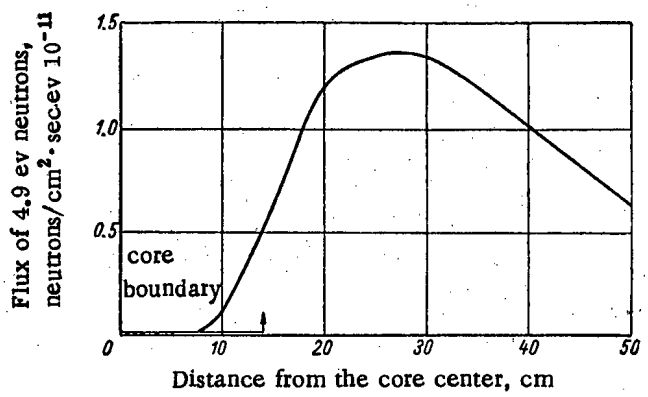

Fig. 5. Spatial distribution of the neutron flux with E_n = 4.9 ev along the experimental channel.

In contrast to the distributions plotted by means of detectors which are sensitive to slow neutrons, the distributions of Th^{232} fissions and Al (n, α) reactions display a sharp drop in the reactor's reflector, which was to be expected, since the energy of fast neutrons drops below the threshold of these reactions due to elastic scattering in nickel.

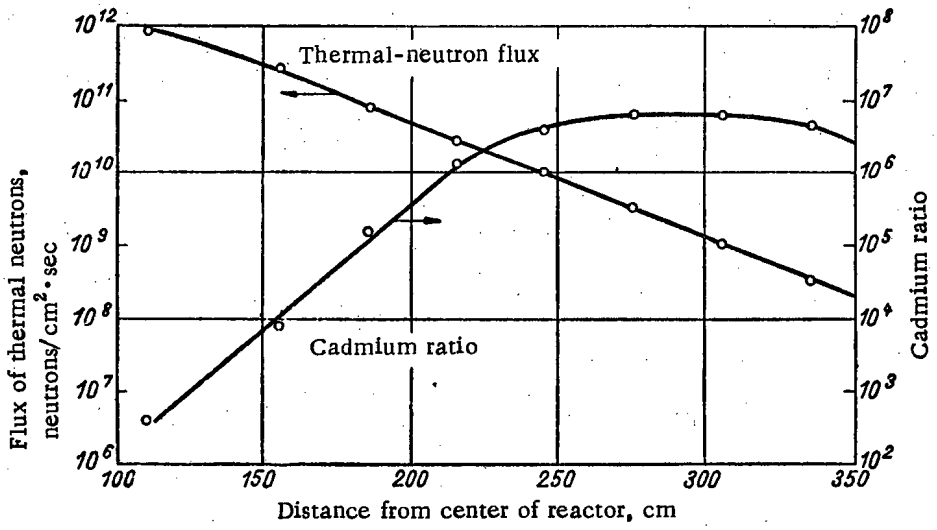

Fig. 6. Distribution of the thermal neutron flux and of the cadmium ratio along the thermal column.

The distributions given in Fig. 3 were plotted in relative units. For normalization, it is necessary to know the cross sections of the corresponding reactions at the center of the reactor core.

The ratios of the U^{235} and U^{238} fission cross sections and of the Au^{197} capture cross section to the Pu^{239} fission cross section were measured at the center of the reactor core. The obtained results are given in the second column of Table 1.

A summary of data on the fluxes is given in Table 2. The distribution of the thermal neutron flux and of the cadmium ratio along the axis of the thermal column was measured by means of Au^{197} and In^{115}, and Cu^{63} radioactive indicators. The averaged data are given in Fig. 6. The thermal-neutron flux curve was normalized with respect to the value obtained for the AK channel. The cadmium ratios were converted with respect to a detector with a 1/v sensitivity. The indicated neutron-flux values pertain to the 5000 kw power, which is generated in the reactor core

(the fission of U^{238} and U^{235} in peripheral packages is taken into account). The power level was determined on the basis of the counting rate of the Pu^{239} fission chamber with a known amount of matter and the nonuniformity factor of the fission distribution in the reactor core. Moreover, the power was calibrated with respect to the heat balance for high reactor power levels that were close to the rated power.

TABLE 1. Cross Sections of Various Reactions at the Reactor Core Center

Reaction	Experiment		Calculation
	σ/σ_f (Pu^{239})	σ, b	σ, b
Pu^{239} (n, f)	1	1.81	1.81
U^{235} (n, f)	0.82±0.03	1.48±0.06	1.46
U^{238} (n, f)	0.090±0.004	0.163±0.007	0.16
Au^{197} (n, γ)	0.121±0.005	0.22±0.01	0.21

Figures 7 and 8 illustrate the neutron spectrum in the B-3 beam, which originated at the reactor core surface. The spectrum was determined by analyzing the transmission curve and by using the photoemulsion method. The second maximum in Fig. 7, which is located in the low-energy region, is due to neutrons that are moderated in the reflector. For energies greater than 2.5 Mev, the above spectrum coincides with the spectrum of fission neutrons. The neutron spectrum in the OK-70 channel, which was measured by means of a chamber filled with He^3, is given in Fig. 9.

The quantitative calculations of the space-energy neutron distributions in the BR-5 reactor were performed for 9 and 18 groups. The neutron distribution which was obtained for nine groups by solving the kinetic equation in the S_4-approximation according to Carlson's method was in satisfactory agreement with experimental data for

TABLE 2. Neutron Fluxes in the Core and the Experimental Devices of the BR-5 Reactor (neutrons/$cm^2 \cdot sec$)

Measurement location	Thermal	Resonance (per single interval)	Fast (over 1.4 Mev)	Total flux
Reactor core center	0	0	$(2.4\pm0.2)10^{14}$	$(8.2\pm0.3)10^{14}$
Beam in B-1 and B-3 . . .	0	0	$(2.2\pm0.21)10^{9}$	$(3.0\pm0.2)10^{10}$
Beam in P-2	0	—	$(1.2\pm0.4)10^{8}$	—
Beam in T-4	$(8.5\pm0.5)10^{7}$	$(3.4\pm0.5)10^{6}$	$(1.0\pm0.3)10^{8}$	—
Maximum neutron flux in the thermal column	$(5\pm2)10^{12}$	—	—	—

Pu^{239} and U^{238} and the activation of gold in the reactor core (see Table 1). This indicates that the theoretical spectrum in the reactor core was calculated correctly. The neutron spectrum which was measured in the OK-70 channel for the 0.1-1.4 Mev interval was also in good agreement with theoretical data. However, the experimental curves for Pu^{239} and U^{235} fission and the activation of gold in the reflector did not agree well with the theoretical curves. Thus, the theoretical gold activation curve abates in the reflector, while the experimental curve has a sharply-defined maximum. In connection with this, we calculated the space-energy neutron distribution in the 18-group approximation for a spherical reactor model. These calculations resulted in a better agreement with experimental data, which is illustrated in Fig. 10, where the theoretical and experimental distributions of capture in gold are compared. In spite of the obvious improvement, there is no complete agreement between theoretical and experimental data. Apparently, the main cause of this discrepancy is the fact that the initial spherical and homogenized variants of the system which were used in calculations cannot adequately represent the actual design of the reactor. An exact consideration of the structural characteristics (annular clearances, reactor parts which are

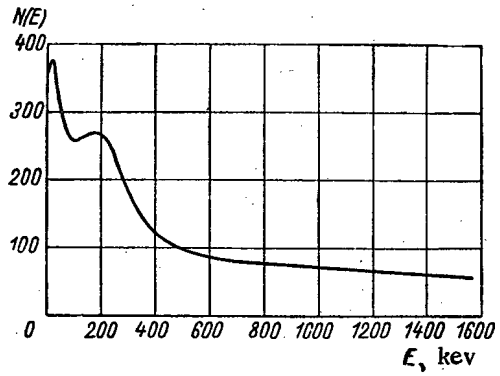

Fig. 7. Spectrum of neutrons in the beam of B-3. The measurements were performed by using the method of transmitting neutrons through a hydrogenous medium (n-hexane).

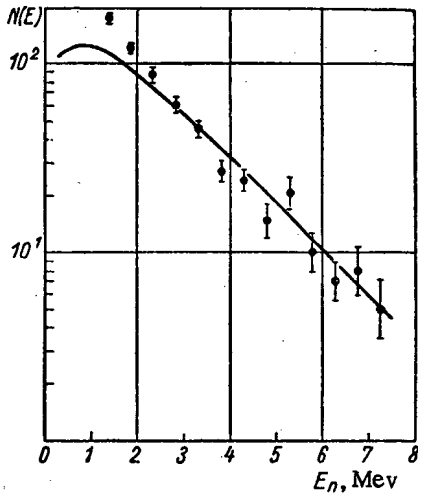

Fig. 8. Hard portion of the spectrum of neutrons outgoing from the reactor core, which was measured by using the photoemulsion method. The experimental data are compared with the theoretical $N(E_n) \sim \sqrt{E_n} e^{-\frac{E_n}{\theta}}$ curve for the spectrum of instantaneous Pu^{239} fission neutrons. (According to the measurement results obtained by V. F. Kuznetsov, the value of θ was assumed to be equal to 1.4 Mev).

located beyond the reflector, etc.) constitutes a complex problem. It is also possible that the system of constants was not quite correctly chosen. However, it should be noted that the separately performed investigation of the space-energy neutron distribution in nickel yielded results which were in satisfactory agreement with theoretical data.

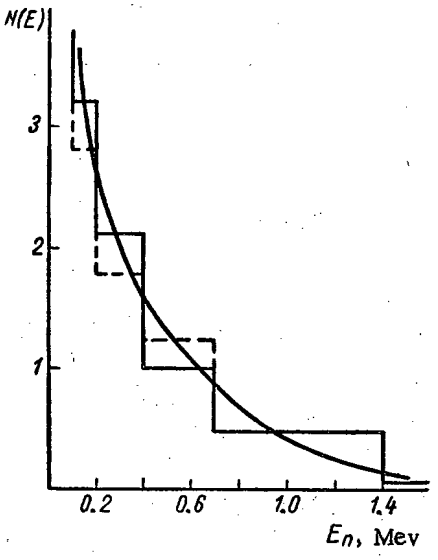

Fig. 9. Neutron spectrum in the OK-70 channel. (The smooth curve represents the experimental results, and the histogram represents the results of calculations for 9 (dotted lines) and 18 groups. The N_i values were assumed to be equal in the 0.7-1.4 Mev interval).

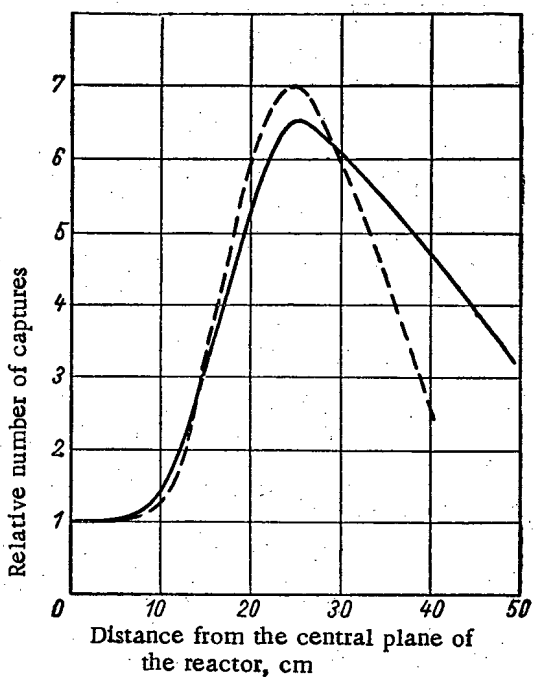

Fig. 10. Comparison between the experimental and the theoretical gold activation curves. The solid line represents the experimental results, while the dotted line shows theoretical data.

The authors extend their thanks to D. S. Pinkhasik, N. N. Aristarkhov and to the entire personnel who serviced the reactor for their help in the experiments.

LITERATURE CITED

1. A. I. Leipunskii et al., Transactions of the Second International Conference on the Peaceful Uses of Atomic Energy (Geneva, 1958). Reports by Soviet Scientists [in Russian] (Atomizdat, 1959), Vol. 2, p. 215.
2. V. I. Golubev et al., Atomnaya Énergiya 11, 6, 522 (1961).

All abbreviations of periodicals in the above bibliography are letter-by-letter transliterations of the abbreviations as given in the original Russian journal. *Some or all of this periodical literature may well be available in English translation.* A complete list of the cover-to-cover English translations appears at the back of this issue.

ON SOME METHODS FOR RAISING THE POWER LEVEL OF REACTORS WITH GASEOUS COOLANTS

P. I. Khristenko

Translated from Atomnaya Énergiya, Vol. 11, No. 6, pp. 506-514,
December, 1961
Original article submitted February 18, 1961

The present article is concerned with certain methods for raising the power level of reactors with gaseous coolants: additional cooling of the gas ahead of the gas compressor, increasing the pressure in the loop, and profiling the coolant flow through the reactor.

Equations for calculating the theoretical thermodynamic cycle for a reactor with a gaseous coolant, the coolant temperature at the downstream end of the reactor, and the profiling of the coolant flow are derived.

The cost $\overline{C}$ of the electric power produced by a reactor can be determined from the expression

$$\overline{C}\left[\frac{\overline{A}_1}{N_T n(\eta_t')}+\frac{\overline{A}_2}{N_T n(\eta_t')}+\frac{\overline{b}}{(\eta_t')}\right]\frac{1}{1-\beta}\frac{1}{\eta_{oe}} \tag{1}$$

or

$$C=(\overline{a}_1+\overline{a}_2+\overline{b}_1)\frac{1}{1-\beta}\frac{1}{\eta_{oe}} \tag{1a}$$

where $\overline{A}_1$ is the sum of annual deductions from the investment in the reactor and equipment, which take into account the servicing, amortization, and the paying-off of the investment;* this figure also includes the annual expenditures for overhauling the equipment and the salaries of the servicing personnel; $\overline{A}_2$ is the same for the power section of the station (machine room, electrical section, water supply, etc.); $\overline{b}$ is the cost of the fuel expended in producing 1 kw-hr of heat power; N_T is the reactor's heat output; η' is the efficiency of the entire device; and $\underline{n}$ is the time during which the power output of the station is utilized (hr/year).

The $\frac{1}{1-\beta}$ factor takes into account the effect of the power dissipated in coolant circulation through the reactor on the electric power cost, while the $\beta=\frac{N_{II}}{N_T(\eta_t')}$ coefficient represents the relative power dissipation in circulation; η_{oe} is the efficiency factor which takes into account other equipment necessary for the power station itself (circulation pumps for turbines, steam generator feed pumps, etc.). For single-loop systems using gas turbines, the factor $\frac{1}{1-\beta}$ in Eq. (1) should be omitted, while (η_t') should be understood as the internal efficiency of the gas turbine unit.

The contributions of the terms which determine the electric power cost in expression (1) are not equal. For gaseous-coolant reactors which operate with natural uranium [1], the main component of the electric power cost is determined by the first term of expression (1). With an increase in the reactor's power level, the value of the first term will decrease, and, consequently, the economic efficiency of boosting the power level of such a reactor is obvious. This can be done, for instance, by increasing its dimensions or by raising the temperature of the fuel

* The additional deductions from the investment, which are equal to the total investment divided by the amortization period, are also included in this figure.

elements. In the latter case, not only the power level, but also the factor of utilization of the nuclear fuel will increase. However, the problem of raising the temperature is connected with the search for new materials and designs of fuel elements. If we do not resort to larger reactor dimensions and to raising the temperature of the fuel elements, the useful power output of the station can be augmented only by intensifying the coolant flow through the reactor and by reducing the power dissipated on coolant circulation. We shall analyze here these possibilities.

1. The simplest and the best-known method for intensifying the coolant flow through the reactor is that of increasing the coolant pressure in the loop. With an increase in the coolant pressure, the power level of the reactor increases almost at the same rate, while the portion of power which is expended on gas circulation remains virtually unchanged. Therefore, increasing the pressure is always advisable.

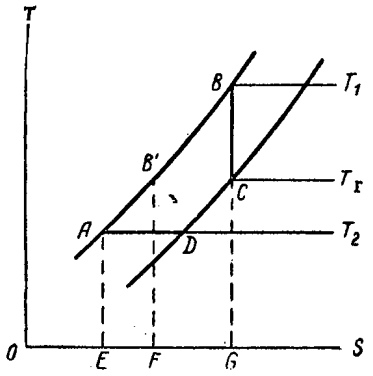

Fig. 1. Theoretical thermodynamic cycle of a reactor with a gaseous coolant.

The theoretical thermodynamic cycle of a gaseous-coolant reactor with complete heat regeneration is represented graphically in Fig. 1.* Such a cycle could be realized if the heat from the reactor is used directly in the gas turbine; however, due to heat losses in the turbine and the compressor, this cycle becomes advantageous only if the initial gas temperature is above 750 °C. For lower temperatures, it is more convenient to utilize the heat by means of a single-step or a multistep steam power plant cycle, where the utilization factor of the theoretical cycle is always less than unity. The gas, which is heated in the reactor to the temperature T_1 (point B on the TS diagram), expands adiabatically along BC until its temperature attains the regeneration temperature T_r (point C). Along the isobar DC, the heat is then taken away from the gas in the regenerative heat exchanger. The gas in then compressed by a compressor along the isotherm DA** to a pressure equal to the pressure in the reactor, after which it is heated along the isobar first in the regenerative heat exchanger (curve AB') and then in the reactor (curve B'B).

If the specific heat of the gas is $c_p = \text{const}$, and $c_p\,dT = T\,dS$, the thermal efficiency of this cycle can be written thus:

$$\eta_t = 1 - T_2 \frac{\ln\left(\frac{T_1}{T_r}\right)}{T_1 - T_r}. \qquad (2)$$

The power level of the reactor depends on the coolant discharge g, its specific heat c and the preheating temperature $(t_2 - t_1)$ of the coolant in the reactor:

$$N_T = gc\,(t_2 - t_1). \qquad (3)$$

The coolant temperatures at the upstream and the downstream ends of the reactor enter Eqs. (2) and (3). The maximum temperature $(t_n)_m$ of the fuel element surfaces and the coolant temperature at the reactor's upstream end are usually assigned. The latter temperature is assigned on the basis of the technological operating conditions of the reactor or is determined on the basis of engineering and economic calculations.

The coolant temperature at the exit from the channel of a reactor without end-reflectors (with a cosine energy distribution along the height) is determined by the equation

$$t_2 - t_1 = A\left(\sqrt{\frac{A^2}{4} + 1} - \frac{A}{2}\right)[(t_n)_m - t_1] = \varphi(A)\,[(t_n)_m - t_1]; \quad (\varphi(A) \leqslant 1) \qquad (4)$$

* This cycle has the greatest thermal efficiency.

** In operative gas turbine units, adiabatic compression is used instead of isothermic compression in several compressor stages with intermediate cooling between the stages. For a large number of stages, compression with intermediate cooling approximates isothermic compression.

This equation can be derived from the equation

$$\Delta t_y = \sqrt{(t_n)_m^2 - 2(t_n)_m t_{av} + t_2 t_1}; \quad (5)$$
$$t_{av} = \frac{1}{2}(t_1 + t_2),$$

if we use the heat balance equations for the reactor's channel

$$Q = gc(t_2 - t_1) \text{ and } Q = H\alpha\Delta t_{cy}\eta_h, \quad (6)$$

and if we denote by

$$A = \frac{t_2 - t_1}{\Delta t_{cy}} = \frac{H\alpha\eta_h}{gc}, \quad (7)$$

the coefficient which depends on the surface area H of the fuel elements, the coefficient α of heat transfer from the fuel elements to the coolant, and the coefficient of equalization η_h of the gas discharge g through the reactor and of the specific heat c of the gas along the height of the reactor, and if we substitute in Eq. (5) the maximum difference Δt_{cy} between temperatures of the fuel element surfaces and the coolant, which is given by Eq. (7).

For reactors with end-reflectors, the equations, which are similar to Eqs. (4) and (5), have the following form:

$$t_2 - t_1 = \frac{A\left(\sqrt{\frac{A^2}{4}\frac{1}{\sin^2(n)} + 1} - \frac{A}{2}\right)}{\frac{A^2}{4}\left(\frac{1}{\sin^2(n)} - 1\right) + 1} \times [(t_n)_m - t_1],$$
$$t_2 - t_1 = \Phi(A)[(t_n]_m - t_1]. \quad (8)$$

$$\Delta t_{cy} = \sqrt{[2(t_n)_m - (t_2 + t_1)]^2 - \frac{1}{\sin^2(n)}(t_2 + t_1)^2}. \quad (8a)$$

Eqs. (4), (5), (8), and (8a) were derived from the condition which states that a temperature maximum should exist along the fuel element, i.e., on the basis of the condition $\frac{d(t_n)_x}{dx} = 0$, and the limits within which they can be applied can be determined from the expressions $(t_n)_m \geq \frac{t_2}{2}\left(\frac{1}{\sin^2(n)} + 1\right) - \frac{t_1}{2}\left(1 - \frac{1}{\sin^2(n)}\right)$ or $A \leq 2\frac{\sin^2(n)}{\cos(n)}$. For reactors without end-reflectors [sin (n) = 1], these conditions are always satisfied. In the case of reactors with end-reflectors [sin (n) < 1], the maximum $(t_n)_m$ sometimes does not exist. The fuel elements which are located at the hot end of the reactor have the highest temperature, and, therefore, Eqs. (8) and (8a) are not suitable for calculations; the difference $(t_2 = t_1)$ is then determined from the expression

$$t_2 - t_1 = \frac{A}{A + \cos(n)}[(t_n)_m - t_1].$$

The useful power output of an atomic power station can be defined by the following product:

$$N_n = N_T(\eta_t')(1 - \beta). \quad (9)$$

As an example, we shall consider the increase in the useful power of a reactor with a gaseous coolant if it is possible to raise the pressure in the reactor by 25%. In the reactor described in [1], the maximum temperature of the fuel element surfaces was $(t_n)_m = 500\,^\circ C$, while the temperature of carbon dioxide at the upstream end of the reactor was $t_1 = 100\,^\circ C$. The average value of the coefficient A for such reactors is equal to 2-3. If we assume that

$A_0 = 2.4$, and if we consider that the dependence of A on the coolant density obeys the $\frac{1}{\gamma^{0.2}}$ law, the coefficient A will be equal to 2.3 if the pressure in the reactor is increased by a factor of 1.25, while the $\varphi(A_0)$ and $\varphi(A)$ values corresponding to these coefficients will be equal to 0.869 and 0.855, respectively. In this case, the temperature differences $(t_2 - t_1)_0$ and $(t_2 - t_1)$ will be equal to 347.5°C and 342.5°C, respectively; the increase in the useful power of the device will be 22%.*

How will this affect the cost of the electric power produced? If we assume that $\frac{\bar{a}_1}{\bar{b}_1} = 2$, $\frac{a_2}{\bar{b}_1} = 1$, $\bar{b}_1 = 1$, and $\beta = 20\%$ in Eq. (1a), the comparative cost $\overline{C}$ of electric power will be equal to 5 units, while, after increasing the pressure, it will be 4.55.

2. The possibilities of increasing the coolant pressure in the loop are limited. If we do not resort to an increase in the pressure, the main factor hindering intensification of the gas flow through the reactor and the raising of its power level is the fact that, at a certain time, the power expended on coolant circulation, which is proportional to the third power of the coolant's velocity, will start to increase faster than the reactor's power level. There is no sense in further increasing the coolant discharge, since it would not result in an increase in the useful power of the station.

This difficulty can be surmounted by providing additional cooling of the coolant ahead of the gas compressor and by transferring the thus obtained heat surplus to the cooler. Thus, the coolant discharge and the reactor power level can be increased, while the dissipated heat surplus would correspond to the saved additional power that is expended on coolant circulation. In the end, it makes no difference whether the increase in circulation and the power level is due to the power used up by the gas circulation blowers or due to the additional heat release in the cooler.

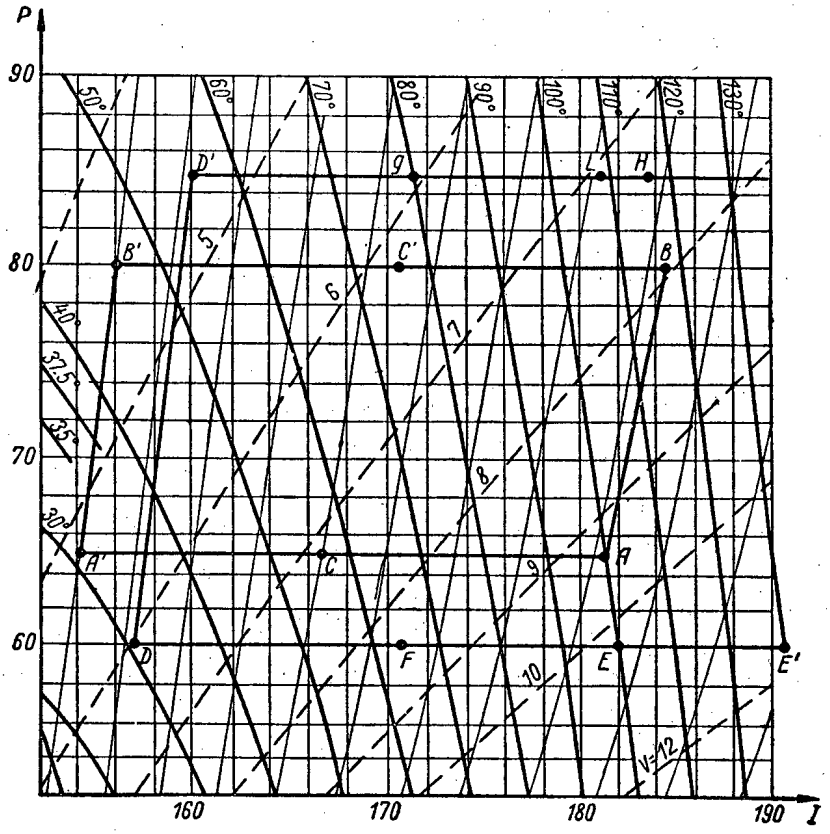

Fig. 2. IP diagram of the process of carbon-dioxide compression with and without additional cooling ahead of the compressor.

* If the temperature of the cooler is assumed to be equal to 35°C.

For instance, in operation without additional cooling, if a coolant whose initial temperature is 100°C (section AB in Fig. 2) is adiabatically compressed from 65 to 80 atm in the compressor, and if the theoretical work of compression is $\Delta i_1 \simeq 3.20$ cal/kg, then, in the case of additional cooling, the gas will be adiabatically compressed with an initial temperature of approximately 30°C * (section A'B'), and we shall have $\Delta i_2 = 1.6$ cal/kg. Due to additional cooling, the power expended on circulation will be reduced by a factor $m = \frac{\Delta i_1}{\Delta i_2} = 2.0$.**

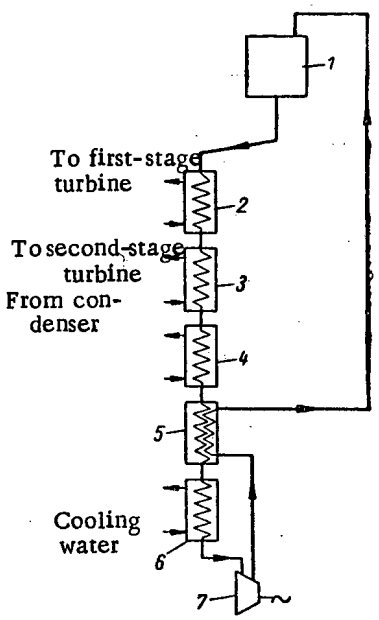

Fig. 3. Diagram of the loop with additional gas cooling ahead of the gas compressor. 1) Reactor; 2) first-stage steam generator; 3) second-stage steam generator; 4) condensate preheater; 5) regenerative heat exchanger; 6) additional gas cooler; 7) gas compressor.

If the relative consumption β was 18%, it will now be equal to 9.0%, i.e., the useful power of the reactor will increase by 9.0%. The increase in power is accompanied by additional expenditure of heat. The portion of heat that was taken away from the gas ahead of the compressor (section AC is equal to the section B'C', which corresponds to 14.6 cal/kg in Fig. 2) can be returned to the gas in the regenerative heat exchanger (Fig. 3).

A portion of the heat (section A'C corresponds to 12.3 cal/kg) is dissipated in cooler 6, which the gas must enter with a temperature higher than the temperature with which it leaves the gas compressor 7. This is necessary for creating a temperature drop in the regenerative heat exchanger 5. In the case under consideration, this difference was assumed to be equal to 10°C. At the gas compressor's outlet, the gas temperature is equal to 47°C (point B' in Fig. 2), while, at the inlet of cooler 6, the temperature is 57°C (point C in Fig. 2).

Due to the fact that, in compressing a gas with an initial temperature of 30°C, the gas compressor returns less heat to the loop than in compressing a gas with an initial temperature of 100°C (1.6 cal/kg instead of 3.2 cal/kg), 13.9 cal/kg (section C'B in Fig. 2) instead of 12.3 cal/kg must be additionally transferred to the gas in the reactor.

As a result of additional cooling, we shall obtain an electrical energy gain corresponding to $\frac{(3.20 - 1.6)}{(0.83 \cdot 0.95 \cdot 0.98)} = 2.07$ cal/kg (0.83, 0.95 and 0.98 are the polytropic, mechanical, and electrical efficiencies of the gas compressor), for which additional 13.8 cal/kg will be expended in the reactor. The efficiency of such reactor power stations is equal to 0.2, and an amount of heat equal to $\frac{2.07}{0.2} = 10.35$ cal/kg would have to be expended for this gain. Consequently, the additional useful power of the electric power station is secured at the expense of a slight deterioration of its efficiency. The question is whether this is advantageous.

After adiabatic compression along AB (see Fig. 2), the cooling gas with an initial temperature of 100°C would have a temperature of 117°C at the reactor's upstream end (the point B on the IP diagram); after adiabatic compression along A'B' and additional preheating in the regenerative heat exchanger, the gas with an initial temperature of 30°C would have a temperature of 77°C (point C') at the reactor's upstream end. If we assume that $A = 2.4$, $\varphi(A) = 0.869$ and $(t_n)_m = 500$°C, then, in the first and the second case, the temperature of the gas in the reactor would be respectively increased by

* The cooling depth is determined by the temperature that can be secured by the cooling water.

** Such a sharp reduction in the work expended on gas compression can be explained by the fact that carbon dioxide is in the state of maximum compressibility at pressures and temperatures of the order of 60 atm abs and 30°C, respectively. At 66 atm abs and 30°C, the specific volume of carbon dioxide is $v = 0.0045$ m^3/kg, while, at 66 atm abs and 100°C, the specific volume is $v = 0.0088$ m^3/kg. At a pressure of 15 atm abs, this effect is much less pronounced; thus, at 30°C, $v = 0.0263$ m^3/kg, while $v = 0.0343$ m^3/kg at 100°C. In the case of other gases (nitrogen, helium, and air), a reduction in the gas temperature ahead of the compressor does not yield such appreciable results as in the case of carbon dioxide in the region close to its critical parameters.

$$t_2 - t_1 = 0.869\,(500 - 115) = 334^\circ\,\text{C};\quad (t_2 = 449^\circ\,\text{C})$$

and

$$t_2 - t_1 = 0.869\,(500 - 77) = 368;\quad t_2 = 445^\circ\,\text{C}.$$

In this case, the thermal deficiency of the thermodynamic cycle would not be greatly different, but the reactor's heat output in the case of additional gas cooling would be increased by a factor of $\frac{368}{334} = \sim 1.1$.

The utilization factor of the reactor's heat output would deteriorate at the same rate, i.e., the fuel cost would be greater, since the electrical power output of the station would not change. If we use the same coefficient relationships $\frac{\bar{a}_1}{\bar{b}_1}$, $\frac{\bar{a}_2}{\bar{b}_2}$, and $\bar{b}_1 = 1$ as in the preceding example, the comparative cost $\bar{C}_1$ of electric power will be equal to 4.97 in the first case (without additional gas cooling ahead of the gas compressor), while, in the case of gas cooling, it will be $\bar{C}_2 = 4.5$.

However, the possibility of reducing the power expended on gas circulation can also be used in a different manner. The power expended on gas circulation can be kept at the same level as in operation without additional gas cooling, and, by utilizing this, the flow of the gaseous coolant through the reactor and the reactor's power level can be increased.* In the case of additional cooling, the gas compressor power is reduced $\underline{m}$ times, i.e., by a factor of $\frac{3.2}{1.6} = 2$. If the average density of the gaseous coolant in the loop can be kept constant, the gas velocity in the reactor's channels and the gas flow through the reactor can be increased by a factor of $\sqrt[3]{m} = \sqrt[3]{2} = 1.26$ while the hydraulic resistance of the circulation channel can be increased by a factor of $\sqrt[3]{m^2} = \sqrt[3]{2^2} = 1.59$. In the previous example, the latter was equal to 15 atm; in this case, it would be 25 atm, while the gas in the gas compressor would have to be compressed from 60 atm to 85 atm (the adiabatic curve DD' in Fig. 2) by raising its temperature in the gas compressor from 30 to 55°C (to the point D').

If, as before, we assume that the gas in the condensate preheater 4 (see Fig. 3) is cooled to 100°C, then, in the regenerative preheater 5, the gas will be cooled along the isobar EF (see Fig. 2) from 100 to 65°C and from 65 to 30°C along the isobar FD in cooler 4. The heat corresponding to the section FD = 13.7 cal/kg is dissipated in the cooler; the heat corresponding to the section EF = D' g = 11.3 cal/kg is returned to the gas in the regenerative heat exchanger, where the gas is heated to 80°C, while the heat corresponding to the section gH = 12 cal/kg must be additionally transferred to the gas in the reactor.

Further, if we neglect the insignificant changes in the coefficients A = 2.4 and $\varphi(A) = 0.869$, which are connected with changes in the gas velocity in the loop in transition to the new circulation conditions (the A coefficient is inversely proportional to velocity with an exponent equal to 0.2), the increase in the gas temperature, $t_2 - t_1$, due to preheating, which was equal to 334°C under the initial operating conditions (t_2 = 449°C), will be equal to 365°C (t_2 = 445°C) under the new conditions. Consequently, the specific heat consumption in the reactor will be increased by a factor of $\frac{365}{334} = 1.095$. The heat utilization coefficient will deteriorate in the same ratio if we do not take into account the slight deterioration of the thermal efficiency of the thermodynamic cycle due to the drop of the gas temperature from 449 to 445°C, which will be less than 0.5%. As a result, the electrical power output of the reactor will be increased by a factor of 1.26, while the heat utilization coefficient will be reduced by a factor of 1.095. Considering that $\beta = 0.18/1.26 = 0.143$, the comparative cost of electrical energy produced will be equal to 4.3 under the former assumptions, i.e., the corresponding reduction in the electric power cost will be 13.5%. The useful power output of the station will be in this case increased by a factor of 1.32.

The layout of a circulation loop with additional gas cooling ahead of the gas compressor makes it possible to use an additional procedure for increasing the power output of the station and for lowering the electric power cost. The energy release along the reactor's radius is not uniform.

* A different method can also be used. The surface area of the fuel elements can be developed and the coolant temperature at the reactor's downstream end can be increased, i.e., the thermal efficiency of the thermodynamic cycle can be improved.

Utilizing the nonuniformity of heat release in the reactor, the power level can be raised by supplying to the reactor's central zone gas which is heated to a lesser degree than the gas supplied to the peripheral zone. In this, the average gas temperatures at the upstream and downstream ends of the reactor must remain unchanged, and the gas flow must be increased by using peripheral reactor channels.* In order to realize this, the reactor cooling scheme must be somewhat modified (Fig. 4). Downstream from the second-stage steam generators, the cooling gas should be divided into two streams. One stream (the smaller one) should be directed to the condensate preheater 4, and the other should be directed to the regenerative heat exchanger 5. After it passes through the gas compressor 7, a portion of the cold gas should be directed to the central zone of the reactor 1, while the other portion should be preheated in heat exchanger 5 and then directed to the peripheral zone. Calculations show that, by using this method, the gas circulation can be increased and the electrical and the useful power outputs of the reactor can be augmented by 6-7%.

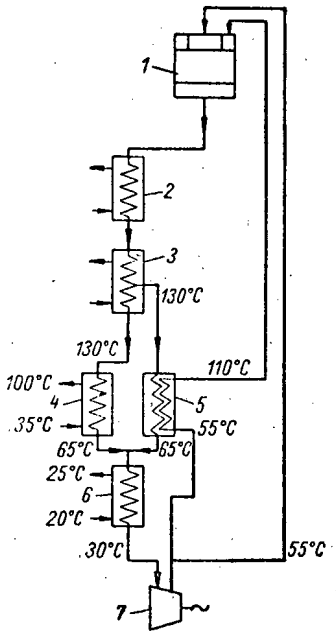

Fig. 4. Diagram of the circuit with additional gas cooling ahead of the gas compressor, where cold gas is supplied to the reactor's central zone. 1) Reactor; 2) first-stage steam generator; 3) second-stage steam generator; 4) condensate preheater; 5) regenerative heat exchanger; 6) additional gas cooler; 7) gas compressor.

As a result of all these measures, the electrical and the useful power outputs of the reactor would increase by factors equal to 1.6 and 1.7, respectively, while the cost of the electric power produced would be reduced to 15-25%. A further increase in the initial pressure of the coolant ahead of the gas compressor (for instance, from 60 to 80 atm) with simultaneous additional cooling would result in an even sharper reduction in the power expended on gas compression.

The cooling of the coolant ahead of the gas compressors would require that the heating surface of the tail-end parts of steam generators be increased three- to fivefold and that of the entire steam generator by a factor of 1.5, which constitutes a disadvantage of this method.

3. If the fuel elements of the reactor consist of rods, the outside rods screen the inside rods, which results in a "heaping up" of the neutron density toward the center of the channel. Due to this, the existing possibilities of removing heat from the reactor are fully utilized only in those rods of the reactor's central channel which are most heavily loaded. All the other elements in the reactor are underloaded, and this sharply reduces, sometimes by a factor larger than 2, its thermal and electrical power outputs. However, by redistributing within allowable limits the cross-sectional area of the coolant flow and the coolant velocity in the channels, by enlarging the channels at places of intensive heat exchange, and by lowering the coolant temperature at the entrance to the central channel and raising it at the entrance to the peripheral channels, we come close to a reactor which is "ideal" with respect to power generation, i.e., a reactor with uniform intensity of heat release along its radius and over the channel cross section, where the channels are chosen with respect to the optimum possibilities of heat removal under conditions where the reactor is utilized with the most advantageous power parameters.

The electrical power of the reactor can be defined as the product of the thermal power N_{cc} of its central channel, the number of channels n, the factor η_r of power equalization over the reactor's surface, and the power plant efficiency η_t':

$$N_e = N_{cc} n \eta_r (\eta_t'). \tag{10}$$

For instance, if it is possible to increase the central channel's power by a factor of $\frac{1}{\eta_r}$ while preserving the initial optimum parameters of the power plant (its thermal efficiency and the amount of power expended on coolant

* Such equalization was used in the French power reactors with gaseous coolants.

circulation) without exceeding the surface temperature of the fuel elements, then the problem of equalizing the energy release in the reactor can be completely solved by heat engineering methods, i.e., by means of thermal equalization.

The heat release in fuel elements can be equalized in a similar manner.

The redistribution of the cross section of the coolant flow and the related redistribution of the coolant velocities in the fuel elements as well as in the reactor's channels in dependence on the heat released constitute an efficient method of thermal equalization. In this case, the more heavily-loaded reactor channels or portions of the fuel elements will be cooled by a larger amount of coolant, but the coolant will be heated to a lesser degree, and vice versa. In this, the average coolant temperature at the reactor's downstream end may be left unchanged, while the coolant flow through the reactor and its thermal and electrical power outputs will increase.* Two cases are possible in such thermal equalization:

1) The case where the coolant flow velocity in the channels can be varied by providing channels with variable passage cross sections while keeping the hydraulic resistance of the reactor (the coolant head at the reactor's upstream end) at a constant level, i.e., by maintaining $\Delta p = \text{const}$. In this, the flow cross sections $\underline{f}$ and the coolant velocity W will be variable. This case pertains to reactors with gaseous coolants;

2) the case where the coolant velocity is limited (for instance, due to water cavitation in reactors with aqueous coolants). The constancy of the coolant velocity in all reactor channels, i.e., $W = \text{const}$, can be used as the necessary condition in calculations for the profiling of the coolant flow in such reactors. In this case, the coolant flow cross sections will be used in the most efficient manner. In this, the central instead of the peripheral channels will be throttled by means of gate valves. This is feasible, since the portion of the energy expended on circulation is small in reactors with liquid coolants.

The calculation of thermal equalization for a reactor can be reduced to the selection of coolant flow cross sections in dependence of the ratio $\frac{\mu^*}{\mu_0}$ of the heat outputs of two fuel assembly rods or of two reactor channels. For large Reynolds numbers and a uniform distribution of spacing devices along the fuel element (the resistance factor $\xi = \frac{a}{Re^n} z$ also takes into account the local resistances), the condition $\Delta p = \text{const}$ can be written in the following form: **

$$\left[\frac{(d_e)_0}{(d_e)_1}\right]^{(1+n)} \left(\frac{W_1}{W_0}\right)^{2-n} = 1. \tag{11}$$

If we assume that ϵ_1 is the surface portion occupied by the rods in the fuel assembly [1], $\underline{f}$ is the flow cross section per single rod, d_1 is the rod diameter and d_e is the process channel's equivalent diameter which is reduced to a single rod, then

$$f = \left(\frac{1-\varepsilon_1}{\varepsilon_1}\right)\frac{\pi d_1^2}{4} \text{ and } d_e = \left(\frac{1-\varepsilon_1}{\varepsilon_1}\right) d_1. \tag{12}$$

* Such equalization was used, for instance, in the design of a heavy-water reactor with gas cooling [1]. Such equalization somewhat improves the heat release curve along the reactor's radius, since the amount of absorbing structural materials decreases and the amount of moderator material per single cell of the process channel increases if the channel diameter decreases from the center to the periphery.

** This can be done if we do not take into account the effect of the coolant's heating in the reactor channels and if neglect the dynamic head, which is permissible in the small range of changes in ϵ under consideration. Actually, condition (11) can be written as

$$\left[\frac{\frac{l}{(d_e)_1}\frac{a}{Re_1^n}z+1}{\frac{l}{(d_e)_0}\frac{a}{Re_0^n}z+1}\right]\frac{W_1^2}{W_0^2} = 1.$$

For two rods with different porosities $(1 - \epsilon)$, i.e., with different passage cross sections per single rod, the $\frac{\mu_1}{\mu_0}$ ratio can be written thus:

$$\left(\frac{\mu'}{\mu_0}\right) = \frac{g_1}{g_0} \frac{(t_2 - t_1)}{[(t_2)_0 - (t_1)_0]}. \tag{13}$$

If we consider Eqs. (8) and (12) and take into account that

$$\frac{A_1}{A_0} = \frac{\alpha_1 f_0 W_0}{\alpha_0 f_1 W_1} = \left(\frac{1-\varepsilon_0}{\varepsilon_0} \frac{\varepsilon_1}{1-\varepsilon_1}\right)^{\frac{3m+2-n}{2-n}}$$

(since $\frac{\alpha_1}{\alpha_0} = \left(\frac{W_1}{W_0}\right)^{1-m} \left[\frac{(d_e)_0}{(d_e)_1}\right]^m$), we shall obtain the ratio of power outputs for two rods by using expression (13):

$$\left(\frac{\mu_1}{\mu_0}\right) = \left(\frac{1-\varepsilon_0}{\varepsilon_0} \cdot \frac{\varepsilon_1}{1-\varepsilon_1}\right)^{\frac{2(3m-n)+1}{2-n}} \times \frac{\left(\sqrt{1+\frac{4}{A_1^2}} - 1\right)}{\left(\sqrt{1+\frac{4}{A_0^2}} - 1\right)}. \tag{14}$$

This equation can be used for profiling a reactor channel with rod fuel elements as well as for determining the average reactor channel porosities if variable-diameter channels are provided in profiling.

The equations for determining the porosities under conditions where W = const can be derived in a similar manner; they are written in the following form:

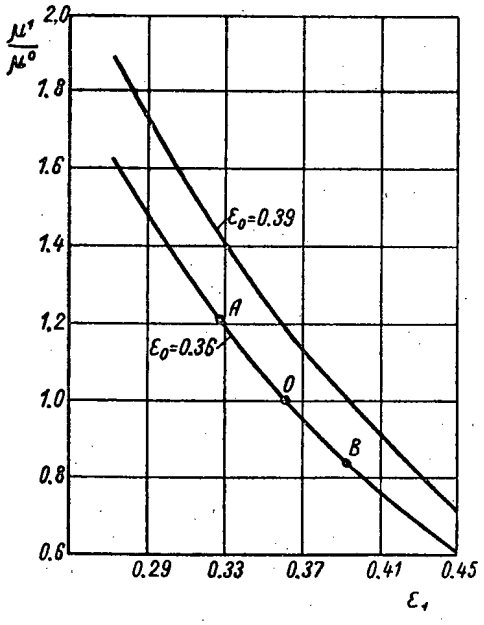

Fig. 5. Curves for calculating the thermal equalization in the reactor under conditions where Δp = const for $A_0 = 2.3$, m = 0.2 and n = 0.

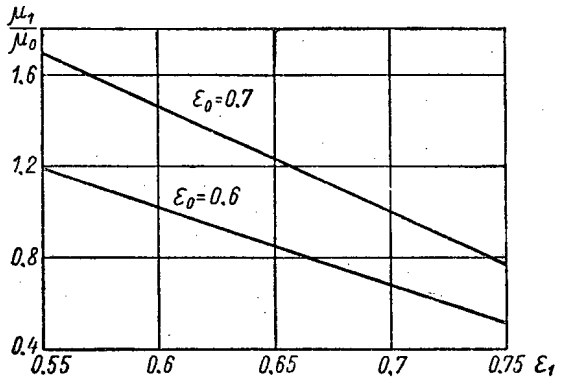

Fig. 6. Curves for calculating the reactor's thermal equalization under conditions where W = const for $A_0 = 5$, m = 0.2, and n = 0.

$$\left.\begin{aligned}\left(\frac{\mu'}{\mu_0}\right)&=\left(\frac{1-\varepsilon_0}{\varepsilon_0}\cdot\frac{\varepsilon_1}{1-\varepsilon_1}\right)^{1+2m}\\&\times\frac{\left(\sqrt{1+\frac{4}{A_1^2}}-1\right)}{\left(\sqrt{1+\frac{4}{A_0^2}}-1\right)},\\A_1&=A_0\left(\frac{1-\varepsilon_0}{\varepsilon_0}\cdot\frac{\varepsilon_1}{1-\varepsilon_1}\right)^{1+m}\end{aligned}\right\}\qquad(15)$$

Figures 5 and 6 show the curves for calculating the reactor's thermal equalization and for profiling the fuel assemblies; these curves were calculated by using Eq. (14) for Δp = const and Eq. (15) for W = const.*

The mixing of the coolant in the channels [1] of a reactor with a gaseous coolant is limited. In the absence of mixing, the reactor's power output will be considerably reduced if profiling is not applied. Profiling prevents this reduction and, in certain cases, it results in almost complete equalization. The possibility of complete equalization results from the fact that the range in which the porosity varies (the range of changes in the filling factor ϵ – the points A and B in Fig. 5) is not so large; within these limits, the curve AB $\left[\varepsilon_1=f\left(\frac{\mu'}{\mu_0}\right)\right]$ is sufficiently close to a straight line, i.e., the condition $\frac{d(\mu'/\mu_0)}{d\varepsilon}=\text{const}$ is satisfied. Hence, it follows that the redistribution of rods over the cross section of channels can be performed in such a manner that the equalization factor is equal to unity, i.e., the screening can be neglected in calculating the fuel assembly. In this case, the following condition will apply. The free cross-sectional area for the passage of gas at the periphery increases in the amount by which it decreases at the center.

In profiling the reactor and its process channels, it is necessary to take into account the possibility that the porosity will change from the point of view of the reactor's physics. For instance, the profiling of the fuel assembly in a reactor [1] does not cause considerable changes in the curve for the neutron density in the assembly. Simultaneous profiling of the reactor and of its process channels is a very efficient method for raising the reactor power level, although, like any thermal equalization, in comparison with physical equalization, it has a disadvantage which consists of the fact that, while increasing the reactor power level, it does not eliminate the nonuniformity of the burn-up of fuel material, and it intensifies the thermal stresses in the central channels.

The application of these methods will make it possible considerably to reduce the cost of the electric power supplied by atomic power stations which are equipped with gaseous-coolant reactors.

LITERATURE CITED

1. P. I. Khristenko, et al., Transactions of the Second International Conference on the Peaceful Uses of Atomic Energy (Geneva, 1958). Reports by Soviet Scientists [in Russian] Vol. 3 (Moscow, Atomizdat, 1959), p. 655.

All abbreviations of periodicals in the above bibliography are letter-by-letter transliterations of the abbreviations as given in the original Russian journal. *Some or all of this periodical literature may well be available in English translation.* A complete list of the cover-to-cover English translations appears at the back of this issue.

---

* The curves for determining the average porosities of reactor channels with a constant diameter can be obtained by multiplying the ordinates of the curves in Figs. 5 and 6 by $\frac{\epsilon_1}{\epsilon_0}$. Investigation of these curves shows that, for Δp = const and W = const, the reactor's heat output is at a maximum for a certain porosity value.

THE CRITICAL HEAT FLUX FOR BOILING WATER IN TUBES

Z. L. Miropol'skii and M. E. Shitsman

Translated from Atomnaya Énergiya Vol. 11, No. 6, pp. 515-521,
December, 1961
Original article submitted April 8, 1961

An analysis of the experimental results obtained by various authors on critical heat flux is carried out by using nondimensional criteria. Recommendations are given for the numerical methods of determining values of the critical heat flux in the case of a steam-water mixture, underheated to saturation in tubes and in ring-shaped and plane slotted channels.

During recent years, both in the USSR and in foreign countries, a large amount of experimental data has been obtained, which is sufficient to clarify the influence on the boiling crisis of various factors: the specific heat and velocity of the medium, the geometric parameters, etc. It would therefore be useful to generalize the available results and to develop a method of calculating q_{cr}, taking into account the factors that are important in the process under consideration.

In [1], for the case of the boiling crisis in a liquid in forced motion in channels, when gravitational forces can be neglected, the following system of criteria was proposed:

$$\frac{q_{cr} l_0}{a' r \gamma''} = f\left(\frac{W_0 l_0}{\nu'}, \frac{W_0 l_0}{a'}, \frac{r}{c_p' T_s}, \frac{W_0''}{W_0'}, \frac{\gamma''}{\gamma'}\right). \quad (1)$$

In the application of this system for obtaining general theories from the available experimental results, we must keep in mind the following considerations:

1. The choice of a characteristic length l_0. An analysis of the available experimental data shows that the dimensions of the cross section of the channel do not have a great influence on q_{cr} if the internal diameter of the tube is greater than 4 mm [2], if the radial clearance is greater than 1-2 mm [3, 4], and if the width of the plane slot is greater than 1.3 mm [5-7].

The influence of the length of the heated portion of the channel on q_{cr} is of importance only up to a certain value of the ratio $\frac{l}{d_{eq}}$, which becomes smaller the greater the values of p, W_g and x.

For example, the comparison in Fig. 1 of results obtained in experiments with uniformly-heated tubes and annular channels of various lengths shows that, under these conditions, the influence of the heated length of the channels on q_{cr} is only noticeable for $l/d_{eq} < 100$.

For larger values of p and W_g, the influence of the length on q_{cr} ceases for still smaller values of l/d_{eq}. We may therefore assume that, for parameters that are important in practice for technical establishments, the limiting value of l/d_{eq} is about 100. Thus, if we exclude from consideration the experimental results obtained in experiments with channels of small dimensions ($d < 4$ mm, $\delta < 1.3$ mm, $l/d_{eq} < 100$), then the geometrical dimensions of the channel can be omitted from the parameters determining the behavior of the system (1).

As a characteristic linear dimension l_0 for boiling water in large volumes, we take the quantity $\sqrt{\frac{\sigma}{\gamma' - \gamma''}}$, proportional to the break-away diameter of steam bubbles when the latter are acted upon only by gravitational and surface-tension forces. In forced motion of a boiling liquid in channels, the break-away of a bubble from the wall occurs as the result of the interaction between the dynamic thrust of the medium and the surface-tension forces. Under these conditions, the characteristic linear dimension l_0 is a function of the surface tension σ and those same variables occurring in the right-hand side of the system (1).

2. From a consideration of experimental results obtained for a boiling liquid in a large volume, it follows that the effect of the heat conductivity λ' of the liquid on q_{cr} can be neglected [1, 9]. Thus, in the system (1), the criterion $\frac{W_0 l_0}{a'}$ can be eliminated when the criterion $\frac{W_0 l_0}{\nu'}$ is present.

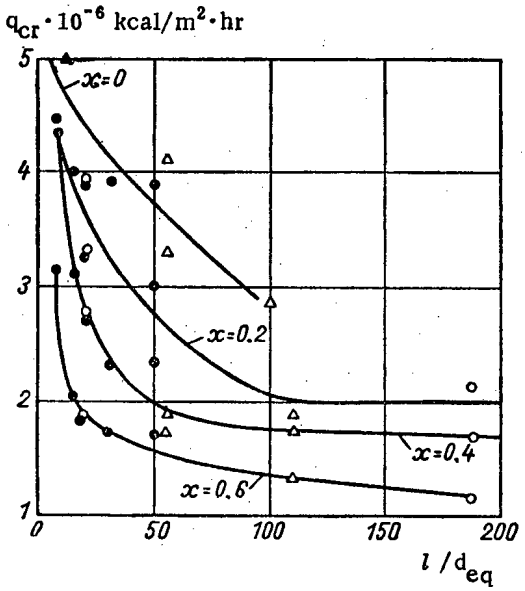

Fig. 1. The influence of the relative length of a channel on the critical heat flux for p = 100 atm, W_g = 800-850 kg/m²·sec (non-pulsating regime). Cylindrical tubes: ●) results from [13]; ○) results from [11]. Annular channel: △) results of Miropol'skii, Shitsman, Mostinskii, and Faktorovich; ▲) results from [14].

3. For the parameters characterizing the velocity and phase state of the medium, it is convenient to take the rate of mass transfer W_g (since it does not vary with the length of the channel for constant cross section), and the difference between the heat content of the medium and water at the saturation line $\Delta i = i - i'$.

It follows from this that the system (1) in dimensional form becomes $q_{cr} = f(W_g;\ \gamma';\ \gamma'';\ \mu';\ \sigma;\ r;\ c_p';\ T_s;\ \Delta i)$, and so, from the methods of dimensional analysis, we obtain the following system of criteria:

$$\frac{q_{cr}\mu'}{\sigma\gamma' r} = f\left(\frac{W_g\mu'}{\sigma\gamma'},\ \frac{r}{c_p' T_s},\ \frac{\gamma'}{\gamma''},\ \frac{\Delta i}{r}\right). \qquad (2)$$

The system (2) is a special case of the general relation obtained in [8] by using the hydrodynamic theory of the boiling crisis. Thus, for example, we have

$$\frac{W_g\mu'}{\sigma\gamma'} = \left(\frac{F_r^*}{A_r^*}\right),$$

where

$$F_r^* = \frac{W_0^2}{g}\sqrt{\frac{\gamma'-\gamma''}{\sigma}}$$

and $A_r^* = \frac{g}{\nu^2}\left(\frac{\sigma}{\gamma'-\gamma''}\right)^{3/2}\left(1-\frac{\gamma''}{\gamma'}\right)^2$.

Experimental Results for Channels of Various Shapes

Channel shape	Cross section dimensions, mm	$\frac{l}{d_{eq}}$	p, atm	W_g, kg/m²·sec	x	References
Tube	$d=8$	100—220	100—200	1000—5000	−0.5+0.25	[2]
»	$d=6$	106	35—141	1300—10000	−0.4+0.5	[10]
»	$d=5,1$	80	35—52	2000—4000	+0.3+0.7	[7]
»	$d=8$	188	100	400—1300	0+0.8	[11]
Plane slot	1.27×25.4	123	42—141	600—3000	+0.2+0.7	[7]
» »	1.5×25.4	242	131—141	900—1400	+0.3+0.7	[7]
» »	2.47×25.4	70—150	42—141	1000—4000	+0.2+0.8	[7]
» »	2.47×25.4	140	141	600—4000	0+0.7	[5]
» »	1.5×25.4	100—230	141	400—2700	−0.15+0.7	[6]
Annular channel*	$d=6/10$	110	20—100	200—5000	−0.1+0.8	—

* Experiments with the uniform heating of both tubes, forming an annular channel, were carried out by the authors, I. L. Mostinskii and L. E. Faktorovich.

The complex $\frac{q_{cr}\mu'}{\sigma\gamma' r}$ is the product of the criterion discussed above and the known criterion $\frac{q_{cr}}{rW_g}$, where the latter is the ratio of the mass rate of evaporation (perpendicular to the wall) to the axial flow velocity.

The criterion $\frac{r}{c'_p T_s}$ can be considered as a measure of thermodynamic similarity. It takes into account the factors that are not reflected in the hydrodynamic criteria.

The criterion $\frac{\Delta i}{r} = x$ refers to the enthalpy of the flow. In the interval of values between 0 and 1, it is numerically equal to the vapor content by weight. For water underheated to the saturation temperature we have $x < 0$, while for superheated steam $x > 1$. Since, in the case of uniform heating, the boiling crisis usually occurs at the outlet part of a channel, we will take the value of $\underline{x}$ for the channel outlet in all the calculations that follow.

In calculating the concrete form of the relation between the criteria of system (2), we use the results of experiments carried out with channels of various shapes (see the table). The limits of the ratios of the geometrical dimensions of the channels, described in 1, are also taken into account.

In comparing experimental results obtained by different authors, it is necessary to take into consideration the fact that, with a definite range of values of the pressure, velocity, and heat content of the medium, the values of q_{cr} can be strongly dependent on conditions that determine the general circulation of the flow. Here two different types of regime must be distinguished [12, 13]: a) regimes with free development of pulsations (pulsating regimes) in the presence of a compressible medium at points in the flow located between the heated section and a choking element or an element for stimulating the circulation; b) regimes with restricted development of pulsations (non-pulsating regimes), with an incompressible medium at the points in the flow referred to above.

The analysis of experimental results has shown that the difference between these regimes effects the value of q_{cr} only when $K_W = \frac{W_0 \mu'}{\sigma \gamma'} \times \left(\frac{\gamma'}{\gamma''}\right)^{0.2} < 2 \cdot 10^{-2}$.

The concrete form of the relation between the criteria of the system (2) can be written in the form of the following equations:

1. Non-pulsating regime, $x \geq 0$.

The motion of a water-steam mixture in tubes and annular channels:

$$\frac{q_{cr}}{\sigma \gamma' r} = 0.174 \left(\frac{c'_p T_s}{r}\right)^{0.8} K_W^{0.4} (1 - x)^n, \tag{3}$$

where $n = 0.8$ for $K_W < 1.6 \cdot 10^{-2}$;
$n = 50 K_W$, for $1.6 \cdot 10^{-2} < K_W < 6 \cdot 10^{-2}$;
$n = 3$, for $K_W > 6 \cdot 10^{-2}$.

The motion of the water-steam mixture in plane slot channels

$$\frac{q_{cr} \mu'}{\sigma \gamma' r} = 0.224 \left(\frac{c'_p T_s}{r}\right)^{0.8} K_W^{0.4} (1 - x)^n, \tag{4}$$

where $n = 33.3 K_W$, for $2 \cdot 10^{-2} < K_W < 9 \cdot 10^{-2}$;
$n = 3$, for $K_W > 9 \cdot 10^{-2}$.

2. The pulsating regime (for $K_W < 2 \cdot 10^{-2}$ with a compressible medium in the specially included elements of the path of the flow); $x \geq 0$. Motion of a water-steam mixture in tubes and annular channels:

$$\frac{q_{cr} \mu'}{\sigma \gamma' r} = 0.7 \left(\frac{c'_p T_s}{r}\right)^{0.8} K_W (1 - x)(1 + 4x). \tag{5}$$

3. Non-pulsating regimes; $x < 0$.

The experimental results obtained for the motion of water, underheated to the saturation temperature in tubes and annular channels, agree well with the results of the hydrodynamic theory of the boiling crisis, in that, to a first approximation, q_{cr} for $x < 0$ is a linear function of $x = \frac{\Delta i}{r}$. In the case under consideration, it was found that

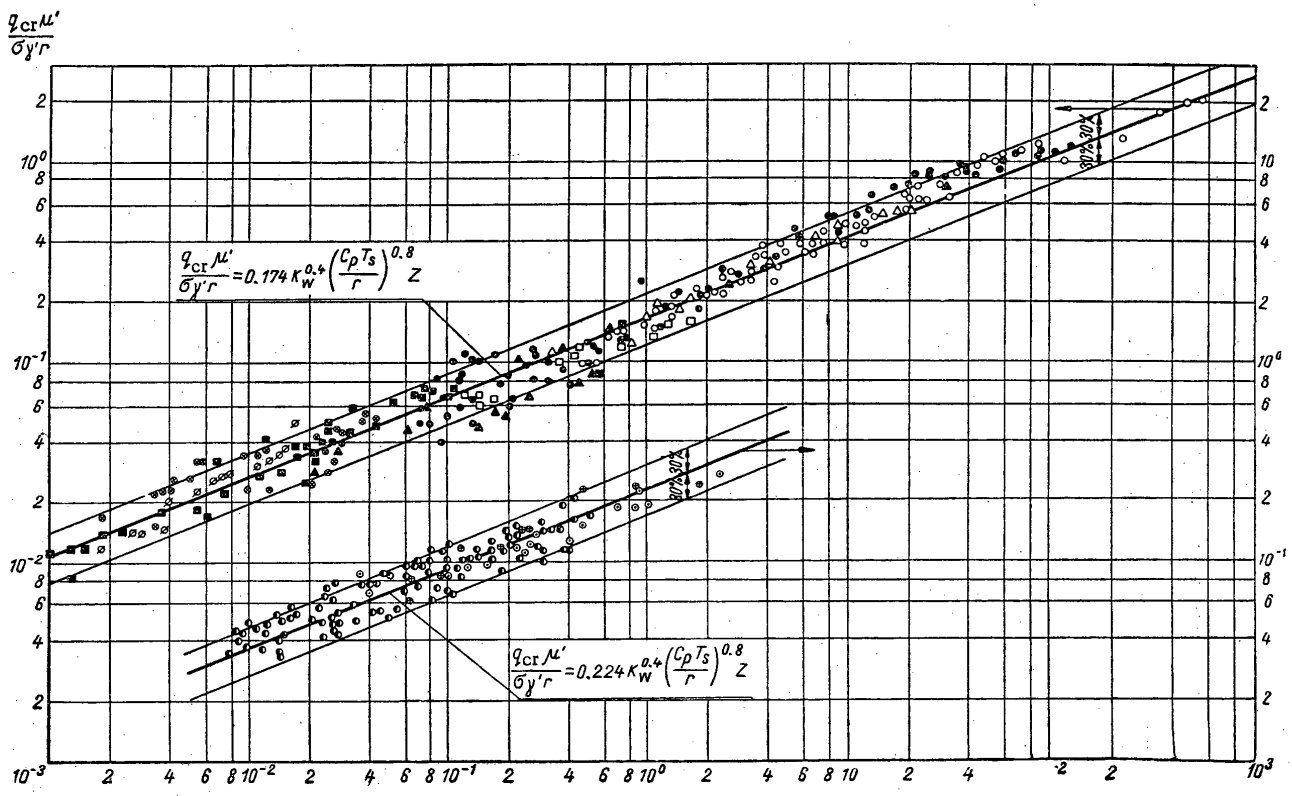

Fig. 2. The dependence of q_{cr} on W_g and $\underline{x}$ in nondimensional coordinates (non-pulsating regimes).

	$x>0$	$x<0$	
Tubes	●	○	[2]
	▲	△	[10]
	⊕		[11]
	⌀		[7]

Annular channels: ■ □ results of Miropol'skii, Shitsman, Mostinskii and Faktorovich.

Plane slot channel ◐ [7], ⊕ [6], ⊙ [5]

for $x>0$ $z=(1-x)^n$.

for $x<0$ $z=1-0.45\,x\left(\frac{\gamma'}{\gamma''}\right)^{0.85}$

$$\frac{q_{cr}\mu'}{\sigma\gamma' r} = 0.174\left(\frac{c'_p T_s}{r}\right)^{0.8} K_W^{0.4} \times \left[1 - 0.45x\left(\frac{\gamma'}{\gamma''}\right)^{0.85}\right]. \quad (6)$$

We show, in Fig. 2 and Fig. 3, the results of an analysis of the experimental results corresponding to Eqs. (3), (4), (5) and (6). A satisfactory agreement was established between the experimental and the calculated results; about 90% of the experimental results agreed with the calculated results to within ± 30%, and about 80% agreed to within ± 20%.

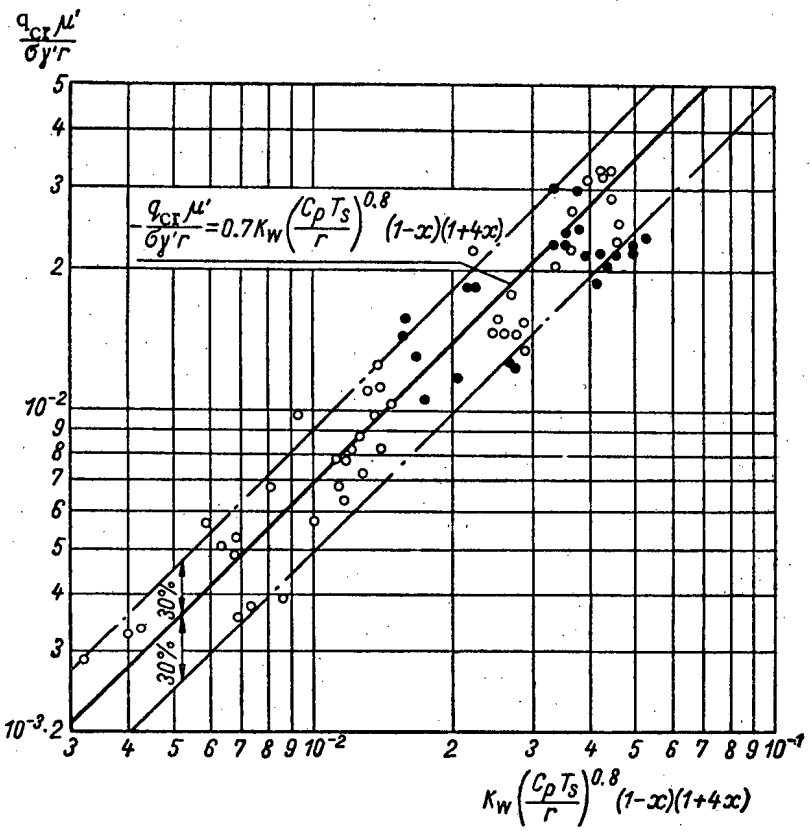

Fig. 3. The dependence of q_{cr} on W_g and x in nondimensional coordinates (pulsating regime). Cylindrical tubes: ●) data from [11]. Annular channels: ○) results of Miropol'skii, Shitsman, Mostinskii and Faktorovich.

In applying the Eqs. (3), (4) and (5), it should be noted that as the steam content, the pressure, and the mass-transfer rate increase, the temperature jump occurring at the transition from bubbling-boiling to full-boiling becomes smaller, and the operation of steam-generating channels becomes safe under worsening heat-transfer conditions. The heat flux obtainable in this case exceeds the values of q_{cr} calculated from the formulas (3), (4) and (5). In the present article, we have assumed that for $q = q_{cr}$, the wall temperatures exceeded t_s by more than 100-150° C. For mass rate of flow in steam-generating units in contemporary steam-generating plants, we may, for a start, assume that the Eqs. (3) to (5) can be applied within the following limits of steam content relative to pressure:

p = 20 atm – up to 0.9;
p = 100 atm – up to 0.6;
p = 180 atm – up to 0.4;
p = 200 atm – up to 0.25.

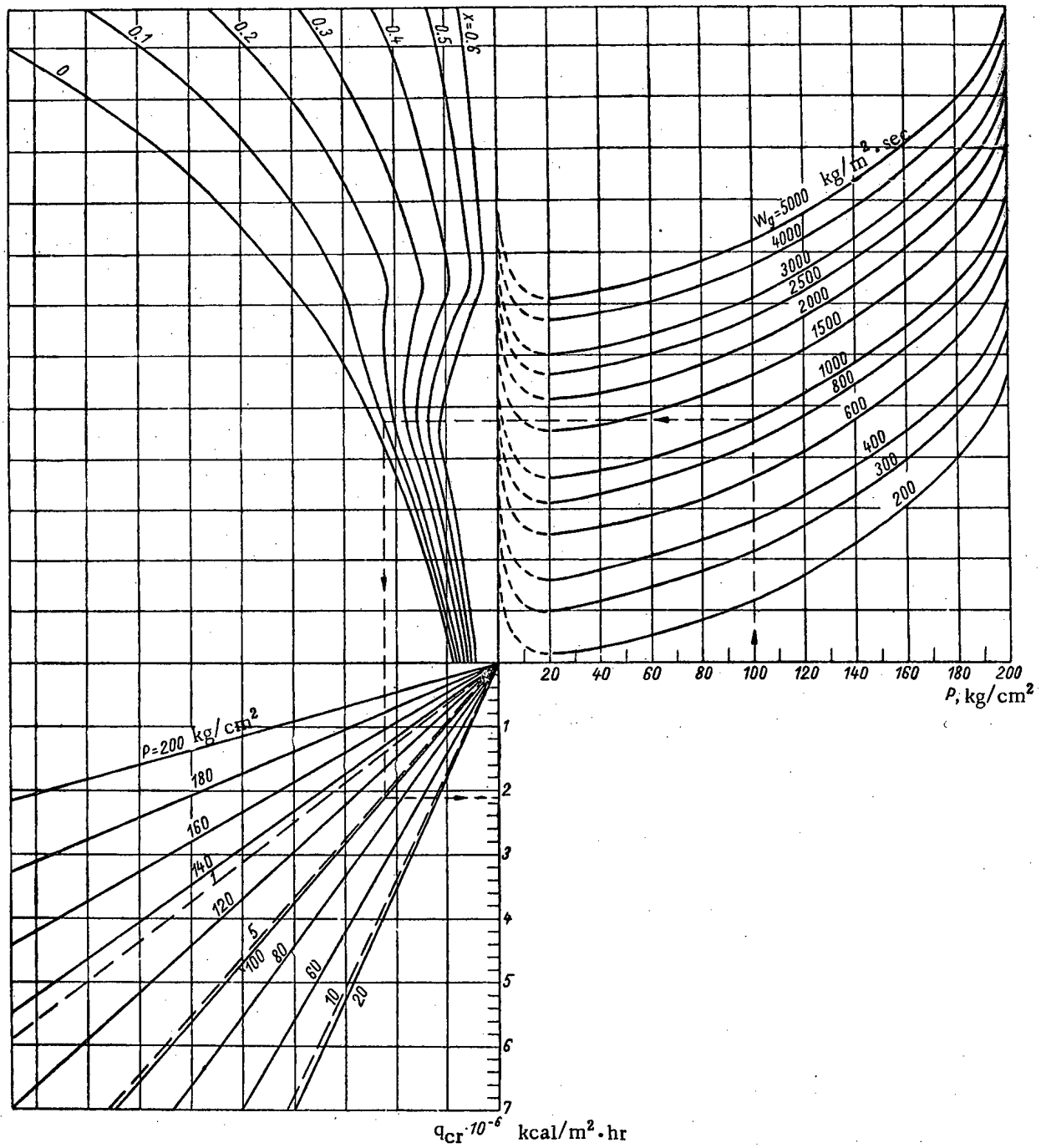

Fig. 4. Nomogram for the determination of q_{cr} in tubes and annular channels (non-pulsating regime; $\frac{l}{d_{eq}} > 100$).

The application of Eq. (6) for high rates of flow and large negative values of $\underline{x}$ is also associated with definite limits, obtained from the following considerations. For water moving in a tube and underheated to the saturation temperature, surface boiling can arise only after the temperature of the wall has reached the value t_s. At this point, the corresponding heat flux can be determined from the equation

$$q_s = 0.023 \frac{\lambda}{d} Pr^{0.4} \left(\frac{W_0 d}{\mu g} \right)^{0.8} (t_s - t_f). \qquad (7)$$

Since the boiling crisis cannot occur for $t_w < t_s$, the Eq. (6) can be used only when the inequality $q_{cr} > q_s$ is satisfied. Calculations show that the limiting values of W_g that are obtained are significantly greater than the mass rates of flow used in contemporary steam-generating plants.

To simplify the calculations, we have included Fig. 4, a nomogram for the determination of q_{cr} in tubes and annular channels ($l / d_{eq} > 100$) from the values of $\underline{p}$, W_g, and $\underline{x}$ for non-pulsating regimes and values of $x \geq 0$.

NOTATION

The prime ' refers to the liquid, and the double prime " to steam at saturation;

γ) specific weight, kg/m^3;
c_p) specific heat, kcal/kg °C;
ν) kinematic viscosity, m^2/sec;
μ) dynamic viscosity, kg · sec/m^2;
σ) surface tension, kg/m;
r) heat of vaporization, kcal/kg;
λ) heat-conduction coefficient, kcal/m · hr °C;
a) temperature-transfer coefficient, m^2/sec;
g) acceleration of gravity, m/sec^2;
t_s, T_s) saturation temperature, °C; °K;
t_f) flow temperature °C;
t_w) wall temperature °C;
i) heat content of the medium, kcal/kg;
Δi) $i - i'$, kcal/kg;
$x = \frac{\Delta i}{r}$, rate of enthalpy;
W'_0, W''_0) reduced velocities, m/sec;
W_g) mass rate of flow, kg/m^2 · sec;
q) specific heat flux, kcal/m^2 · hr;
q_{cr}) specific critical heat flux, kcal/m^2 · hr;
l_0) characteristic linear parameter, m;
δ) slot width, mm.

LITERATURE CITED

1. L. S. Sterman, ZhTF, 23, 2, 341 (1953).
2. V. I. Subbotin, B. P. Zenkevich, O. N. Sudnitsyn, A. A. Ivashkevich, N. D. Sergeev, and O. L. Peskov, Collection - An investigation of heat transfer to steam, in water boiling in pipes at high pressure [in Russian], (Moscow, Atomizdat, 1958) pp. 95, 120.
3. V. S. Chirkin and V. P. Yukin, ZhTF 7, 1542 (1956).
4. N. L. Kofengauz and I. D. Bocharov, "Teploénergetika," 3, 76 (1959).
5. H. Jacket, J. Rourty and J. Zerbe, Trans. ASME 80, 2, 391 (1958).
6. D. Bell, Nuclear Science and Eng. 7, 3, 245 (1960).
7. A. Cicchitti, M. Silvestri, G. Soldaini and R. Zavattaralli, Energia Nucleare (Milano) 6, 10, 407 (1959).
8. S. S. Kutateladze, The Elements of Heat-Transfer Theory [in Russian] (Moscow, Mashgiz, 1957).
9. S. S. Kutateladze and M. A. Styrikovich, The Hydraulics of Gas-Liquid Systems [in Russian] (Moscow, Gosénergoizdat, 1958).

10. H. Buchberg, Studies in boiling heat transfer,Final Report 1951. U. S. Atomic Energy Commission.
11. Z. L. Miropol'skii, M. E. Shitsman, A. A. Stavrovskii and I. L. Mostinskii, "Teploenergetika," 1, 80 (1959).
12. M. A. Styrikovich, Z. L. Miropol'skii, M. E. Shitsman, I. L. Mostinskii, A. A. Stavrovskii and L. E. Faktorovich, "Teploénergetika," 5, 81 (1960).
13. V. E. Doroshuk and F. P. Frid, "Teploénergetika," 9, 74 (1959).
14. I. T. Alad'ev and L. D. Dodonov, In the Collection "Convective and Radiative Heat-Exchange," [in Russian] (Moscow, Izd-vo AN SSSR, 1960) p. 65.

All abbreviations of periodicals in the above bibliography are letter-by-letter transliterations of the abbreviations as given in the original Russian journal. *Some or all of this periodical literature may well be available in English translation.* A complete list of the cover-to-cover English translations appears at the back of this issue.

THE USE OF RESONANCE DETECTORS FOR THE INVESTIGATION OF NEUTRON SPECTRA IN FAST-NEUTRON REACTORS

V. I. Golubev, V. I. Ivanov, M. N. Nikolaev,

and G. N. Smirenkin

Translated from Atomnaya Énergiya, Vol. 11, No. 6, pp. 522-527,
December, 1961
Original article submitted April 17, 1961

The possibility of the investigation of the low energy portion of the neutron spectra in reflecting fast reactors by activated resonance detectors is considered.

Absorber difference and "1/v absorption" methods are illustrated by an example of the measurement of the flux distribution of resonance neutrons with energies of 4.9 ev (Au^{197}) and 2.95 kev (Na^{23}) in the reflecting reactors BR-1 and BR-5. It is shown that the neutron spectrum region from one to several thousand electron volts can be studied in adequate detail with the aid of the set of detectors described.

The resonance detector method has been used with success for many years for the investigation of neutron spectra in intermediate- and thermal-neutron reactors. The use of thin foils or layers of material having strong isolated resonance activation cross sections as detectors permits the determination of neutron fluxes, at energies corresponding to the resonance maximums [1].

The resonance detector method can also be useful for the study of comparatively soft spectra arising in fast neutron reflecting reactors. However, in this case, the contribution of the primary, usually the strongest, resonance to the detector activation can prove to be comparable with the resonances at high and lower energies. Therefore, it is necessary to use special methods to separate the activity induced by the neutrons which correspond to the resonance energy.

One of such methods is the absorber difference method. If the detector foil is covered on both sides during irradiation by layers of the same material which is thin in all neutron energy regions except in the neighborhood of the resonance at $E = E_0$, then the portion of the total activity due to the resonance neutrons will be decreased, because of the screening, in comparison with the case when the detector foil was irradiated without screening layers (filters).

It can be shown that the difference of the absolute magnitude of the saturation activity ΔA, which refers to unit volume of the detector foils without filters and with filters of thickness t, when irradiated in identical isotropic neutron fluxes, can be represented by the following expression:

$$\Delta A = \varphi(E_0)\frac{\pi}{2}\Gamma_\gamma \Sigma_{0,a}\eta + 2t\int \Sigma_a(E)\,\Sigma_c(E)\left\{1-\frac{1}{2}\times Ei[-\Sigma_c(E)\,t]\right\}\varphi(E)\,dE. \quad (1)$$

Here $\varphi(E)$ is the neutron flux with energy E; Γ_γ is the radiation width; $\Sigma_{0,a}$ is the activation cross section at the resonance maximum; Σ_a and Σ_c are the activation cross sections of the isotope being irradiated and the total absorption cross section of the detector respectively (all macroscopic cross sections).

The first term in formula (1) is dependent on the screening of the resonance neutrons which is characterized by the factor η. The second term, to a first approximation, takes into account the absorption of the neutrons which lie outside the resonance being studied (the integration is carried out over all of the energy region except the

neighborhood of the resonance). It is assumed that, for these neutrons, $\Sigma_c t \ll 1$, and that the detector thickness can be neglected in comparison with the filter thickness. From relation (1) it is obvious that with $\Sigma_0 \gg \Sigma_c(E)$ it is always possible to make the second term negligibly small in comparison with the first. Thus, by measuring the activity difference ΔA and knowing the resonance parameters and the dependence of the absorption factor η on them, it is possible to determine the flux of resonance neutrons.

The absorption factor η can be calculated easily with the aid of the Gurevich-Pomeranchuk resonance absorption theory (see for example [2]) in the limiting cases of narrow ($\Gamma \ll \xi E_0$) and broad ($\Gamma \gg \xi E_0$) isolated resonances and also for isolated absorption resonances ($\Gamma \approx \Gamma_\gamma$). We will, for convenience, introduce the parameters $\beta = \Sigma_0' t$, $\beta_0 = \Sigma_0' t_0$; the relation of the filter thickness t and the detector thickness t_0 to the "drawing-out" length of neutrons from the resonance region is $\frac{I}{\Sigma_0'}$ which corresponds to its maximum. It is obvious that

$$\Sigma_0' = \begin{cases} \Sigma_0 & \text{for } \Gamma \ll \xi E_0 \\ \Sigma_0 \dfrac{\Gamma_\gamma}{\Gamma} & \text{for } \Gamma \gg \xi E_0 \text{ and } \Gamma \approx \Gamma_\gamma. \end{cases} \tag{2}$$

Then the factor $\eta(\beta, \beta_0)$ in Eq. (1) will be determined by the relation

$$\begin{aligned} \eta(\beta, \beta_0) &= F(0, \beta_0) - F(\beta, \beta_0) \\ &= f(\beta_0) - f(\beta + \beta_0) - \beta \frac{f(\beta+\beta_0) - f(\beta)}{\beta_0}, \end{aligned} \tag{3}$$

where

$$F(\beta, \beta_0) = \frac{(\beta+\beta_0) f(\beta+\beta_0) - \beta f(\beta)}{\beta_0} \tag{4}$$

is the factor which takes into account both the self-screening of the detector and the screening by its filters.

$$f(\beta) = \int_0^1 e^{-\frac{\beta}{2\mu}} \left[I_0\left(\frac{\beta}{2\mu}\right) + I_1\left(\frac{\beta}{2\mu}\right) \right] d\mu \tag{5}$$

is the function which describes the self-screening of the resonance neutrons in a plane layer of thickness t [2]; I_0 and I_1 are Bessel functions of order zero and one, with imaginary argument. From formula (4) it is obvious that the factor $F(\beta, \beta_0)$ is proportional to the difference between the activities of layers of thickness $\beta + \beta_0$ and β. The values $\eta(\beta, \beta_0)$ can be calculated from tables of functions of $f(\beta)$ given in [2]. However, in practice, one has to deal mostly with the case $\beta \gg \beta_0$ when the calculation of the difference between the close values of $f(\beta + \beta_0)$ and $f(\beta)$ can lead to a significant error in the value of η . In this case one should use for $\eta(\beta, \beta_0)$ the formula which is obtained by a Taylor's series expansion of $f(\beta + \beta_0)$ and which is correct to third-order terms in β_0^3:

$$\begin{aligned} \eta(\beta, \beta_0) &= f(\beta_0) - f(\beta)\left(2 + \frac{\beta_0}{\beta}\right) \\ &+ \frac{e^{-\frac{\beta}{2}}}{\beta} \left[\left(\beta + \beta_0 - \frac{\beta_0^2}{12} + \frac{\beta_0^3}{192}\right) I_0\left(\frac{\beta}{2}\right) \right. \\ &\left. + \left(\beta + \frac{\beta_0}{2} + \frac{\beta_0^2}{12} - \frac{\beta_0^3}{192}\right) I_1\left(\frac{\beta}{2}\right) \right]. \end{aligned} \tag{6}$$

Values of the function $\eta(\beta, \beta_0)$ for certain β and β_0 calculated from formula (6) are given in Table 1. The interference resonance and potential scattering has been neglected in the calculation of $\eta(\beta, \beta_0)$. When $\Gamma \sim \xi E_0$ and $\Gamma_n \gg \Gamma_\gamma$ the calculation is difficult and consequently must be carried out separately, by numerical methods, for each specific resonance.

In order to determine the difference ΔA with sufficient accuracy, it is necessary that the contribution to the total detector activity of the neutrons which correspond to the first resonance level energy be sufficiently large. For a Fermi spectrum this contribution is determined by the ratio of the magnitude of $\frac{\pi\Gamma_\gamma\Sigma_0}{2E_0}$ to the total resonance integral I_R. Although the spectra in fast-neutron reflecting reactors can be substantially different from Fermi spectra, this ratio is a convenient detector characteristic. When detectors are used with highly situated primary resonances, the effect of the slower neutrons can be substantially decreased if the detectors, both with and without filters, are covered on both sides by additional borate filters.

TABLE 1. Values of the Absorption Factor $\eta\ (\beta, \beta_0)$

β_0 \ β	0.25	0.5	0.75	1.0	1.5	2.0	2.5	3.0	4.0	5.0	7.0	10.0
0.0	0.308	0.422	0.508	0.570	0.654	0.709	0.743	0.769	0.805	0.827	0.857	0.882
0.25	0.186	0.295	0.368	0.427	0.496	0.546	0.577	0.601	0.634	0.656	0.684	0.708
0.5	—	0.234	0.300	0.349	0.416	0.454	0.489	0.513	0.544	0.565	0.592	0.615
0.75	—	—	0.257	0.309	0.346	0.403	0.430	0.451	0.480	0.501	0.527	0.550
1.0	—	—	—	0.266	0.319	0.343	0.383	0.403	0.431	0.451	0.476	0.499

One should choose, as resonance detectors, those isotopes whose primary resonance activation cross sections are separated from the remainder by an adequately large energy interval. For such detectors the absorption of the second and succeeding resonances [see Eq. (1)] will be small in comparison with the absorption of the primary resonance since they have greater width and smaller cross section at the maximum. Table 2 gives some characteristics of resonance detectors recommended for spectra measurement. The characteristics of all the isotopes given in the table are such that it is possible, in the case of investigation of spectra close to $1/E$, to neglect deliberately the second term in formula (1) for $\beta \ll 1$. For all detectors given in the table except Na^{23}, the contribution of the primary resonance to the total resonance integral is almost 100%. For Na^{23} this contribution is 30%. From Table 2 it is obvious that condition (2) is satisfactorily fulfilled only for three detectors In^{115}, Au^{197} ($\Gamma > \xi E_0$ and $\Gamma_\gamma \sim \Gamma$), La^{139} ($\Gamma < \xi E_0$). An experimental determination of the "drawing out" cross section Σ_0^* is necessary for the use of the remaining detectors.

TABLE 2. Characteristics of Resonance Detectors

Isotope	E_0, ev	σ_0, barn	Γ_γ, ev	Γ_n, ev	ξE_0, ev	α, %*
In^{115}	1.46	$3.90 \cdot 10^4$	0.072	0.003	0.025	95.8
Au^{197}	4.91	$3.74 \cdot 10^4$	0.124	0.016	0.050	100.0
W^{186}	18.8	$1.19 \cdot 10^5$	0.047	0.282	0.20	28.4
La^{139}	73.5	1760	0.150	0.027	1.05	100.0
Co^{59}	132	$8.92 \cdot 10^3$	0.5	4.9	4.4	100.0
Na^{23}	2950	550	0.4	220	250	100.0

* α is the content in a naturally-occurring isotopic mixture.

If the neutron spectrum being studied decreases with energy with sufficient rapidity in the resonance region, then neutrons which correspond to the second and higher resonances do not give a marked contribution to the detector activity. In this case, it is possible to use the so-called "1/v absorption" method to separate the activity induced by neutrons lying in the neighborhood of the primary resonance level.

In the case under discussion, the saturation activity of a thin detector can be represented as a sum of the contribution from the region where the activation cross section obeys the 1/v law and from the region of the primary resonance:

$$A_1 = \left[\Sigma_a^m \sqrt{E_m} \int \varphi(E) \frac{dE}{\sqrt{E}} + \varphi(E_0) \frac{\pi}{2} \Gamma_\gamma \Sigma_0 \right] \cdot \zeta. \quad (7)$$

Here Σ_α^m is the activation cross section for thermal neutrons (at energy E_m), ζ is the detector efficiency.

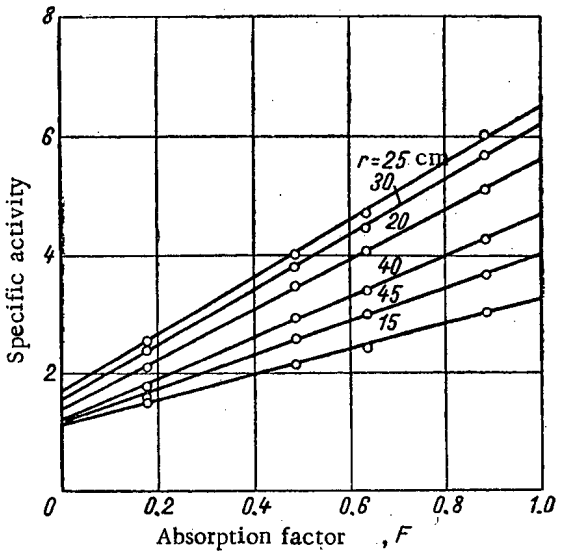

Fig. 1. The dependence of the specific activity of gold detectors on the absorption factor of the primary resonance for various distances from the center of the active zone.

We will discuss two isotopes, one of which has a resonance in the activation cross section for $E = E_0$, while the cross section of the other obeys the 1/v law. It is obvious that the second term of formula (7) will be absent in the expression for the second detector's activity. The neutron flux near E_0 can be determined from the following relation:

$$\varphi(E_0) = \frac{A_1 - A_2 \frac{\Sigma_{a,1}^m}{\Sigma_{a,2}^m} \frac{\zeta_1}{\zeta_2}}{\frac{\pi}{2} \Gamma_\gamma \Sigma_0 \zeta_1}. \quad (8)$$

The B^{10} (n, α) reaction can be employed as a detector possessing $\frac{1}{v}$ sensitivity.

In order to build-up spectra from data obtained with the aid of various detectors, it is necessary to compare their efficiencies in an identical thermal-neutron flux. The BF_3 chamber (or counter), which is used to separate the "$\frac{1}{v}$ contribution," must be calibrated in the same flux.

Let us now illustrate the proposed methods with results obtained from the investigation of neutron spectra in fast reflecting reactors. The difference method was used to measure the flux distribution of neutrons with an energy of 4.9 ev in the BR-5 reflecting reactor [3]. Gold foils with a density of 1.38 mg/cm^2 ($\beta_0 = 0.14$) were used as detectors; the filters were gold foils with densities of 3.05 and 6.10 mg/cm^2 ($\beta = 0.31$ and 0.62). The activity distribution of foils with density of 195 mg/cm^2 was also measured. In the latter case, the self-absorption of β-particles was taken into account in processing the measured results. The measurements were made in a vertical channel which was 50 mm from the axis of the reactor and passed through the active zone and below the end reflector which was made of nickel with small amounts of sodium and stainless steel.

Figure 1 shows the dependences of the specific activity of the detector used on the parameter $F(\beta, \beta_0)$ which was calculated from formula (4) for the primary resonance of Au^{197}. As is obvious from the figure, these dependences are linear for all detector positions in the reactor. Consequently, the contribution from neutrons which lie below the primary resonance in the region being blocked by the thicknesses of the filters employed is negligibly small. Extrapolation of these data to the absorption factor value $F = 1$ gives the activity of an infinitely-thin detector:

$$A(F \to 1) = C \int \varphi(E) \Sigma(E) dE. \quad (9)$$

The difference between this quantity and the activity which is obtained from a linear extrapolation to the absorption factor value $F = 0$ ($t \to \infty$) is proportional (with the same proportionality coefficient) to the resonant neutron flux:

$$A(F \to 1) - A(F \to 0) = C\varphi(E_0) \frac{\pi}{2} \Gamma_\gamma \Sigma_0. \quad (10)$$

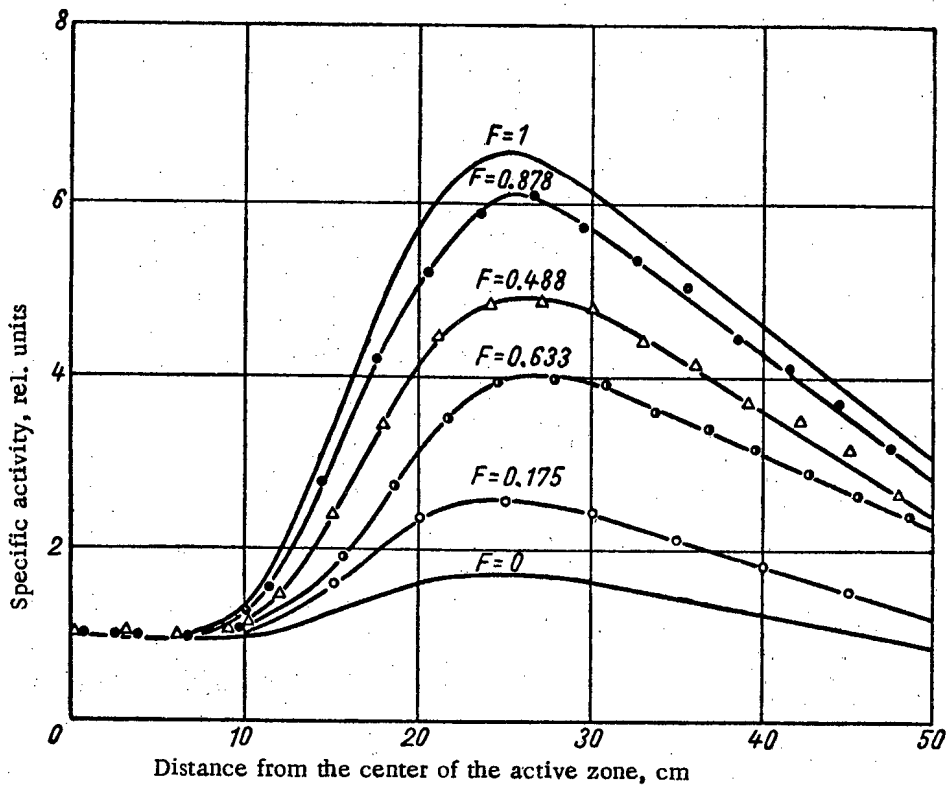

Fig. 2. Activity distribution of gold detectors as a function of the distance from the reactor center. Values of the absorption factor are shown as numbers on the curves.

Figure 2 gives the specific activity distributions along the axis of the channel for the detectors used and also the extrapolated activity distributions. The neutron flux distribution at an energy of 4.9 ev at 5000 kw nominal reactor power is shown in Fig. 3. For the measurement of the latter distribution, the activity differences of detectors calibrated in the thermal column of a reactor together with a layered Pu^{239} fission chamber were used.

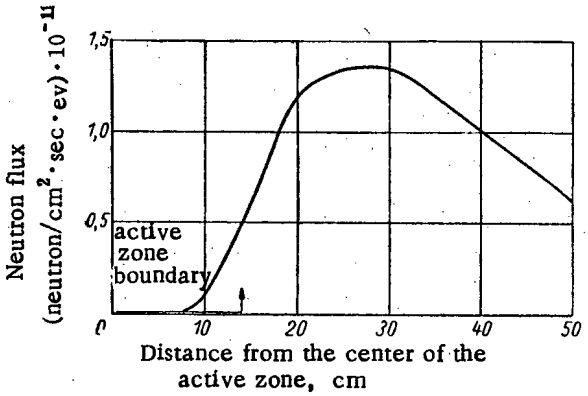

Fig. 3. Distribution of neutron flux at 4.9 ev energy for 5000 kw reactor power.

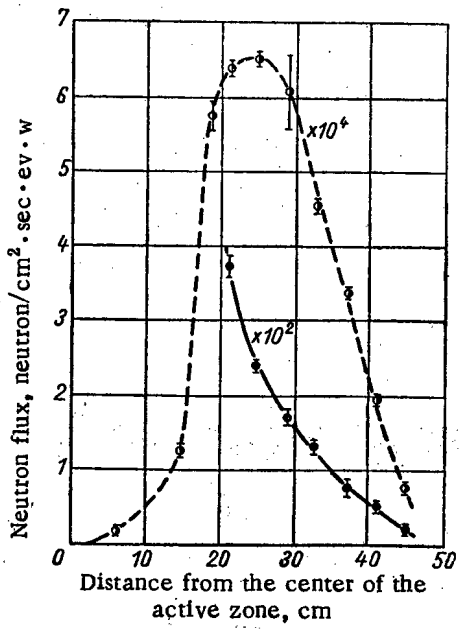

Fig. 4. Distribution of neutron flux with energy 2.95 kev in the BR-1 reactor's nickel shield, obtained from sodium detectors by the "1/v absorption" method.

The described measurements were carried out in detail with the aim of checking the method. For practical application of the method, as a rule, the use of one filter thickness is sufficient; the resonant neutron flux is calculated from this according to the formulas (1), (3) or (6).

The "1/v absorption" method was used to measure the neutron flux at the 2.95 kev energy in the BR-1 reactor [4] with a nickel reflector. The measurements were carried out using salt (Na_2CO_3) detectors of thickness 100 mg/cm^2 ($\beta_0 \sim 0.3$); a small size BF_3 chamber was used as a 1/v detector. The contribution of the resonance neutrons to the total activity of the sodium detectors ranged from 20 to 50%, depending on their position in the reactor. Measurements were not made near the active zone where the second (55 kev) and higher sodium resonances could add a noticeable contribution to the detector activity. The results are presented in Fig. 4. The neutron flux distribution at an energy of 4.9 ev, measured by the absorber difference method with gold foils, is shown by the same dotted curve.

The authors express deep thanks to A. I. Leipunskii for interest in the work and to I. I. Bondarenko and V. V. Orlov for helpful advice and comments.

LITERATURE CITED

1. D. Yuz, "Neutron research in nuclear reactors" [in Russian] (Moscow, published in Foreign Literature, 1954).
2. G. I. Marchuk, "Numerical calculation methods for nuclear reactors" [in Russian] (Moscow, Atomizdat, 1958).
3. A. I. Leipunskii, et al., Transactions of the Second International Conference on the World Utilization of Atomic Energy (Geneva, 1958). Reports of Soviet Science. 3 (Moscow, Atomizdat, 1959), p. 215.
4. A. I. Leipunskii, et al., "Atomnaya Énergiya," 5, 277 (1958).

All abbreviations of periodicals in the above bibliography are letter-by-letter transliterations of the abbreviations as given in the original Russian journal. *Some or all of this periodical literature may well be available in English translation.* A complete list of the cover-to-cover English translations appears at the back of this issue.

DETERMINATION OF THE SEPARATION FACTOR OF LITHIUM ISOTOPES IN ION EXCHANGE

S. G. Katal'nikov, V. A. Revin, B. M. Andreev,

and V. A. Minaev

Translated from Atomnaya Énergiya, Vol. 11, No. 6, pp. 528-532,
December, 1961
Original article submitted January 30, 1961

The isotopic equilibrium between the solutions of lithium salts (LiOH and LiCl) and SBS, KU-2, and Dowex-50 cationites is investigated. It is shown that, in the first place, the Li^7 isotope was concentrated in the solution in all the cases which were investigated; in the second place, there is a dependence of the separation factor value α on the nature of the cationite; in the third place, in 1 N to 5 N solutions of LiCl, the value of α does not depend on the concentration of the solution.

Taylor and Urey [1] made the first attempt to separate lithium isotopes by using ion exchange. They demonstrated the theoretical possibility of separating lithium, potassium, and nitrogen isotopes in the exchange between their salts with a zeolite-type aluminosilicate ion exchanger, and they determined the equilibrium separation factor α of the $R^7Li + {}^6Li^+ \rightleftarrows R^6Li + {}^7Li^+$ ion-exchange reaction. Taylor and Urey showed that, at room temperature, the above reaction is characterized by a separation factor $\alpha = 1.022$. In connection with the development of artificial ion-exchange materials, experiments on the separation of lithium isotopes by using organic ion exchangers were performed in the postwar years [2-4]. The experiments performed by Glueckauf, et al. [2] on the chromatographic separation of lithium isotopes in a column filled with the Zeo-Karb H. I. ionite showed that the value of α is much smaller than the 1.022 value obtained in [1]. Menes, et al. [4] came to the same conclusion; according to the results of their experiments on the isotopic exchange between lithium salts and the Dowex-50 cationite, the value of α is equal to 1.002. The paper by Lee and Begun [5] is devoted to the effect of the degree to which the Dowex-50 cationite is bonded on the magnitude of α for lithium isotopes. It was shown in this paper that, if the percentage of divinylbenzene (DVB) (which characterizes the degree to which the cationite is bonded) varies from 2 to 24% in the resin, the α values vary from 1.0010 to 1.0038. In all the above-mentioned experiments, the separation of lithium isotopes occurred in such a manner that the solution was enriched in heavy isotopes. A paper by G. M. Panchenkov et al. [6], which appeared in 1959, was devoted to a study of the influence exerted by the concentration of the exchanging salts and their nature as well as the nature of the ion exchanger itself on the separation factor value. In this paper it was shown that in the exchange between LiOH, Li_2CO_3 and C_6H_5COOLi and sulfocarbon, the solution is enriched with the light isotope, while, in the exchange between LiCl and the same cationite, the heavy isotope is concentrated in the solution. All the above papers are concerned to various degrees with the assessment of such influences on the separation factor as the nature of the cationite and its structure, the chemical nature of the exchanging salt, the salt concentration in the solution, and the temperature. The present article is concerned with the determination of the separation factors of lithium isotopes in the exchange between LiOH and LiCl in different concentrations and certain domestically-produced sulfocationites, such as SBS and KU-2, as well as the Dowex-50 cationite.

Experimental

Preliminary investigations of cationites. A 0.25-0.50 mm cationite fraction in the air-dry state and in hydrogenous form was used in our experiments. The static exchange capacity (SEC) for all the above-mentioned cationites was determined according to the standard method [7] by using a LiOH solution instead of NaOH. Table 1 shows the results obtained in determining the capacities of the SBS, KU-2, and Dowex-50 cationites and of their swelling ability in a 1 N solution of LiOH. Table 1 also provides the values of the distribution factor K_{Li}^{H} and of the exponent

p in the expression $K_{Li}^{H}\left(\frac{RH}{RLi}\right)\left(\frac{LiCl}{HCl}\right)^{p}$ which describes the ion exchange in the RH + LiCl ⇌ RLi + HCl system. The distribution factor for Li^+ and H^+ ions was determined graphically with respect to the relative equilibrium concentration of lithium and hydrogen in the solution and in the resin; a graph (Fig. 1) which expresses the $\log\frac{RH}{RLi} = f\left(\log\frac{LiCl}{HCl}\right)$ dependence was plotted for this purpose.

TABLE 1. Certain Characteristics of the SBS, KU-2, and Dowex-50 Sulfocationites*

Cationite type	SEC, mg-eq/g of resin		Swelling ability, %	K_{Li}^{H}	p
	air-dry	dry			
SBS (1)	2.68	3.40	50	4.16	1.00
SBS (2)	2.46	3.16	40	3.46	0.65
SBS (3)	4.86	5.20	110	6.01	1.00
SBS (4)	3.65	4.57	40	4.68	1.00
SBS (5)	2.34	3.06	40	2.82	0.65
KU -2	3.60	4.85	—	—	—
Dowex -50	3.54	—	—	—	—

* The SBS batches which we used, which will be subsequently denoted as Nos. 1, 2, 3, 4, and 5, were produced by various organizations at different times. We obtained SBS [5] from SBS (4) by additional sulfonation.

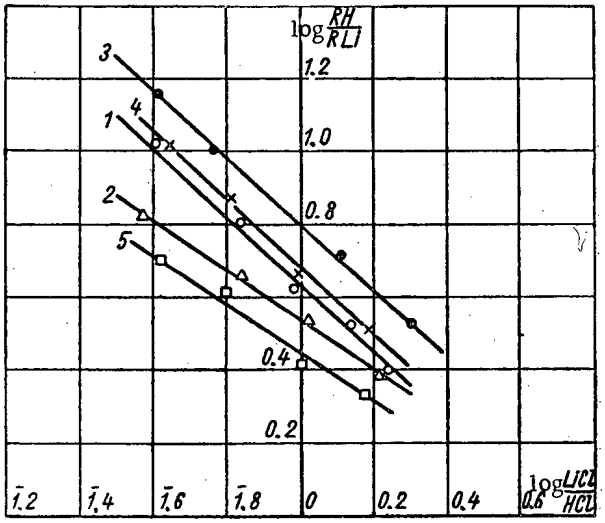

Fig. 1. Determination of the distribution factor K_{Li}^{H} in the exchange with SBS cationite from different batches. The numbers 1, 2, 3, 4, and 5 denote different batches of the SBS cationite.

A comparison between the static capacity, the swelling ability, and the distribution factor for different SBS cationite batches indicates the existence of definite differences between their physical and exchange properties. It was natural to assume that the above differences will manifest themselves in the isotopic exchange process. In connection with this, we organized experiments on the exchange between lithium isotopes and all of the above-mentioned cationite types.

The experimental method. One of the simplest methods for determining the value of the isotope separation factor

$$\alpha = \left(\frac{Li^6}{Li^7}\right)_{ap} / \left(\frac{Li^6}{Li^7}\right)_{bp}$$

is the method of single equilibration with the subsequent calculation of the α value with respect to the difference between the equilibrium concentrations. The greatest difference between the concentrations of equilibrium phases is secured in work with samples which are enriched up to 50% (in isotopes). We had at our disposal lithium hydroxide that was enriched with Li^6 to 48.4%, with which a concentration difference of approximately 0.25 ($\alpha - 1$) could be secured in single experiments. In order to increase the accuracy of α determination even in work with samples that are enriched with Li^6, it is advisable to perform the so-called multistep experiments, which have been described in [8].

In multistep experiments, the separation factor value can be calculated by using the equations given in [9], or it can be determined graphically, as was described in [8]. In processing the results of our multistep experiments, the value of α was determined only graphically.

In using the graphical method for determining the separation factor, it is necessary to know the amount of lithium that is introduced in RLi form at each exchange step. Therefore, after performing each exchange step, the

cationite was regenerated by means of a 2-3 N solution of HCl, and the lithium percentage in the solution was determined; the remaining LiOH solution was concentrated by evaporation in order to maintain a constant concentration. The isotope concentrations were determined according to the flotation method by comparing the flotation temperatures of the specimen crystals and of the standard. The residue of the LiOH solution as well as LiCl solutions, which were obtained at individual exchange stages, were used as samples. Some of the experiments were performed at a temperature of 0 °C, since the separation factor of Na and Li isotopes increases with a decrease in temperature [10, 11].

Experimental Results

The experiments concerning the dependence of α on the nature of cationites were performed with a 1 N solution of LiOH. The experimental results are given in Table 2.

TABLE 2. Values of α in the Exchange Between Lithium Isotopes and SBS, KU-2, and Dowex-50 Cationites

Cationite	Expt. No.	α	α_{av}	Temp. °C
SBS (1)	1	1.006±0.001 1.006±0.001	1.006±0.001	0
SBS (2)	1	1.004±0.001	1.004±0.001	0
SBS (3)	1	1.019±0.001 1.022±0.002	1.020±0.002	0
SBS (4)	1	1.010±0.001		
	2	1.010±0.001	1.009±0.002	0
	3	1.008±0.002		
SBS (5)	1	1.004±0.001		
	2	1.005±0.001	1.004±0.001	0
	3	1.004±0.001		
KU-2	1	1.008±0.002	1.008±0.002	25
Dowex-50	1	1.006		
	2	1.006		
	3	1.008	1.006±0.002	25
	4	1.006		

TABLE 3. Exchange of Lithium Isotopes Between SBS (5) and LiCl Solutions

Expt. No.	Initial concentration of LiCl, g-eq/liter	Equilibrium conc. of LiCl, g-eq/liter	Lithium share in the cationite, $\frac{RLi}{RLi+RH}$	α
1	1.230	0.877	0.283	1.005±0.001
2	1.360	0.869	0.290	1.004±0.001
3	1.150	0.800	0.286	1.005±0.001
4	1.050	0.720	0.278	1.007±0.002
5	1.010	0.975	0.322	1.010±0.002
6	1.020	1.010	1.000	1.003±0.001
7	1.290	1.280	1.000	1.005±0.001
8	5.20	4.64	0.362	1.005±0.002
9	5.40	4.83	0.372	1.006±0.002

In order to investigate the effect of the solution characteristics on the value of the separation factor for lithium isotopes, we performed experiments on the exchange between the SBS (5) cationite and LiCl and LiOH solutions.

In multistep experiments where LiCl solutions are used, a progressive accumulation of hydrochloric acid in the solution takes place (due to the $RH + LiCl \rightleftharpoons RLi + HCl$ reaction). As a consequence of this, the exchange equilibrium is shifted toward the hydrogenous form of resin, which makes the performance of multistep experiments very difficult. Therefore, only single-step experiments were performed with LiCl solutions, the results of which are given in Table 3.

In experiments 6 and 7, we used a cationite which was first saturated with lithium that had the same concentration of Li^6 as the solution.

The dependence of the α value on the lithium concentration in the solution that was used in exchange with the cationite in the RH-form (SBS, 5) was investigated by means of 1 N and 5 N solutions of LiCl. The choice of lithium chloride solutions was based on the fact that cationites are unstable in intensely alkaline solutions. Moreover, exchange experiments with solutions whose concentrations are higher than 5 N cannot be readily performed.

The results of the experiments performed with 5 N solutions of LiCl are also given in Table 3.

Discussion of the Results

The sulfo group, in which hydrogen possesses the exchange ability, constituted the functional group in all the cationites which we used. Therefore, we cannot draw any conclusions concerning the effect of the ion exchanger's functional group on the separation factor value. At the same time, our results as well as the results given in papers

that were published earlier [6] indicate that the value of α depends on the cationite's nature. By the term "nature" of the cationite, we understand the chemical properties of the cationite's frame as well as its physical structure. Both of the above factors determine the difference between the selective properties of a single cationite type (KU-2 and Dowex-50 with different DVB percentages and SBS, which is prepared by using different initial materials and which is sulfonated according to different procedures) as well as the difference between the selective properties of different cationite types.

In [5], the difference between the selective properties of Dowex-50 cationites with various DVB percentages can be reduced mainly to a decrease in the number of water molecules which hydrate a lithium ion in the resin phase. In the above experiments, this reduction was caused by the different degrees to which the cationite is bonded, which are expressed in percentages of DVB that is introduced into the resin's structure during its synthesis. As a rule, cationites with a large percentage of DVB swell to a lesser degree. If the results of determining α by using the SBS cationite are interpreted from this point of view, our results cannot be explained by the dehydrating action of the ionite. The maximum value of the separation factor was obtained for the SBS (3) cationite, which had the maximum swelling ability. It must be emphasized that this cationite type is characterized by the greatest value of the distribution factor K^H_{Li}. If we compare the K^H_{Li} and α values for all SBS cationite batches except SBS (5), we arrive at the following conclusion: The lesser the affinity of the cationite to lithium, the larger the lithium isotope separation factor. For the SBS cationite, this dependence is quantitatively given in the shape of an $\alpha = f(\log K^H_{Li})$ graph, which is shown in Fig. 2. This inference enables us to state that the distribution factor value, which expresses the affinity of the cationite to lithium, can determine to a certain extent the value of α.

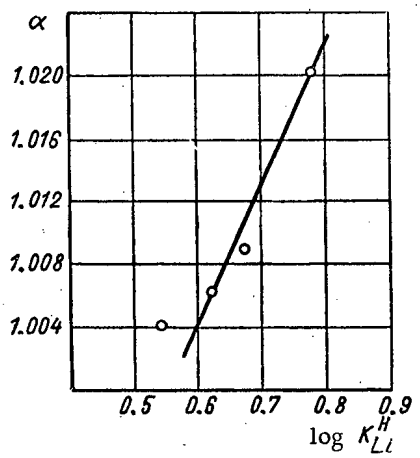

Fig. 2. Dependence of α on log K^H_{Li} for the SBS cationite.

Unfortunately, the article [5] does not provide the elution curves, which could be used for estimating the lithium distribution between the solution and the cationite and, consequently, the molar portion of lithium in the cationite phase. In fact, according to data given by Reichenberg [12] and Bonner [13], the value of K^H_{Li} for the Dowex-50 cationite depends on the molar portion of lithium in the cationite phase. If there is a relationship between K^H_{Li} and α and if it has the character indicated above, the fact that different values of α were obtained in [5], where HCl and NH_4Cl were used as elution agents, becomes understandable. It is known that, with respect to their affinity to cationites, lithium, ammonia, and hydrogen ions can be arranged in the following order: $Li < H < NH_4$. This means that the lithium peak of an elution curve that was obtained by using an NH_4Cl solution will be more constricted in comparison with a similar peak that is obtained by washing-out lithium with a HCl solution. In the peak of lithium that is washed out by an NH_4Cl solution, the influence of the tail and head portions of the peak on the effective separation factor will be less pronounced due to the fact that the molar portion of lithium in the cationite phase is smaller in these sections of the peak (consequently, the K^H_{Li} value is also smaller). Therefore, it can be expected that the α_{eff} value in washing-out lithium with an NH_4Cl solution would be larger, which was confirmed in [5].

This confirms the fact that α depends on the molar portion of lithium in the cationite or on the values of the K^H_{Li} and $K^{NH_4}_{Li}$ distribution factors. On the other hand, if there is a dependence of α on the molar portion of lithium in the cationite, then, the α values which are determined by using the chromatographic method are integral, and they are not comparable with the α values obtained in lithium exchange in a solution with a cationite that is used entirely in lithium form, as was the case in our experiments with LiOH. In our experiments with the SBS cationite, for which no dependence of K^H_{Li} on the molar portion of lithium in the cationite was detected, the separation factor value was also independent of the molar portion of lithium in the cationite.

It is also interesting to note the fact that additional sulfonation of the SBS cationite results in a change in all of its properties, including the separating ability with respect to isotopes, which follows from Tables 1 and 2 (specimens 4 and 5).

The results of experiments with the SBS cationite and LiOH and LiCl solutions indicate that, within the limits of measurement errors, the α value remains the same in the exchange between lithium that is bonded to the cationite and a LiOH solution as well as a LiCl solution. With respect to the character of the dependence of α on the nature

of the solution, our results differ from those obtained in [6]. It seems that the presence of some functional groups is the main cause of these discrepancies.

SUMMARY

1. As a result of isotopic exchange of lithium between SBS, KU-2, and Dowex-50 cationites, and LiOH and LiCl solutions, it was shown that: a) The Li^6 isotope is concentrated in the cationite, while the Li^7 isotope is concentrated in the solution; b) the value of the separation factor α depends on the nature of the cationite.

2. Within the limits of measurement errors, the values of α are equal in the exchange of lithium isotopes in LiCl and LiOH solutions, while, in 1-5 N solutions of LiCl, the α value does not depend on the concentration.

3. The mutual dependence between the distribution constant for the $Li^+ - H^+$ system and the lithium isotope separation factor was demonstrated qualitatively. It was shown that a cationite with the minimum affinity to lithium has a maximum value of the separation factor. A similar relationship between K_{Li}^{H} and α also holds for cationites in which the distribution factor value depends on the molar portion of lithium in the exchanging cationite (Dowex-50).

In conclusion, we extend our sincere thanks to Professor G. K. Boreskov for his advice and continued interest in the work.

LITERATURE CITED

1. T. Taylor and H. Urey, J. Chem. Phys. 5, 597 (1937); 6, 429 (1938).
2. E. Glueckauf, K. Barker and G. Kitt, Disc. Faraday Soc. 7, 199 (1949).
3. I. Gross, Nucl. Sci. Abstrs. 5, 169 (1951).
4. F. Menes, E. Saito and E. Roth, Proceedings of the International Symposium on Isotope Separation, p. 227. North-Holland Publishing Co. Amsterdam (1958).
5. D. Lee and G. Begun, J. Am. Chem. Soc. 81, 10, 2332 (1959).
6. G. M. Panchenkov, E. M. Kuznetsova and O. N. Kaznadzei, Atomnaya Énergiya 7, 6, 556 (1959).
7. GOST 5695-52.
8. G. K. Boreskov and S. G. Katal'nikov, Zh. Fiz. Khimii 35, 6, 1240 (1961).
9. E. M. Kuznetsova, A. V. Makarov and G. M. Panchenkov, Zh. Fiz. Khimii 32, 11, 2641 (1958).
10. R. Betts, W. Harris and M. Stevenson, Canad. J. Chem. 34, 1, 65 (1956).
11. D. Lee, J. Phys. Chem. 64, 187 (1960).
12. D. Reichenberg and D. Mc Cauley, J. Chem. Soc. 2741 (1955).
13. O. Bonner, J. Phys. Chem. 58, 4, 318 (1954).

All abbreviations of periodicals in the above bibliography are letter-by-letter transliterations of the abbreviations as given in the original Russian journal. *Some or all of this periodical literature may well be available in English translation.* A complete list of the cover-to-cover English translations appears at the back of this issue.

SOME PROBLEMS IN NUCLEAR METEOROLOGY

B. I. Styro

Translated from Atomnaya Énergiya, Vol. 11, No. 6, pp. 533-538,
December, 1961
Original article submitted March 11, 1961

A group of problems associated with radioactive contamination of the atmosphere is discussed. Principal attention is given to the study of natural radioactivity and to those phenomena which are closely connected with meteorology or which assist in the solution of a number of meteorological problems. While setting forth the results obtained thus far, several questions are raised which need investigation.

With the widespread use of atomic energy, large quantities of radioactive gases and aerosols of artificial origin have been deposited in the atmosphere during the last fifteen years; contamination of the atmosphere has occurred, presenting a biological hazard. Aware of this, scientists have exhibited great interest in the study of atmospheric radioactivity. The area of investigation, both for artificial and natural radioactivity, has been broadened, since the fate of radioactive aerosols of both natural and artificial origin is identical in many respects despite a number of fundamental differences.

The term "nuclear meteorology" is not a standard one, but we find it convenient for the definition of those geophysical problems connected with radioactive contamination of the atmosphere and with the solution of a number of meteorological problems by radiometric methods.

This paper is chiefly devoted to the study of natural atmospheric radioactivity. There have been numerous papers, published both here [1, 2] and abroad, on radioactive contamination of the atmosphere caused by man.

Immediately after the discovery of radioactivity [3, 4], scientists set about the study of radioactive contamination of the atmosphere, and a wealth of material, which is summarized in a monograph [5], has been accumulated up to the present time.

One of the fundamental problems of nuclear meteorology is the study of the radioactive materials which form part of the atmosphere [6, 7]. In papers published in the past sixty years [3, 6, 7], analyses were made of the nature of atmospheric radioactivity, and it was shown that all the members of the radioactive families of uranium, thorium, and actinium were present in air in the atomic state or as aerosols.

In recent years, a number of radioactive isotopes [5, 8] have been detected in the atmosphere, a list of which is given in the table. This list will be increased continually, as our knowledge grows.

The assumption that the creation of these isotopes is explained by cosmic ray irradiation of the atmosphere is bolstered by the increase in their concentration with height above the Earth's surface [5], and by the existence of a latitude effect on the concentration [9, 10] which coincides with the change in cosmic ray intensity. The possibility of atmospheric contamination by radioactive elements carried in with meteoritic matter [11, 12] is not excluded either. Finally, an important source of radioactive contamination is the activity of man as a result of which the atmosphere is contaminated by radon, thoron, and C^{14}, as well as by Sr^{90}, Cs^{137}, I^{131}, and other fission products which originate from nuclear weapons testing and from the use of atomic energy for peaceful purposes.

The formation of radioactive isotopes in the atmosphere, as a result of natural processes, and their radioactive decay enrich the air with both radioactive and stable isotopes. Such a situation, firstly, calls for the assumption that there is a possibility of quantitative variations in atmospheric composition when there is a variation in the intensity of the cosmic radiation which penetrates the atmosphere. For example, this can occur with variations in the intensity of the Earth's magnetic field. Secondly, along with the continuous creation of some isotopes in the atmosphere, there occurs deposition on the surface of the Earth, thus one can conclude that some materials in the crust of the Earth and in the deep sediments of the oceans owe their origin to nuclear reactions of atmospheric gases with cosmic ray particles.

All the things mentioned change our view of the atmosphere somewhat. It has been discovered that the atmosphere is a medium in which intense changes in isotopic and chemical composition occur.

Some Radioactive Isotopes Which Are Formed in the Atmosphere as a Result of Interactions of Protons, Neutrons, and Mesons of Cosmic Origin with Nitrogen, Oxygen, and Argon Nuclei

Radio-active isotope	Half-life	Type of decay and particle energy, Mev	End product of decay
H^3	12.25 yr	$\beta^-(0.018)$	He^3
Be^7	53 d	$\gamma(0.48)$	Li^7
Be^{10}	$2{,}7\cdot10^6$ yr	$\beta^-(0.55)$	B^{10}
C^{14}	5720 yr	$\beta^-(0.15)$	N^{14}
Na^{22}	2.6 yr	$\beta^+(0.54)$ $\gamma(1.27)$	Ne^{22}
Si^{32}	100 yr	$\beta^-(\sim0.1)$	$P^{32} \longrightarrow S^{32}$
P^{32}	14.3 d	$\beta^-(1.70)$	S^{32}
P^{33}	25 d	$\beta^-(0.26)$	S^{33}
S^{35}	87 d	$\beta^-(0.17)$	Cl^{35}
Cl^{36}	$4{,}4\cdot10^5$ yr	$\beta^-(0.71)$	Ar^{36}
Cl^{39}	55 min	$\beta^-(1.65; 2.96)$ $\gamma(0.36; 1.31)$	K^{49}
Ar^{41}	110 min	$\beta^-(1.24; 2.5)$ $\gamma(1.37)$	K^{41}

In the quantitative determination of the concentration of radioactive material in air, rainfall, individual rain drops, or cloud elements, the experimenter encounters great difficulties which are associated with the lack of precise knowledge about the isotopic composition of radioactive contamination. This applies especially to the determination of levels of short half-life contamination, since it then becomes necessary to determine from the calculated concentration the isotopic activity not in the measured sample but in the actual meteorological unit. Analysis of air sample activity is done with all the instruments which are in the armamentarium of the present-day nuclear physicist. Sample collection is a separate, and often very difficult, task for which one of the following methods is used; accumulation in charcoal or a liquid, activation, freezing, air filtration, aerosol electrodeposition, sedimentation collection on sticky paper or in pots, dynamic sample collection on a photoemulsion layer, etc.

Unfortunately, each of the collection methods has its disadvantages. In activation, for example, there is a selectivity with respect to the sign of the charge on the ions [5]. Porous filters are selective for aerosol dispersions and absorb practically no inert gases. The electro-deposition method has a similar disadvantage. Absorption of radioactive materials in charcoal and liquids permits the obtaining of results for radon only. Dynamic activation of a photoemulsion layer [7, 13] is advantageous because it permits a simultaneous determination of the kind of radioactive material and an estimate of its concentration, but the determination of concentration still requires great improvement. A selectivity, which has not been successfully evaluated yet, is possible in connection with the air flow over the photoemulsion and with the capture of aerosols. Up to now, studies have been made of α-radiograms only, but the use of β-radiograms should be no less a possibility.

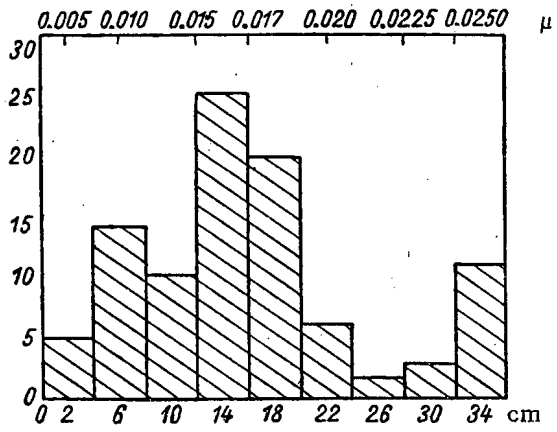

Fig. 1. Mass spectrum of ions carrying natural radioactivity (radon decay products).

At the present time, radiochemical methods are used ever more widely for the separation of the different components of radioactive atmospheric contamination. These methods are quite effective for the determination of long-lived isotopes, but, unfortunately, they are not suitable for isotopes with short half-lives.

Many of the difficulties mentioned here are also met with in the determination of radioactivity in rainfall. Thus, the making-up of mixtures of rainwater with scintillating liquids seems a very good possibility for the future.

Methods were first developed in [6, 14, 15] and radioactivity measured for separate raindrops and various cloud elements, in connection with which the radiographic method proved to be very effective.

Radioactive material in the atmosphere is usually transported by aerosols, therefore the study of the composition, dispersion and behavior of these aerosols is one of the most important problems. From the work of Wilkenning [16], it is known that radon daughter products are associated with finely-dispersed aerosols. The distribution in mobility and size of those aerosols which carry natural radioactivity is shown in Fig. 1. As can be seen from the

figure, most particles have dimensions from 0.009 to 0.018 μ. Similar experiments were repeated in [17] with somewhat improved methods. The results obtained did not contradict the ones presented above. The nature of these aerosols and the selectivity of aerosols of a particular dispersion for radioactive materials is still unexplained. Nor is the problem definitely settled with respect to the state in which radon exists in the atmosphere; in the form of individual gas atoms, or as a gas which is absorbed on aerosols [5]. Individual particles of high activity, amounting to 10^{-9} C [18], were detected recently by autoradiography. These particles were called "hot". Their occurrence sharply increases the activity of a sample and can create a false impression of the average concentration of contamination in the air. Hot particles appear after atomic weapons tests and are detected in amounts of one particle per 100-1000 m^3 of filtered air.

The concentration of radioactive materials in the atmosphere changes both periodically and nonperiodically with time. The periodic changes are associated with the periodicity in the change of day and night or of the seasons of the year, the nonperiodic with features of atmospheric circulation, with changes in the weather or even in individual meteorological elements. Numerous attempts to establish a connection between changes in meteorological elements and atmospheric radioactivity have generally turned out to be unsuccessful; different authors have established only correlated, and often diametrically opposed, relationships. Atmospheric radioactivity is more or less precisely correlated with wind speed (turbulence) and absolute humidity [5]. Generally, the concentration of radioactive contamination in the surface layer decreases with increasing wind speed because of increased mixing. The amount of natural atmospheric radioactivity and the absolute humidity change in one and the same direction. Usually, the connection between complex meteorological elements, i.e., weather, and the concentration of radioactive materials in the air is complicated and not well-defined, therefore the group of studies in this area should be extended in the future.

The establishment of a connection between the concentration of radioactive materials in the air and large-scale atmospheric processes is of great interest. Marine air masses, as a rule, have less natural radioactivity than continental air masses. Artificial radioactive contamination of the atmosphere leads to particularly heavy contamination of the middle latitudes of the northern and southern hemispheres of the Earth because of the peculiarities of atmospheric circulation.

In this situation, some correlation with atmospheric pressure is observed, but the development or breaking-down of vertical motion, which may be associated with pressure or may be the cause of its change, is the actual reason for changes in the radioactive contamination of the surface air layer.

Changes in meteorological elements cause marked variations in atmospheric radioactivity; thus, for example, two measurements of natural radioactivity at the very same spot can differ from one another by two to three orders of magnitude [5], with the average value of radon concentration above dry land approximately 10^{-10} C/cm^3. Above the sea, that kind of radioactivity is less by one to three orders of magnitude [5, 19], as a rule. The activity of thoron and its decay products in the air has been studied considerably less well. On the average, thoron activity over dry land is approximately $5 \cdot 10^{-17}$ C/cm^3. Knowledge of the actinon group and its decay products is even less reliable, but its activity is obviously an order of magnitude less than radon activity. Activity in the surface air layer of the products from nuclear explosions is 0.01-0.001 that of radon activity.

Recently, a number of papers have been published in which the variations of the relative concentrations of the different components that contribute to atmospheric activity were studied. These referred equally to natural [5] and artificial activity [20-22]. However, the presentation of measurements still does not give a complete picture of the phenomenon.

Rainfall, being an important scavenger of radioactive aerosols from the atmosphere, can concentrate them in large amounts. On the average, the amount of natural radioactivity in rain and snow is $2\text{-}3 \cdot 10^{-11}$ C/g [5].

Regularity in the distribution of radioactive isotopes in the depth of the atmosphere, on the one hand, is associated with the mechanism of penetration into it or the creation of radioactive isotopes within it, and, on the other hand, reflects the structural properties of the atmosphere. Experimental studies point to great uniqueness in this distribution. It is characterized by inversions and intermittent changes in the transition from one layer to another. At the present time, the distribution of radon and its daughter products has been studied more than any other, and several theoretical schemes for its circulation have been constructed [23, 24].

Interesting work has been done in the USA where the concentration of C^{14} and H^3 in the stratosphere [25] was studied by collecting samples with large plastic balloons and analyzing the samples in laboratories on the ground. These experiments indicated a sharp increase in the concentration of C^{14} and H^3 in the stratosphere in comparison to that in the troposphere, which can be explained, firstly, by more intense creation in the stratosphere, and, secondly, by their accumulation in the stratosphere as a consequence of thermonuclear weapons testing.

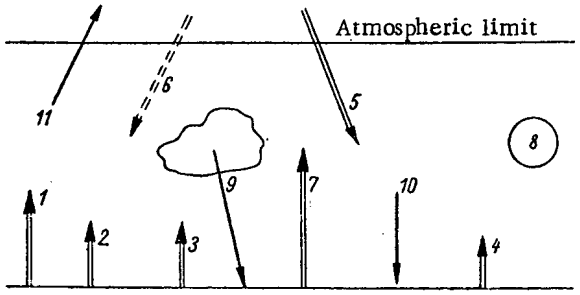

Fig. 2. A qualitative scheme for the circulation of radioactive materials in the atmosphere; positive terms: 1) inflow of radioactive material (r. m.) because of emission of emanations from the soil; 2) inflow of r. m. with dust; 3) inflow of r. m. by evaporation and penetration of spray into the atmosphere; 4) inflow of r. m. by the combustion of carbonaceous fuels; 5) inflow of r. m. with meteoritic material; 6) creation of isotopes by the action of cosmic rays; 7) penetration of r. m. through atomic weapons testing and the use of atomic energy for peaceful purposes: negative terms: 8) radioactive disintegration; 9) washing-out of r. m. by rain; 10) deposition of r. m. with dust; 11) departure of r. m. beyond the limits of the atmosphere.

Study of the time variations in the concentration of radioactive isotopes in the air make it possible to investigate atmospheric turbulence. Yearly variations in artificial contamination of the atmospheric surface layer points out the existence of seasonal variations; a maximum is observed in the spring, a minimum in the fall [26, 27]. These seasonal variations are connected with seasonal changes in the penetrability of the tropopause and with mobility of the stratospheric air mass, and, in turn, can serve as a means for investigating the properties of the tropopause and the mechanism of interchange between troposphere and stratosphere.

A scheme for the processes of atmospheric contamination by radioactive isotopes and atmospheric purification is shown in Fig. 2. It would be advisable to evaluate quantitatively the various components in the balance of radioactive isotopes which get into the atmosphere and to set up the problem of the quantitative study of the circulation of the different isotopes between the atmosphere, on the one hand, and the lithosphere and hydrosphere of the Earth, on the other. The study of these processes has only begun at the present time. Only the circulation of radon and its daughter products has been described quantitatively [28]. There has also been an attempt to calculate quantitatively the entrance of radiocarbon, beryllium, and tritium into the lithosphere and hydrosphere [5]. However, this problem is still unsolved because of the great complexity in the interactions of the lithosphere, hydrosphere, and atmosphere.

At the present time, the study of the penetration of radioactive materials into the atmosphere from the Earth's surface along with dust, about which there is no quantitative data whatever, is of interest. As a verification of the important role of this process, one might perhaps consider the work [29] in which it was shown that, in connection with measurements of artificial radioactivity, the ratio of the concentration of long-lived isotopes (observed one to two months after sample collection) to a short-lived isotopes was always less than one on a mountain, and more than one in a valley. Quantitative evaluations of this process are of paramount importance for calculation of the accumulation of radioactive fallout on the Earth [30].

No less ahead of us is the problem of investigating the transfer of radioactive materials, along with air masses, between continents and oceans, between various latitudes, and between the northern and southern hemispheres.

Radioactive isotopes which are created in the stratosphere, then penetrate into the troposphere, and from it are deposited on Earth. This situation can serve as a source of information about air mass mixing processes between stratosphere and troposphere which is of great interest to meteorology. Thus, the problems of radioactive material balance in the atmosphere open up a very broad perspective. In connection with this, it is possible to set up the problem of study of the density of deposition of the various radioactive and nonradioactive isotopes on the Earth, their ultimate fate, and their possible role in the formation of the elements distributed in the Earth's crust.

Artificial contamination of the atmosphere by atomic weapons testing and by industrial use of atomic energy puts a number of problems before the research meteorologist. First of all, it is possible to study the processes of turbulent mixing and diffusion in the surface layer of the atmosphere because of the presence of easily detected

radioactive material in the air. Recommendations for the placing of nuclear reactors must be based on the technical results of these studies.

The study of the temporal course of meteorological processes by the investigation of the radioactivity of meteorological elements is also of interest, for example, the residence time of water and carbon dioxide in the atmosphere, the transfer of air masses between continents, the time for formation and growth of drops in a cloud, etc. [5].

In conclusion, one can say that nuclear meteorology is beginning to attract the attention of numerous investigators, and that the group of problems calling for solution is very broad and interesting.

LITERATURE CITED

1. L. I. Gedeonov, "Atomnaya Énergiya," 3, 3, 260 (1957).
2. O. I. Leipunskii, "Atomnaya Énergiya," 4, 1, 63 (1958).
3. J. Elster and H. Geitel, Phys. Zs. 2, 40, 590 (1901).
4. V. Gess, Ionization of the Atmosphere and Its Causes [in Russian] (Moscow-Leningrad, Gosizdat, 1930).
5. B. I. Styro, Problems of Nuclear Meteorology [in Russian] Inst. Geol. i Geograf. AN Lit. SSR, Vil'nyus (1959).
6. B. I. Styro and Ch. A. Garbalyauskas, Tr. AN Lit. SSR, Ser. B, 2, 21 (1955).
7. Ch. A. Garbalyauskas, Tr. AN Lit. SSR, Ser. B, 1, 69 (1956).
8. D. Lal, E. Goldberg and M. Koide, Phys. Rev. Let. 3, 8, 350 (1959).
9. W. Libby, Scient. Am. 4, 38 (1954).
10. D. Lal, P. Walhotra and B. Petrs, J. Atmos. and Terr. Phys. 4, 12, 306 (1958).
11. T. Kohman and W. Ehmann, Cosmic-ray induced radioactivity in meteorite and tektites, Radioisotopes Scient. Res. (International Conference, Paris, Sept. 9-20, 1957), Vol. 2 London - New York - Paris - Los Angelos - Pergamon Press (1958), p. 661.
12. F. L. Fureman and Derelice, J. Geophys. Res. 64, 8, 1102 (1959).
13. B. I. Styro and Ch. A. Garbalyauskas, Tr. AN Lit. SSR, Ser. B, 3, 55 (1955).
14. B. I. Styro, Nauchnye soobshcheniya AN Lit. SSR, Inst. Geol. i Geograf., 3, 61 (1956).
15. V. Yu. Potsyus, Nauchnye soobshcheniya AN Lit. SSR, Inst. Geol. i Geograf. 10, 1, 63 (1959).
16. M. Wilkenning, Rev. Scient. Instrum. 23, 1, 13 (1952).
17. K. Stierstadt and M. Papp, Atomkernenergie 5, 12, 459 (1960).
18. W. Marquardt, Z. Meteorol. 13, 9, 10, 237 (1959).
19. S. G. Malakhov, Izv. AN SSSR, Ser. geofiz. 4, 620 (1961).
20. D. Peirson, R. Crooks and E. Fischer, Radioactive fallout in air and rain, Atomic Energy Res. Establ. No. 3359 (1960).
21. W. Anderson et al., Nature (England) 186, 4720, 223 (1960).
22. A. Wensel, Atompraxis 5, 10-11, 419 (1959).
23. B. I. Styro, Nauchnye soobshcheniya AN Lit. SSR. Inst. Geol. i Geograf. 10, 1, 39 (1959).
24. S. G. Malakhov, Izv. AN SSSR, Ser. geofiz. 9, 1344 (1959).
25. F. Hagemann et al., Science 130, 3375, 542 (1959).
26. N. Stewart, Bull. Schwez. Akad. met. Wiss. 14, 5-6, 407 (1958).
27. L. Machta and R. List, J. Geophys. Res. 64, 9, 1267 (1959).
28. B. I. Styro, Nauchnye soobshcheniya AN Lit. SSR. Inst. Geol. i Geograf. 1, 55 (1959).
29. R. Reiter, Naturwissenschaften 47, 13, 300 (1960).
30. V. P. Shvedob et al., "Atomnaya Énergiya," 5, 5, 577 (1958).

All abbreviations of periodicals in the above bibliography are letter-by-letter transliterations of the abbreviations as given in the original Russian journal. *Some or all of this periodical literature may well be available in English translation.* A complete list of the cover-to-cover English translations appears at the back of this issue.

LETTERS TO THE EDITOR

DELAYED-NEUTRON YIELDS IN THE FISSION OF Pu^{239} AND Th^{232} BY 14.5 MEV ENERGY NEUTRONS

V. I. Shpakov, K. A. Petrzhak, M. A. Bak,

S. S. Kovalenko and O. I. Kostochkin

Translated from Atomnaya Énergiya, Vol. 11, No. 6 , pp. 539-540,
December, 1961
Original article submitted July 18, 1961

A knowledge of the delayed-neutron yields as a function of the neutron energy causing the fission is of theoretical and practical importance. Existing data [1] on the fission of various nuclei by thermal neutrons and fission spectrum neutrons show that the total delayed-neutron yield per fission event for odd nuclei does not depend to a great extent on the excitation energy of the fissioning nucleus. Measurements of delayed-neutron yields in the fission of U^{235} by monochromatic neutrons with energies of 2.4, 3.3 and 14.5 Mev [2] show that up to 3.3 Mev the yield does not change, at an energy of 14.5 Mev it is doubled. The delayed-neutron yields during the fission of even nuclei (U^{238} and Th^{232}) are also doubled when the energy of the bombarding neutrons from the fission spectrum is increased to 14.5 Mev [3]. In the theoretical consideration [4] it is assumed that the probability of emission of a delayed neutron from a given nucleus is constant. The change in the delayed-neutron yield with increase in the excitation energy of the fissioning nucleus is therefore determined by the change in the yield of nuclei emitting the delayed neutrons. These nuclei are mainly near the peaks of the mass distribution curve. It is known that the yield of fragments corresponding to a peak remains practically constant over a wide range of energies of particles causing fission. Furthermore, with increase in the excitation energy the radioactive chains are shortened, which should lead in the general case to a reduction in the total yield of the nuclei emitting delayed neutrons. In the region of symmetrical fission, where the yields of fragments increase considerably with increase in the excitation energy, there is little probability of the existence of nuclei emitting delayed neutrons since these nuclei are at a distance from the closed neutron shells. This is confirmed by an analysis of the decay curves given in [3]. It might therefore be expected that the total yield of delayed neutrons should decrease somewhat with increase in the excitation energy.

As shown above, the yield of delayed neutrons was measured with thermal neutrons, fission neutrons and with 14.5 Mev energy neutrons only for U^{235}. We measured the yield of delayed neutrons in the fission of Pu^{239} by 14.5 Mev energy neutrons. For this nucleus we know the yield of delayed neutrons for fission by thermal neutrons and neutrons of the fission spectrum. For comparison with known data, we also measured the delayed-neutron yield for the fission of Th^{232} by neutrons with the same energy.

The delayed-neutron yield was defined as the ratio of the number of delayed neutrons forming in the fissioning material in 1 sec with saturation, to the number of fissions in the specimen during this time. A diagram of the experiment is shown in the figure. The plutonium or thorium specimens were 5 cm discs (2), enclosed in cadmium containers of 1 mm thickness. They were irradiated by a stream of neutrons (1) with an energy of 14.5 Mev, obtained in a neutron generator in the T (d, n) He^4 reaction. The target (3) immediately behind the specimen was irradiated at the same time in order to determine the number of fissions in the specimen. The target was a thin layer of fissionable material applied to a stainless steel backing and was one of the electrodes in the ionization chamber (4). The diameters of the target and specimen were the same.

To determine the number of delayed neutrons emitted by the specimen, after irradiation the specimen was placed for about 0.2 sec in a neutron detector (5), at a distance of 1.5 m from the neutron source. The detector was in the form of 17 SNM-5A boron counters enclosed in a common paraffin block. The efficiency of the neutron detector and its dependence on the neutron energy was determined by means of calibrated neutron sources with energies of 50, 200, 850 kev and 5 Mev. The pulses from the neutron detector were recorded on motion picture film together with time marks.

The moment of the end of irradiation, i.e., the switching-off of the neutron generator ion current, made to coincide with the ejection of the specimen, was also recorded on the film with an accuracy of 0.02 sec. The neutron activity decay curve was plotted from the obtained data. The number of delayed neutrons forming in the specimen was determined by extrapolating this curve to the end of irradiation. Since the time for feeding the specimen into the neutron detector was 0.2 sec and the shortest period of the delayed neutrons was 0.16 sec, it was essential to estimate the contribution of neutrons with such a period to the total delayed-neutron yield. For this purpose, the specimen was placed inside the neutron detector and irradiated for various periods of time followed by recording of the delayed neutrons. The time of irradiation varied between 0.1 sec and 10 min.

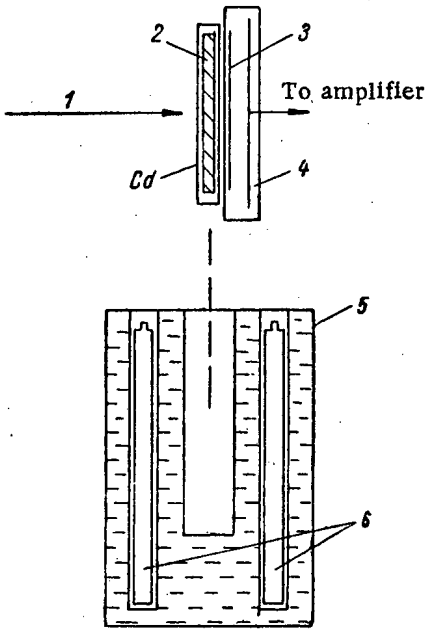

Diagram of experiment on the determination of delayed-neutron yields: 1) direction of neutron stream; 2) specimen in cadmium container; 3) target; 4) ionization chamber for recording fission events; 5) delayed-neutron detector; 6) SNM-5A neutron counters; 7) paraffin block.

The obtained data indicate that during irradiation to saturation the contribution of neutrons having a period of 0.16 sec does not exceed the error of the experiment. The number of delayed neutrons at the zero time can therefore be obtained by extrapolating the curve from 0.4 sec. The time of irradiation needed for saturation was determined experimentally by irradiating specimens for 1 hour and then analyzing the neutron activity decay curve. It was found that if there are neutrons with periods between 1 min and 1 hour, their contribution does not exceed the error of the experiment.

The following data were obtained from the measurements: The total delayed-neutron yield per fission is 0.0130 ± 0.0015 for Pu^{239} and 0.075 ± 0.007 for Th^{232}. The data for Th^{232} agree with the results of [2, 3]. The delayed-neutron yield for the fission of Pu^{239} by thermal neutrons is 0.0061 and during fission by fission spectrum neutrons it is 0.0063 of a neutron per fission [1]. It therefore also follows from our data that the total delayed-neutron yield for the fission of Pu^{239} is doubled on changing to neutrons with an energy of 14.5 Mev. The increase in the total delayed-neutron yield is presumably due to the increased probability of emission of a neutron from the given nucleus, depending on certain characteristics of the fission process. This hypothesis can be checked by studying the emission of delayed neutrons from certain nuclei at different excitation energies of the fissioning nuclei and also by studying the correlation between the β-particles, γ-quanta and delayed neutrons.

LITERATURE CITED

1. G. Keepin, T. Wimett and R. Zeigler, Phys. Rev. 107, 1044 (1957); J. Nucl. Energy 6, 1 (1957); G. R. Keepin and T. F. Wimett, Reports of the International Conference on the Peaceful Uses of Atomic Energy (Geneva, 1955), Vol. 4 [in Russian] (Moscow, Acad. Sci. USSR Press, 1957), p. 197.
2. B. P. Maksyutenko, "Atomnaya Énergiya," 7, 474 (1959).
3. K. Sun, R. Charpie, F. Pecjak, B. Jennings, J. Nechaj and A. Allen, Phys. Rev. 79, 3 (1950).
4. G. R. Keepin, "Atomnaya Énergiya," 4, 3, 250 (1958); A. K. Pappas, Transactions of the Second International Conference on the Peaceful Uses of Atomic Energy [Geneva, 1958). Vol. 2, Selected Reports of non-Soviet Scientists [in Russian] (Moscow, Atomic Energy Press, 1959), p. 308.

All abbreviations of periodicals in the above bibliography are letter-by-letter transliterations of the abbreviations as given in the original Russian journal. *Some or all of this periodical literature may well be available in English translation.* A complete list of the cover-to-cover English translations appears at the back of this issue.

THE KINETIC ENERGY OF Th^{232} PHOTOFISSION FRAGMENTS

B. A. Bochagov, A. P. Komar, G. E. Solyakin

and V. I. Fadeev

Translated from Atomnaya Énergiya, Vol. 11, No. 6, pp. 540-543,
December, 1961
Original article submitted April 24, 1961

By studying the kinetic energy distribution of fragments, using the pulse conservation law, we can obtain the most probable ratio of the fragment masses $\frac{m_2}{m_1}$ and compare it with the ratio determined radiochemically. By comparing these ratios obtained by such different methods we can obtain reliable values of $\frac{m_2}{m_1}$, free from errors resulting from the use of each method separately. The presence of radiochemical data [1] on the fragment masses of Th^{232} photofission, obtained under very similar conditions ($E_{\gamma\ max} = 69$ Mev), led us to undertake the present work. It would be interesting to compare the results obtained in the study of Th^{232} photofission with results obtained in the study of Th^{232} fission by neutrons with an energy of 14 Mev [2].

The experimental method used in this work is the same as the method used in our laboratory to study the photofission of U^{238} [3]. Changes were made in the recording part of the apparatus. The pulses corresponding to heavy and light fragments, after amplification and forming, were fed to the vertical and horizontal plates, respectively, of a cathode oscillograph. In this way each fission event was marked on the oscillograph screen by a bright spot, the coordinates of which were proportional to the kinetic energies of the fragments. The coordinate axes (the axes of the kinetic energy of the fragments) were marked on the screen with a special device. The position of the bright spots on the screen was recorded automatically by a photographic apparatus. Usually about 150 spots were recorded on one exposure. This number was determined by the probability of superimposition of individual spots. The calibration and quality of operation of the coordinate circuit were checked after each five frames.

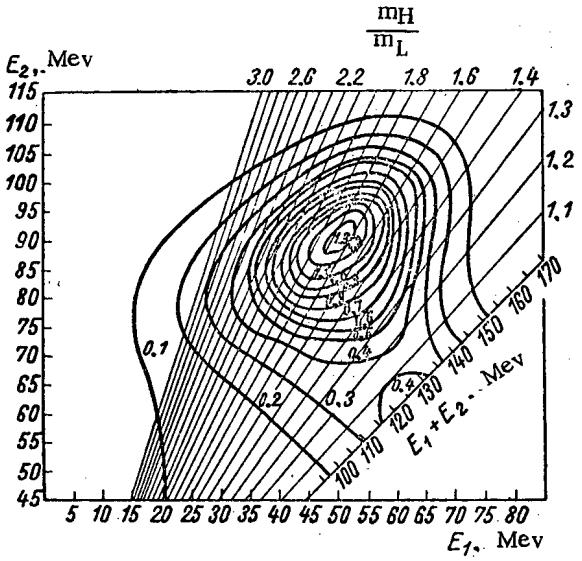

Fig. 1. Contour diagram of the energy distribution of Th^{232} nuclei photofission fragments at $E_{\gamma\ max}$ = 70 Mev.

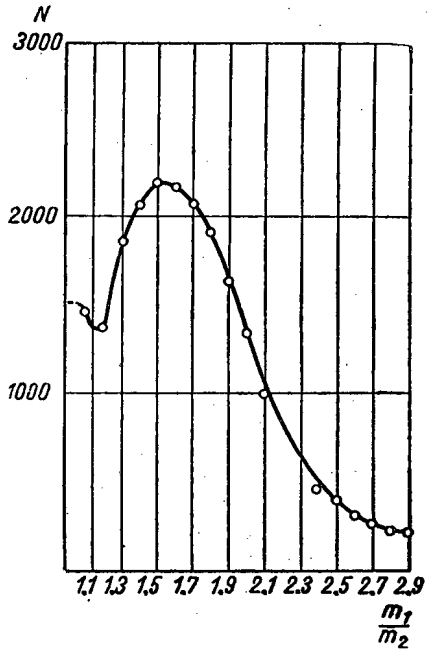

Fig. 2. Mass distribution of photofission fragments of Th^{232} nuclei.

The target was a preparation of thorium nitrate of 150 $\mu g/cm^2$ thickness, applied to an aluminized collodion film of 30 $\mu g/cm^2$ thickness (aluminum + collodion). The target was at a distance of 2 m from the γ-radiation source. About 10 fission events were recorded in 1 min.

When processing the results of the investigations, 26,000 recorded fission events were used. Figure 1 shows a half of the contour diagram where, as for all subsequent curves, in accordance with established tradition the kinetic energy values were used without corrections for losses in the target and for the ionization defect. On the contour diagram for Th^{232}, as for U^{238}, two "hills" and "crosspieces" can readily be seen. The peaks of the "hills" correspond to the most probable kinetic energies of the light and heavy fragments.

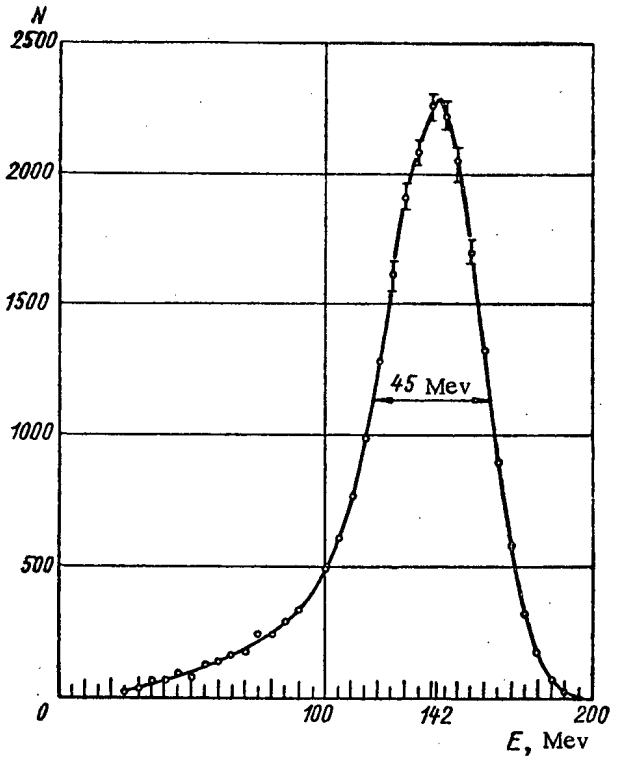

Fig. 3. Spectrum of total kinetic energy of photofission fragments of Th^{232} nuclei.

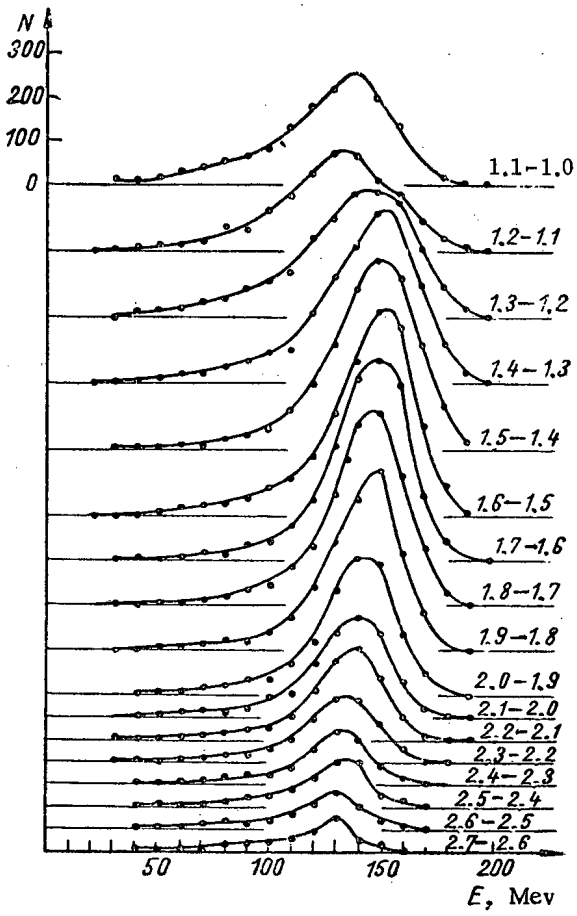

Fig. 4. Distribution of total kinetic energy $E = E_1 + E_2$ of photofission fragments of Th^{232} nuclei for various mass ratios of the fragments $\frac{m_2}{m_1} = \frac{E_1}{E_2}$. The scale along the ordinate axis for all graphs is the same and is shown on the graph for $\frac{m_2}{m_1} = 1.1 - 1.0$.

The presence of two "hills" and "crosspieces" is probably due to the existence of two types of nuclear fission: asymmetric and symmetric. The crosspiece is obviously partially due to the energy losses of the fragments in the target. However, this effect is not decisive. The clearly expressed third peak in the mass distribution, corresponding to symmetrical fission, was detected previously in the fission of the Ra^{226} nucleus [4]. In a number of cases the position of the peak of the heavy fragments in the mass distribution is constant. This leads to a systematic reduction in the ratio $\frac{m_2}{m_1}$ as the mass of the fissioning nucleus increases. For example, the ratios of $\frac{m_2}{m_1}$ for Th^{232}, U^{238} and Cf^{252} are equal to 1.56; 1.36 and 1.31, respectively. Figure 2 is a curve for the fission fragment yield as a function of $\frac{m_2}{m_1} = \frac{E_1}{E_2}$. The most probable value is $\frac{m_2}{m_1} = 1.56$. This value coincides (within the limits of error of the experiment) with the value of 1.52, obtained radiochemically [1]. The total energy distribution of the fragments $E = E_1 + E_2$ is shown in Fig. 3. The most probable value of E is less and the half-width of the maximum of the

curve is greater than the corresponding values for the case of U^{238} photofission. Figure 4 shows the total kinetic energy distribution for various ratios of $\frac{m_2}{m_1}$. In contrast to the curves for U^{238}, the Fig. 4 curves have no clearly-expressed second maximum, although some hints of its existence can be seen on the curve for values of $\frac{m_2}{m_1}$ between 1.1 and 1.2.

Rotating the twin camera through 180° about an axis perpendicular to the γ-radiation beam did not affect the results of the measurements.

In conclusion we give a table of values which are usually used to characterize the energy distributions of nuclear fission fragments.

Characteristics of Energy Distribution of Th^{232} Photofission Fragments

	Most probable values of fragment energies, Mev	
	without corrections for the target thickness and ionization defect	with corrections for the target thickness and ionization defect
Heavy	52 ± 2	52 + 2 + 6.8 = 61 ± 2
Light	89 ± 2	89 + 2 + 5.6 = 97 ± 2
Heavy + Light	141 ± 3	143 + 2 + 12 = 157 ± 3
Half-width of peak of total energy	42 ± 2	
Half-width of peak of light and heavy fragments	28 ± 1	

The authors would like to thank the group operating the synchrotron of the Institute of Physiotherapy, Academy of Sciences, USSR for continuously operating the accelerator and also G. N. Nikolaev and K. Shvets for their technical assistance in this work.

LITERATURE CITED

1. D. Hiller and D. Martin, Phys. Rev. 90, 581 (1953).
2. A. N. Protopopov, M. I. Kuznetsov and É. G. Dermendzhiev, ZhETF 38, 384 (1960).
3. B. A. Bochagov, A. P. Komar and G. E. Solyakin, ZhETF 38, 1374 (1960).
4. R. Jensen and A. Fairhall, Phys. Rev. 109, 942 (1958).

All abbreviations of periodicals in the above bibliography are letter-by-letter transliterations of the abbreviations as given in the original Russian journal. *Some or all of this periodical literature may well be available in English translation.* A complete list of the cover-to-cover English translations appears at the back of this issue.

A PHOTOEMULSION FOR NUCLEAR INVESTIGATIONS (PR-2)

N. A. Perfilov, N. R. Novikova, V. I. Zakharov

and Yu. I. Vikhrev

Translated from Atomnaya Énergiya, Vol. 11, No. 6, pp. 543-544,
December, 1961
Original article submitted April 27, 1961

The first high density (60 grains per 100 μ) in traces of relativistic particles was obtained in our specially fine-grain emulsion (PR) by using the method of double sensitization: sensitization by gold and hypersensitization by triethanolamine [1]. However, in some cases the poor preservation of the photolayers hypersensitized in the triethanolamine means that the second stage has to be left out.

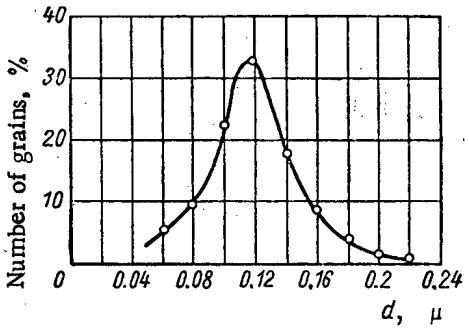

Fig. 1. Curve of distribution of AgBr microcrystals in the finished emulsion PR-2 (d is the crystal dimension).

In order to obtain sufficiently high density in traces of relativistic particles without additional sensitization of the triethanolamine, experiments were conducted to develop a new emulsion. Since the PR emulsion sensitized only with gold records traces of relativistic particles with a density of 20-25 grains per 100 μ, it should be expected that under the conditions of synthesis of our emulsions (an excess of $AgNO_3$ during emulsification) even a small increase in size of the microcrystal could lead to a considerable increase in the trace density. In fact, in our experiments, during the synthesis, an increase in the most probable dimensions of the AgBr microcrystals from 0.08 to 0.12 μ led to an increase in trace density of the relativistic particles to 40-45 grains per 100 μ.

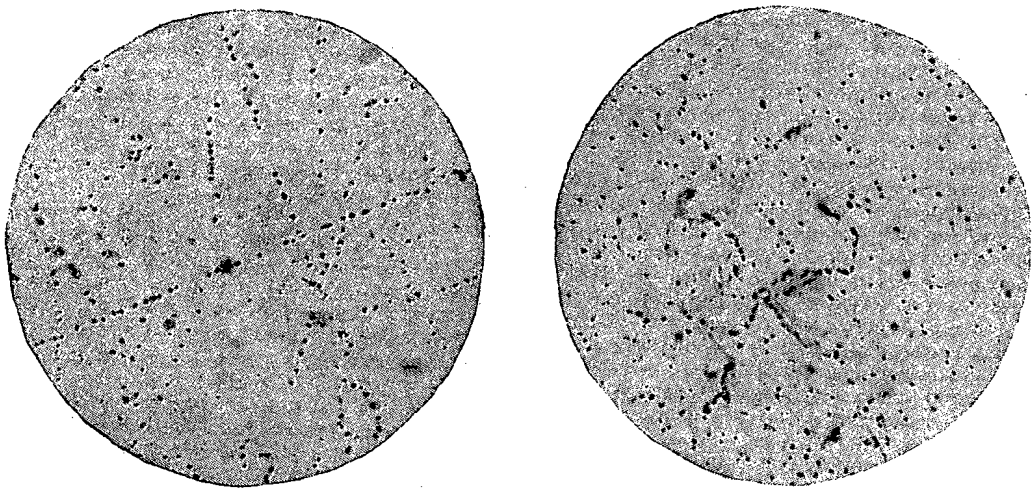

a b

Fig. 2. Microphotographs of traces of relativistic (a) and slow (b) electrons.

Figure 1 shows the distribution of AgBr microcrystals in the finished PR-2 emulsion. Figure 2 shows microphotographs of traces of relativistic and slow electrons recorded in the PR-2 emulsion.

LITERATURE CITED

1. N. A. Perfilov, N. R. Novikova and E. I. Prokof'eva, Reports of the Conference on the Method of Thick-Layer Photoemulsions [in Russian] Dubna, Nuclear Research Institute (1957).

AN APPARATUS FOR STUDYING HEAT EXCHANGE IN FLUIDIZED-BED REACTORS

N. I. Syromyatnikov, L. K. Vasnova, and Yu. N. Shimanskii

Translated from Atomnaya Énergiya, Vol. 11, No. 6, pp. 544-546,
December, 1961
Original article submitted March 28, 1961

Recently, papers have appeared on the leading designs of fluidized-bed reactors in which the nuclear fuel is suspended in the stream of coolant circulating throughout the closed circuit [1, 2]. These reactors have a number of advantages over heterogeneous reactors. However, as yet fluidized-bed reactors have not been studied to any great extent.

In the development of heat exchange equipment with a fluidized bed an important part is played by the experimental study of heat transfer from the particles (the sources of heat) to the medium cooling them. In the S. M. Kirov Urals Polytechnical Institute a high-frequency method [3] has been developed to study heat exchange in a fluidized bed, including heat exchange between particles and the medium under stationary conditions.

For processes of heat exchange between the particles and medium in a fluidized bed the thermal criteria, as for ordinary conditions of heat exchange, are:

$$Nu=\frac{\alpha d}{\lambda} \text{ and } Pr=\frac{\nu}{a},$$

where α is the coefficient of heat transfer from the particles to the medium; d is the particle diameter; λ is the coefficient of thermal conductivity of the medium; ν is the coefficient of kinematic viscosity of the medium; a is the coefficient of temperature conductivity of the medium.

The determining criteria, describing the effect of the hydrodynamics of the process on the heat exchange intensity, are the pseudoliquefaction number W or the Fedorov criterion Fe and also the Reynolds criterion Re. In some cases we must add simplexes, giving the ratio of the reactor diameter to the particle diameter $\frac{D_r}{d}$, to the number of determining criteria.

It is known that heat exchange between the particles and medium in a fluidized bed with a ratio of $\frac{D_r}{d} \geq 20$ becomes self-simulating with respect to the reactor dimensions. This condition is observed even in apparatuses with small diameters, starting with 20 mm, since the dimensions of the particles in the fluidized bed are fairly small. The criterional equation is therefore written in the form

$$Nu=f(Re;\ Pr;\ W)$$

or, for a gas,

$$Nu=f_1(Re;\ W).$$

The operation of the proposed apparatus is based on a method where the continuous liberation of heat in the volume of particles forming the fluidized bed is due to eddy currents of a high-frequency magnetic field. This makes it possible to imitate the liberation of heat in the fuel of a fluidized-bed reactor and the transfer of heat from the fuel elements to the medium. The control of the heat liberated by the eddy currents depends on the frequency and intensity of the magnetic field, on the particle dimensions and the electromagnetic properties of the particle material. To change the magnetic field intensity, various inductors must be used and the operating conditions of the high-frequency generator must be changed.

For each current frequency there is an optimum particle size for which the power liberated per unit volume has the greatest value. The table gives these characteristics for copper and steel.

Optimum Particle Sizes for Copper and Steel

Frequency of current, f, cps	Copper at 20°C, $\rho = 1.7 \cdot 10^{-6}$ Ω·cm, $\mu = 1$	Steel at 20°C, $\rho = 10 \cdot 10^{-6}$ Ω·cm, $\mu = 100$
50	4.4 cm	32 cm
2000	0.7 cm	5 cm
10^6	0.3 mm	2.3 cm

Induction tempering generators with a frequency of 300-500 kc can be used as the high-frequency source for studying the heat exchange of the particles. Materials with a low magnetic permeability must be used to obtain fluidized-bed conditions when using the high-frequency method for heating the particles. Ferromagnetic materials cannot be used for the particles since the particles would be arranged along the magnetic lines of force. Our investigations showed that the most suitable particle materials are copper, aluminum and graphite.

The heat liberation in the bed can therefore be controlled over wide limits by changing the inductor design (diameter, height, number of turns), the quality of the particle material, the particle sizes and the field intensity; high volume densities of the heat flow can then be obtained.

The diagram of an experimental apparatus for studying heat exchange is shown in Fig. 1. It consists of a glass reactor of diameter 20-40 mm, height 300-400 mm, with double walls. The air is evacuated from the space between the walls. Particles with 0.2-2 mm diameters are poured onto the supporting grid. The flow of fluidizing medium is measured by a valve arrangement, the temperature of the medium in the stationary process before and after the reactor is measured by inertialess copper-constantan thermocouples of 0.1 mm diameter. The temperature of the medium at the reactor outlet during the transitional processes is recorded on the tape of an EPP-09 fast electronic potentiometer or a loop oscillograph.

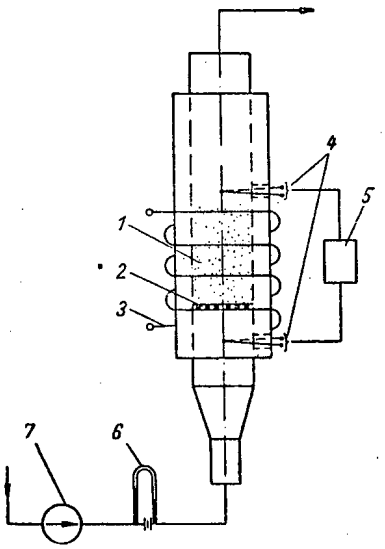

Fig. 1. Apparatus for studying heat exchange: 1) charge forming the fluidized bed; 2) supporting grid; 3) generator inductor; 4) thermocouples; 5) electronic potentiometer; 6) flow meter; 7) blower.

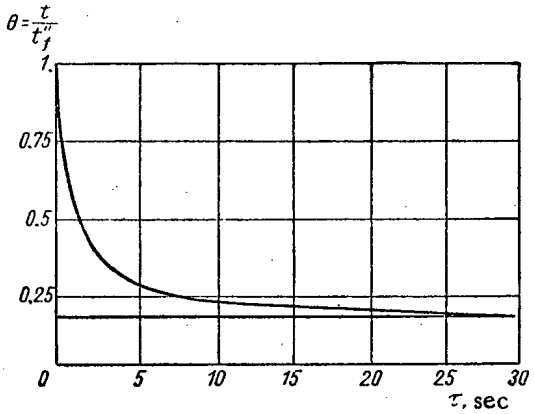

Fig. 2. Cooling curve for the medium of the fluidized bed.

The experiment was performed in the following order. Before the start of the experiment the reactor was filled with material, the amount of which was selected to give a fluidized bed of a certain structure. The blower was then used to set the charge into motion and a high-frequency voltage was applied to the inductor. When stationary conditions were reached the temperatures at the inlet and outlet of the reactor and the flow of the medium were measured. After this the high-frequency generator was switched off and the transitional cooling process commenced, the temperature of the medium being recorded by an electronic potentiometer or oscillograph. To determine the heat transfer coefficient from the measured values and the known total heat exchange surface it was essential to know the temperature of the particle surface. It could be determined calorimetrically with a special calorimeter or by the "flow" method, using the same reactor for this purpose.

The following is used as the main calculation equation for stationary conditions

$$\alpha = \frac{Q_s}{(t_T - t_f) F}, \tag{1}$$

where Q_s is the amount of heat transmitted by the particles to the stream of medium in the stationary process; F is the total surface of particles in the fluidized bed; t_T is the temperature of the particle surface; t_f is the mean temperature of the medium, equal to the arithmetical mean of the temperatures at the inlet and outlet of the reactor. In Eq. (1) the amount of transmitted heat, according to the measurements, is equal to

$$Q_s = Gc (t_f'' - t_f'), \tag{2}$$

where G is the gravimetric flow of the medium; c is the specific heat of the medium; t_f' and t_f'' are the temperatures of the medium at the inlet and outlet of the reactor.

The thermal balance equation compiled for the period of cooling of the particles can be used to determine the temperature of the particle surface t_T with the condition of small internal thermal resistance of the particles and with very small heat losses to the surrounding medium.

When using the "flow" method the flow of medium through the reactor in the cooling process remains the same as under the stationary conditions.

The amount of heat under nonstationary conditions Q_{ns} is determined from the expression

$$Q_{ns} = Gc (t_k - t_f') \tau, \tag{3}$$

where τ is the period of cooling; t_k is the mean integral temperature of the medium, obtained from the cooling curve of the medium, taken with the potentiometer or oscillograph.

The cooling curve obtained experimentally for one of the systems is shown in Fig. 2 in dimensionless coordinates. The value of Q_{ns} can be determined using this curve and the given equation. The particle temperature t_T and then the coefficient of heat transfer α are obtained experimentally from the found value of Q_{ns} from the equation of the thermal balance.

The experiments showed that the developed method is sufficiently simple and accurate, and is perfectly suitable for studying heat exchange in reactors between particles and gas (liquid) and also for studying heat exchange during boiling of the fluidizing medium.

LITERATURE CITED

1. J. Morris, C. Nicholls and F. Fenning, Trans. Instn. Chem. Engrs. 3, 4, 168 (1956).
2. B. V. Petunin, Heat Engineering in Nuclear Installations [in Russian] (Moscow, State Atomic Energy Press, 1960).
3. N. I. Syromyatnikov, A High-Frequency Method for Studying Heat Exchange in a Fluidized Bed, Transactions of the S. M. Kirov Urals Polytechnical Institute, Collection 96 [in Russian] (Sverdlovsk, 1960), p. 70.

All abbreviations of periodicals in the above bibliography are letter-by-letter transliterations of the abbreviations as given in the original Russian journal. *Some or all of this periodical literature may well be available in English translation.* A complete list of the cover-to-cover English translations appears at the back of this issue.

MEASURING THE RELATIVE FAST-NEUTRON FLUX DISTRIBUTION IN THE VVR-M REACTOR WITH SEMICONDUCTOR DETECTING ELEMENTS

R. F. Konopleva and S. R. Novikov

Translated from Atomnaya Énergiya, Vol. 11, No. 6, pp. 546-547, December, 1961
Original article submitted February 13, 1961

When using reactors to study the effect of nuclear radiation on the properties of a solid it is essential to know the fast-neutron distribution in the experimental channels.

For the relative measurement of the fast-neutron flux the "threshold indicator" method is usually used, using foils of sulfur, phosphorus and aluminum [1], the energy thresholds for which are between 1.5 and 6 Mev.

As well as this fairly simple method there is a method based on the use of the electrical conductivity of semiconductors during bombardment by fast neutrons [2].

When semiconductors are irradiated with fast neutrons crystal lattice defects are formed, the concentration of which is proportional to the integral neutron flux. The appearance of defects leads to a change in the concentration of current carriers, i.e., to a change in electrical conductivity.*

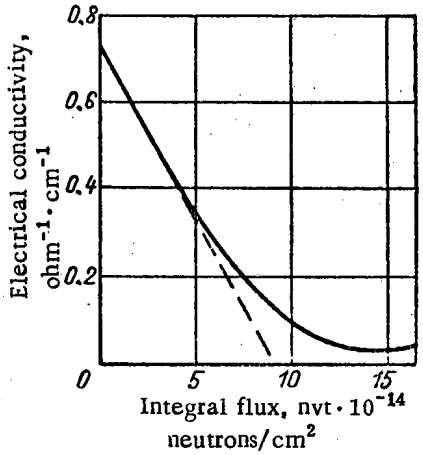

Fig. 1. Dependence of electrical conductivity of n-type germanium on the integral fast-neutron flux.

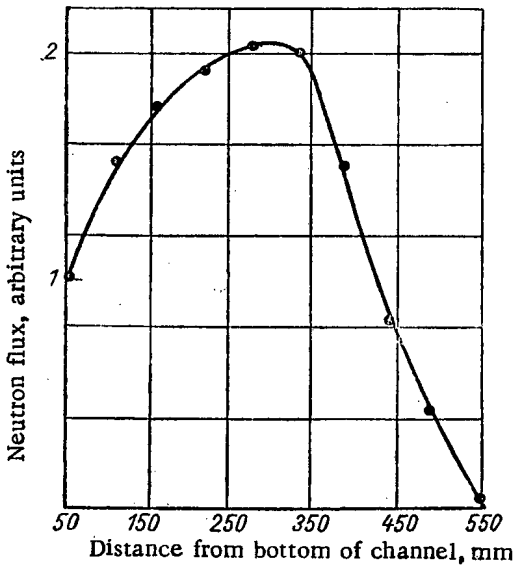

Fig. 2. Relative fast-neutron flux distribution in the vertical channel of the reflector.

* Crystal lattice defects form during irradiation of semiconductors by fast neutrons with energies exceeding a certain critical value. The critical energy depends on the actual crystal structure of the semiconductor. For example, for germanium $E_{cr} \simeq 300$ ev. The defects can also be caused by γ-quanta, however the number of defects formed by one γ-quantum ($N_\gamma = 1.8 \cdot 10^{-4}$) [3] is much less than the number of defects formed by a fast neutron ($N_n = 1.6$) [4]. Since in the described experiment the γ-quanta flux (reduced to 1 Mev) was of the same order as the fast-neutron flux, the fractions of defects caused by the γ-quanta can be neglected.

The dependence of the electrical conductivity of n-type germanium on the integral fast-neutron flux is shown in Fig. 1 [5]. As can be seen from the figure, the electrical conductivity at first changes linearly with the flux.* The rate of change in the electrical conductivity is proportional to the fast-neutron flux intensity, and we used this fact to measure the relative fast-neutron flux distribution in the channels of the reactor in the A. F. Ioffe Physico-technical Institute, Academy of Sciences, USSR.

The neutron-flux detecting elements were specimens of n-type germanium with a specific resistance of 1 ohm · cm, measuring 10 × 1 × 1 mm. The specimens, in 0.5 mm thick cadmium containers,** were placed in the vertical channel of the reflector along the height of the active zone at an equal distance from one another.

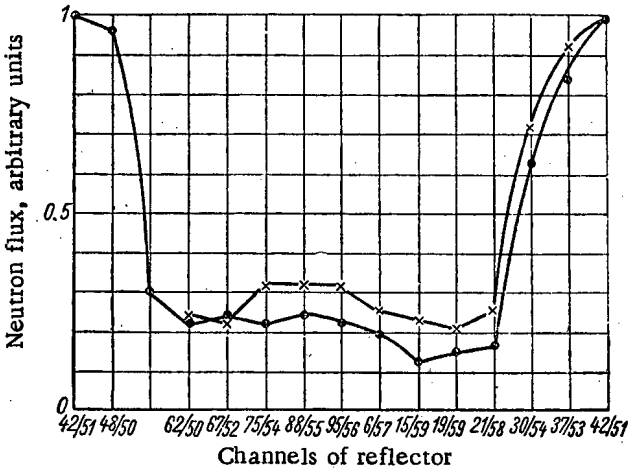

Fig. 3. Relative fast-neutron flux distribution in the experimental channels of a reactor at the level of the center of the active zone: ×) measurements using the activation of gold foils; ●) measurements using the change in electrical conductivity of germanium.

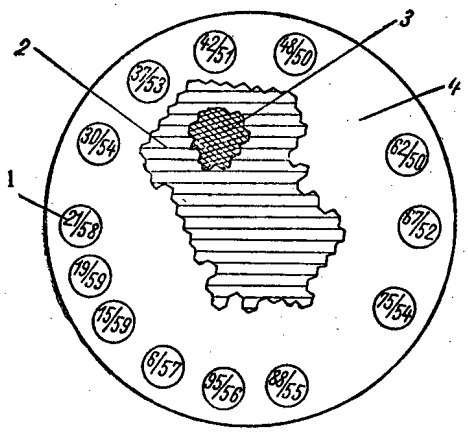

Fig. 4. Arrangement of channels: 1) vertical channels; 2) active zone; 3) water cavity; 4) beryllium reflector.

The electrical conductivity of the specimens was measured during irradiation by the change in the current intensity with a constant voltage applied to the specimen.

Figure 2 gives the relative fast-neutron flux distribution in one of the vertical channels of the reflector. Figure 3 gives the relative fast-neutron flux distribution in all experimental channels at the level of the center of the active zone. The given distribution was obtained for the arrangement of the active zone of the reactor shown in Fig. 4. For comparison, Fig. 3 gives the curve of the relative resonance neutron flux distribution plotted for the activation of gold foils.

This method can therefore be used for the fairly simple measurement of relative fast-neutron flux distributions for energies above 300 ev.

LITERATURE CITED

1. V. A. Dulin, V. P. Mashkovich, et al., "Atomnaya Énergiya," 9, 4, 318 (1960).
2. E. Aleksandrovich and M. Bartenbakh, "Atomnaya Énergiya," 8, 5, 451 (1960).

* The value of the integral flux up to which the change in σ will remain linear is determined by the initial resistance of the specimen and can reach 10^{18} neutrons/cm^2.

** The activation of germanium under the action of thermal neutrons causes chemical impurities which also affect the change in electrical conductivity of the specimens.

In our work the measurements were made in channels where the ratio of the thermal-neutron flux to the fast-neutron flux did not exceed 10 and a 0.5 mm thick cadmium screen was sufficient to reduce the contribution of thermal neutrons to the change in electrical conductivity to a value of about 10%.

3. Fizika tverdogo tela. 1, 9, 1381 (1959).
4. Phys. Rev. 98, 6, 1742 (1955); Phys. Rev. 99, 4, 1171 (1955).
5. Uspekhi fiz. nauk. 50, 1, 51 (1953).

THE USE OF RADIOLUMINESCENCE, CAUSED BY α-RADIATION OF Po^{210}, TO ANALYZE ORES AND MINERALS

I. N. Plaksin, M. A. Belyakov and L. P. Starchik

Translated from Atomnaya Énergiya, Vol. 11, No. 6, pp. 548-549, December, 1961
Original article submitted March 18, 1961

The radioluminescence of minerals has long been known and is a well-studied phenomenon [1] which can be used to analyze ores and minerals. Luminescence under the action of x-rays and γ-rays is used in industry. Cathodoluminescence is widely used for the analysis of ores and minerals [2].

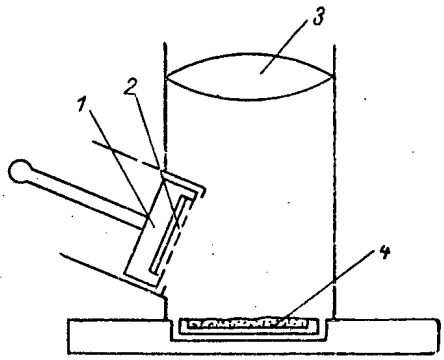

Fig. 1. Instrument for α-luminescence analysis: 1) α-source holder; 2) Po^{210} layer; 3) lens; 4) plate with minerals.

Despite the successful design of the cathodoluminescence apparatus developed by the "Mekhanobr" Institute [3], its use in the field is not always convenient since it is comparatively heavy and needs an electric power supply.

When using radioluminescence to analyze ores and minerals we only need a radioactive isotope, the source of radiation. Beta- and gamma-radiation excite a much weaker luminescence than α-radiation of the same activity. Po^{210} is an especially convenient source of α-radiation.

The half life of Po^{210} is 138.3 days; the energy of α-radiation E = 5.3 Mev; the maximum path of the α-particles in air is 3.8 cm (under normal conditions). The α-radiation of Po^{210} is not accompanied by the radiation of other forms; during the decay of polonium there is only relatively weak gamma-radiation (one gamma-quantum per 10^5 α-particles), which means that this source is comparatively simple to deal with. To prevent contamination of the surrounding objects by the polonium source it is sufficient to cover the layer of polonium with a protective film or thin foil which does not absorb α-radiation, or the film can be applied to the surface of the polonium source. Due to the loss in energy by the α-particles the intensity of luminescence in the film decreases. This decrease is readily compensated for by a small increase in the activity of the polonium α-source.

The visual analysis of ores and minerals with the excitation of luminescence by α-radiation of Po^{210} can be performed with a very simple instrument (Fig. 1). The powder or lumps of rock (up to 20 mm diameter) are placed in a plate under the α-radiator. The luminescence of the minerals is observed by the naked eye or through a lens with appropriate magnification (when using finely-dispersed specimens). The method of analysis of ores and minerals from the number of luminescent particles by means of an α-luminescence apparatus is the same as in cathodoluminescence analysis [3].

When working with such an instrument we used a source with 1.8 C activity. Radioluminescence was observed in calcite, dolomite, fluorite, scheelite and beryl (Table 1).

TABLE 1. Luminescence of Minerals Excited by the α-Radiation of Po^{210}

Mineral	Color	Brightness	Afterglow
Calcite	Red	Large	Weak
Dolomite	Speckled	Very large	"
Scheelite	Violet-blue	The same	Large
Fluorite	Violet	Weak	Very weak
Beryl	Blue	"	The same

TABLE 2. Luminescence of Diamonds Excited by the α-Radiation of Po^{210}

Weight, mg	Size, mm	Brightness	Color
339	− 8 + 4	Large	Blue
182.2	− 10 + 6	Medium	"
239.2	− 8 + 4	Very large	Milky-blue
272.6	− 8 + 4	Large	Greenish

Under the action of α-radiation we also observed intensive radioluminescence of Yakutsk diamonds (Table 2). This means that α-radiation can be used instead of gamma-radiation to sort diamonds.

The described instrument with a photocell (Fig. 2) makes it possible to perform quantitive analysis of minerals, using the photocurrent, as in the cathodoluminescence apparatus [2]. We used the VÉU-1 photoelectron multiplier, working with a photocell.

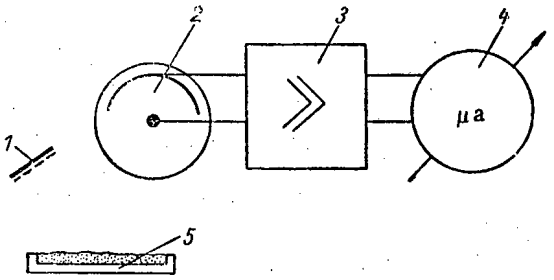

Fig. 2. Diagram of device for radioluminescence analysis using the photocurrent: 1) α-radiator; 2) photocell; 3) direct current amplifier; 4) microammeter; 5) plate with mineral.

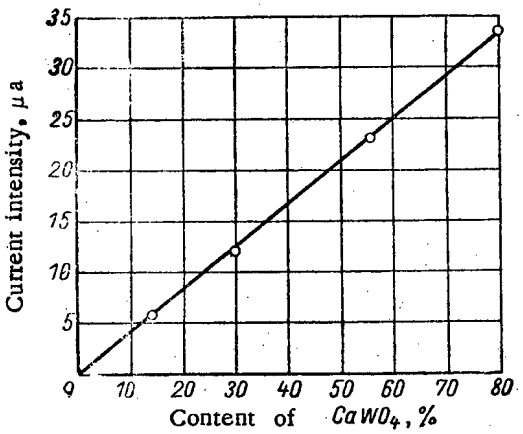

Fig. 3. Dependence of photocurrent on the percentage content of scheelite in the mixture with quartz.

The photocurrent was measured by a direct current amplifier from a "Kaktus" microroentgenmeter with direct current amplification of about 10^4 - 10^5. The photocell was also fed by a "Kaktus" radiometer since the working voltage of the FÉU-1 and the ionization chamber of this microroentgenmeter are the same (220 v).

When determining scheelite in a mixture with quartz the radiator was Po^{210} with an activity of 70 mC. The results of the measurements are given in Fig. 3. During the measurements the photocell was 15 cm from the specimen. By reducing this distance we could analyze specimens with a lower content of mineral. On the other hand, by reducing the distance the Po^{210} activity could be reduced to 5-10 mC.

This apparatus was used to compare the luminescence intensity of scheelite excited by β- and α-radiators with the same activity. The β-radiator was Tl^{204} with an activity of 70 mC ($T_{1/2}$ = 2.71 years, the maximum energy of the β-particles E_m = 0.77 Mev). A plexiglas screen protected the photocell from the direct action of β-radiation. On the average the intensity of radioluminescence under the action of α-radiation was four times that under the action of β-radiation and under optimum geometrical conditions of irradiation by an α-source it was even six times greater.

In the proposed apparatus the α-radiator is used not only because it excites more intensive luminescence than the β- and γ-radiators but also because of the low penetrating capacity of the α-particles in the material (about 20 μ). Since comparatively high activities are needed to excite radioluminescence, the use of an α-source makes the device very simple and practically no shielding is required.

An α-radiator should therefore be used in devices which utilize radiation of radioactive sources to excite the luminescence (for example in devices used to select diamonds). Furthermore, this α-source can be used to determine some elements from nuclear reactions that involve α-particles, as described earlier [4, 5].

LITERATURE CITED

1. K. Pshibram, The Color and Luminescence of Minerals [Russian translation] (Moscow, Foreign Literature Press, 1959).
2. G. F. Komovskii and O. N. Lozhnikova, Luminescence Analysis in the Study of Ores and Minerals [in Russian] (Moscow, State Geology and Technical Press, 1954).
3. P. P. Solov'ev, Recent Advances in the Enrichment of Minerals, Cathodoluminescence Analysis of Ores and Their Enrichment Products, "Mekhanobr," No. 91 [in Russian] (Moscow, Metallurgy Press, 1954).
4. I. N. Plaksin, V. N. Smirnov and L. P. Starchik, Dokl. AN SSSR 128, 6, 1208 (1959).
5. I. N. Plaksin, V. N. Smirnov and L. P. Starchik, Dokl. AN SSSR 127, 3, 618 (1959).

THE ACTIVATION ENERGY OF SOLUTION OF URANIUM DIOXIDE IN A SULFURIC ACID MEDIUM WITH THE PARTICIPATION OF MANGANESE DIOXIDE

E. A. Kanevskii and V. A. Pchelkin

Translated from Atomnaya Énergiya, Vol. 11, No. 6, pp. 549-550, December, 1961
Original article submitted November 9, 1960

Data are given in the literature characterizing the activation energy of solution of uranium dioxide in sulfuric acid solutions in an atmosphere of oxygen (18 kcal/mole) [1] and in carbonate solutions (13.4 kcal/mole) [2]. In connection with the widespread use of pyrolusite in the sulfuric acid leaching of uranium from ores it is of interest to determine the activation energy of the process

$$UO_2 + MnO_2 + 2H_2SO_4 \longrightarrow UO_2SO_4 + MnSO_4 + 2H_2O.$$

The effect of temperature on the solution of uranium dioxide in sulfuric acid, using manganese dioxide as the oxidizing agent, was studied in the temperature range 20-80 °C. The uranium dioxide used in the experiments was obtained by reducing U_3O_8 with hydrogen at 900°C. The content of U (IV) with respect to the total U (IV) and U (VI) was 98%. The "pure" grade of manganese dioxide was used. The grain size of the initial oxides did not exceed 0.074 mm.

The conditions of the experiments were: weight of UO_2 2 g, concentration of H_2SO_4 – 2N; the reaction was carried out in an open beaker, volume of solution 100 ml, speed of stirrer 300 rpm; the temperature, the $UO_2 : MnO_2$ ratio and the duration of the experiment were varied.

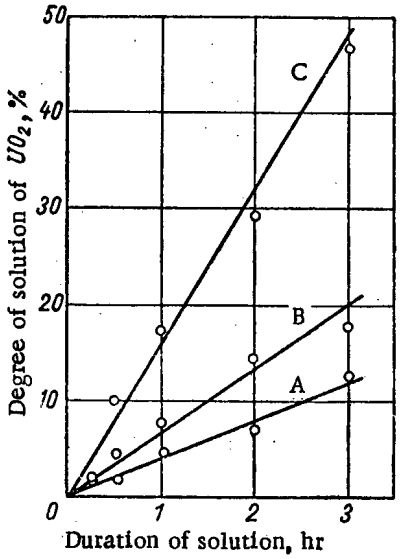

Fig. 1. Effect of the duration of solution and the ratio of the number of moles of MnO_2 and UO_2 on the degree of transfer of uranium dioxide into the sulfuric acid solution. Ratio $MnO_2 : UO_2$; A) 5:1; B) 25:1; C) 125:1.

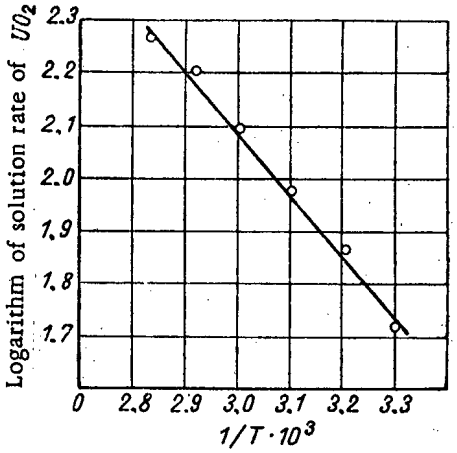

Fig. 2. Dependence of the logarithm of the solution rate of UO_2 on the reciprocal of the absolute temperature.

It can be seen from Fig. 1 that at 20°C the degree of solution of uranium dioxide with an excess of manganese dioxide depends linearly on the duration of the process. It should be emphasized that this dependence is characteristic for the above reaction since the solution of UO_2 in the absence of manganese dioxide was allowed for by means of a blank experiment. In the solution of a relatively small part of the uranium dioxide its rate of solution can therefore be determined readily and with satisfactory accuracy.

As follows from Fig. 2, the solution rates of uranium dioxide in a sulfuric acid medium (mg/liter · min) with manganese dioxide used as the oxidizing agent are described by the Arrhenius equation. From this equation the activation energy of the process was found to be approximately 6 kcal/mole. It should be pointed out that during this process, in which two solid phases and a solution are taking part, steric factors, hindering the reaction, play an important part [3].

LITERATURE CITED

1. T. Mac-Kay and M. Wadsworth, Trans. AIME 212, 597 (1958).
2. V. E. Shortman and M. A. De Sesa, Transactions of the Second International Conference on the Peaceful Uses of Atomic Energy (Geneva, 1958). Selected Reports of non-Soviet Scientists [in Russian] Vol. 7 (Moscow, Atomic Energy Press, 1959), p. 45.
3. E. A. Kanevskii and V. A. Pchelkin, "Atomnaya Énergiya," 10, 2, 138 (1961).

All abbreviations of periodicals in the above bibliography are letter-by-letter transliterations of the abbreviations as given in the original Russian journal. *Some or all of this periodical literature may well be available in English translation.* A complete list of the cover-to-cover English translations appears at the back of this issue.

THE PROBLEM OF AERIAL PROSPECTING IN WOODED REGIONS

A. V. Matveev

Translated from Atomnaya Énergiya, Vol. 11, No. 6, pp. 550-552, December, 1961
Original article submitted May 3, 1961

In [1] an incorrect estimation was made of the screening of γ-radiation of rocks by trees and the authors therefore decided that aerial prospecting in wooded regions was inefficient. In the first place, they used highly-exaggerated data on the reserves of timber in the forests of the USSR, in the second place their method for calculating the absorption of γ-radiation was too approximate, since it did not allow for the anisotropy of the absorbing medium and the dimensions of the localized anomalous sections involved (the calculation formula used in the article, $I = I_0\Phi(\mu d)$, refers to the case of an infinite radiating half-space covered by a homogeneous absorbing layer). Data obtained from more precise calculations and special experimental investigations point to the much lower screening capacity of the trees.

The intensity of γ-radiation at a height h over the center of an anomalous section with a concentration of radioactive material which decreases with the distance from the center according to the law

$$q(x, y) = q_m \exp\left(-4\frac{x^2+y^2}{\lambda^2}\right),$$

is determined by the following approximate expression [2]:

$$I = I_{0m} \exp\left(8\frac{h^2}{\lambda^2}\right) \int_0^{\pi/2} \exp\left(-\frac{8\frac{h^2}{\lambda^2}+\mu_1 h}{\cos\Theta}\right) \sin\Theta\, d\Theta, \quad (1)$$

where $I_{0m} = 2\pi k q_m \varrho_2/\mu_2$ is the γ-radiation intensity at the surface of the section in the center; μ_1 and μ_2 are the effective linear absorption coefficients of the γ-radiation for air and rock; Θ is the polar angle in spherical coordinates with the center at the point of observation (0, 0, h). λ corresponds to the radius of the section.

TABLE 1

Class		H, m	D, cm	No. of trees per 1 hectare	Total wt. of trunks, ton
Pine	I	28.4	33.0	625	680
	II	26.2	30.6	625	560
	III	22.5	26.1	760	440
Spruce	I	29.2	32.3	815	700
	II	25.4	27.2	1010	590
	III	21.4	22.2	1295	440

TABLE 2

λ, m	20	100	∞
$\varkappa$	0.91	0.85	0.70

To allow for the attenuation of the radiation by the trees we introduce in the expression after the integral the factor $M(\Theta) = M_1 M_2$. The factor M_1, determining the screening effect of the trunks, has the apparent value $M_1 = 1 - \alpha(1 - m)$ when $\alpha \leq 1$ and when $\alpha > 1$, is approximated by the formula $M_1 = m^{\alpha}$. Here $m = \exp(-\mu_3 D/2\sin\Theta)$ is the mean value of attenuation by the trunk, of γ-radiation directed at an angle of Θ (μ_3 is the radiation-absorption coefficient for wood; D is the diameter of the lower part of the trunk); $\alpha = \frac{DH}{2S_0}\tan\theta$ is the degree of "shading" of the radiating surface by the tree trunks (H is the height of the trunk, S_0 is the specific area per tree for a given forest density). The values $\alpha > 1$ correspond to overlapping of the "shadows" of the trunks.

The factor $M_2=\exp(-\mu_4 H/2\cos\Theta)$ determines the attenuation of the radiation by the tree tops which form a continuous homogeneous layer of about H/2 thickness. The assumption as to the homogeneity of this layer is justifiable when the degree of density of the tree tops is greater than 0.7-0.8.

Allowing for the tree cover, expression (1) has the form:

for local radiating sections

$$I_M = I_{om}\exp\left(8\frac{h^2}{\lambda^2}\right)\int_0^{\pi/2} M(\Theta)\exp \times\left(-\frac{8\frac{h^2}{\lambda^2}+\mu_1 h}{\cos\Theta}\right)\sin\Theta\, d\Theta, \tag{2}$$

for an infinite radiating surface

$$I_M = I_0\int_0^{\pi/2} M(\Theta)\exp\left(-\frac{\mu_1 h}{\cos\Theta}\right)\sin\Theta\, d\Theta. \tag{3}$$

The corresponding formulas for woodless sections will be expressed for the sake of convenience in calculation by the King function $\Phi(z)=\exp(-z)\cdot -zE_i(z)$:

for local sections

$$I = I_{0m}\exp\left(8\frac{h^2}{\lambda^2}\right)\Phi\left(8\frac{h^2}{\lambda^2}+\mu_1 h\right); \tag{4}$$

for an infinite surface

$$I = I_0\Phi(\mu_1 h). \tag{5}$$

Among the conifers, which occupy about 80% of the whole wooded area of the USSR, mature and over-mature trees predominate. Reference tables on the growth of dense plantations [3] show that the reserve of all timber increases with the age of the plantation (up to the over-mature age), in contrast to the data given in [1]. Table 1 gives average data for mature (100 years old) pine and spruce plantations of the best classes with a degree of completeness equal to 1 [3].

Numerical calculations for the absorption of γ-radiation were performed for a spruce forest of the second class. The mass of the tree top in a dense forest is 10-15% of the mass of the trunk. We increase this figure to 30% to allow for the radiation absorption by the undergrowth and covering rock. The flight altitude h = 50 m is the minimum safety limit for wooded regions. According to the experimental data [4] the effective value of the mass absorption coefficient μ/ρ, approximately allowing for the complex primary spectrum of the γ-radiation of elements in the uranium series and the Compton scattering in the absorber, is 0.03 cm^2/g.

Table 2 gives calculated values of the coefficient of screening of the γ-radiation by the trees $\kappa = I_M/I$ for two local sections and an infinite surface. Calculation according to the formula $I=I_0\Phi(\mu d)$, with the same initial data, gives κ = 0.53. Consequently, because of the incorrect calculation method used in [1], the absorption of radiation by the trees is overestimated by a factor of 5 when λ = 20 m and a factor of 3 when λ = 100 m (47% instead of 9 and 15%, respectively).

In [1], for a similar case (100-year-old spruce forest), κ = 0.109 and the weight of timber per hectare is 2934 tons. The overestimation of gamma-radiation absorption by the trees due to the incorrect data on the amount of timber is still greater for younger forests. For a 40-year-old spruce forest a quite improbable value κ = 0.0056 is given, i.e., 99.5% of the radiation is absorbed.

When the flight is to one side of the center of the anomalous section, the screening effect of the forest is greater than shown in Table 2. An analytical expression for the recorded γ-radiation intensity in this case is very complex and the numerical calculations had to be performed with transparent sheets divided into squares, similar to those described in [5]. We used formula (3) to draw the squared sheet for the absorption by the trees. Calculated graphs for the coefficient of screening κ are shown in Fig. 1 as a function of the distance x from the center of the section. It should be borne in mind that at distances greater than 100-150 m, sections with $\lambda < 100$ m cannot be recorded even when there are no trees since the intensity of radiation falls by a factor of more than 10.

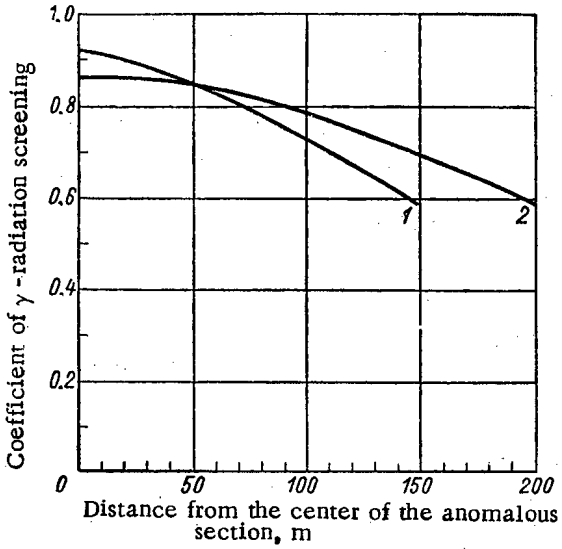

Fig. 1. Dependence of the coefficient of γ-radiation screening by trees on the distance to the center of the anomalous section: 1) $\lambda = 20$ m; 2) $\lambda = 100$ m.

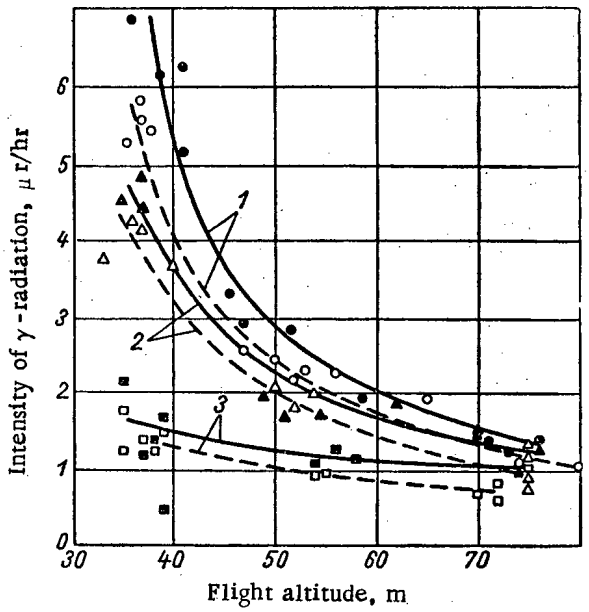

Fig. 2. Data of experimental determination of screening capacity of forest: 1) $\kappa = 0$; 2) $\kappa = 25$ m; 3) $\kappa = 50$ m; —— without trees; – – – with trees.

The absorbing capacity of the trees was determined experimentally by aerial measurements of the γ-radiation intensity of two identical sections, one of which was in a pine forest and the other in a field next to the forest boundary. Anomalous sections were imitated using point radiators (Co^{60} isotope) placed at the corners of a 10×10 m square. The results of one of these experiments are given in Fig. 2. The mean forest parameters were: $H = 15$ m, $D = 0.14$ m and $S_0 = 4$ m^2. The values of κ according to the data of Fig. 2 at $h = 50$ m are within the range 0.8 to 0.9, which agrees satisfactorily with the calculated data.

Paper [1] therefore incorrectly excludes wooded regions from aerial prospecting. The reduction in efficiency of aerial prospecting in these regions is small and is due not so much to the absorption of γ-radiation by the trees as to the difficulty of correct mapping of the survey routes and, possibly, the specific geochemical processes in wooded soils.

LITERATURE CITED

1. G. N. Kotel'nikov and N. I. Kalyakin, "Atomnaya Énergiya," 8, 4, 370 (1960).
2. A. V. Matveev, "Problems of Exploratory Radiometry." Information Collection of the Ministry for Geology and Preservation of the Mineral Resources of the USSR, No. 2 [in Russian] (Leningrad, 1960).
3. A Handbook for Forestry Workers [in Russian] (Minsk, Acad. Sci. Belorus SSR Press, 1959).
4. Radiometric Methods for Surveying and Exploring Uranium Ores, Edited by V. V. Alekseev [in Russian] (Moscow, State Geological and Technical Press, 1957).
5. A. F. Yakovlev, Izv. AN SSSR, Ser. Geofiz. 1, 75 (1958).

A STUDY OF THE FLUORIDES OF SOME MULTIVALENT METALS BY POTENTIOMETRIC TITRATION IN NONAQUEOUS MEDIA

A. P. Kreshkov, V. A. Drozdov, E. G. Vlasova,

S. V. Vlasov and Yu. A. Buslaev

Translated from Atomnaya Énergiya, Vol. 11, No. 6, pp. 553-554, December, 1961
Original article submitted October 14, 1960

There are a number of papers on the properties of various salts in nonaqueous organic solvents [1-3]. Several volumetric methods have been proposed for the analysis of inorganic materials in nonaqueous media [4] and studies have been made of the chlorides of mono-, di-, and trivalent metals and ammonium [5-7]. Very little is known on the fluorides of metals and there have been no investigations into the fluorides of quadri-, penta- and hexavalent metals. In the literature there are only indications of the behavior of higher fluorides toward organic solvents. For example, it is known that TiF_4 dissolves in methanol and pyridine, whereas with ethanol it forms the compound $TiF_4 \cdot C_2H_5OH$ [8]. Niobium pentafluoride dissolves in toluene, ether and alcohol. Tungsten hexafluoride and benzene give a compound with the composition $WF_6 \cdot C_6H_6$ [9].

The fluorides of multivalent metals in aqueous media have been comparatively well studied. The potentiometric titration of niobium, tantalum and molybdenum fluorides [10] has shown that during titration with alkali there is gradual decomposition according to the scheme $H_2NbOF_5 \rightarrow K_2[NbOF_5] \rightarrow Nb_2O_5$. TaF_5 is completely decomposed by alkali to tantalum pentoxide. Molybdenum hexafluoride reacts with alkali forming the metamolybdate $K_2Mo_4O_{11}$ which is further decomposed to K_2MoO_4. The titration of fluorides of multivalent metals by alkalis in aqueous media is accompanied by the hydrolysis of the fluorides by water. In the fluorides of the multivalent metals the fluorine atoms are replaced by oxygen atoms. The replacement of fluorine atoms by oxygen-containing groups has not been studied before.

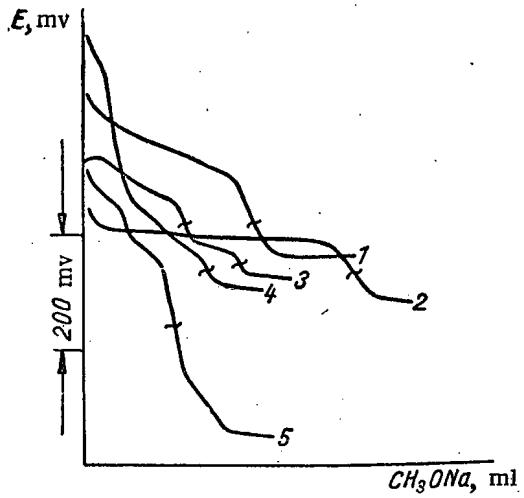

Curves for the potentiometric titration of the higher fluorides of metals in methylethyl ketone by a 0.1 N solution of sodium methylate: 1) niobium pentafluoride; 2) tungsten hexafluoride; 3) molybdenum hexafluoride; 4) tantalum pentafluoride; 5) titanium tetrafluoride.

The higher fluorides of molybdenum, tungsten, niobium, tantalum, zirconium and titanium have been studied. Methods are described in the literature for preparing the higher fluorides, based on fluorination with elementary fluorine [11, 12] and interhalide compounds, for example ClF_3 [13]. In the present work we used the method of fluorination by elementary fluorine, which was obtained in a cell [14] with a working temperature of 110-120°C and electrolyte composition $KF \cdot 2HF$ – 40% HF. A column packed with potassium fluoride tablets was used to remove electrolyte vapors from the fluorine. A quartz reactor with external heating was used for the fluorination. The fluorides were condensed in quartz vessels, cooled by a mixture of dry ice and alcohol. The obtained products were purified by repeated distillation in a quartz apparatus.

During the preparation of the initial 0.1 N solutions of fluorides in absolute methyl alcohol and when removing samples of fluorides for titration all necessary precautions were taken to prevent hydrolysis of the fluorides. The titrating solution was a 0.09840 N solution of sodium methylate in methyl alcohol.

The fluorides were titrated in methylethyl ketone and a mixed solvent – methylethyl ketone-benzene. The methylethyl ketone was purified according to the method described in [15]. The benzene used as the cosolvent ("pure for analysis") was dried over metallic sodium and redistilled; the condensate was kept over potassium hydride and then twice redistilled using a fractionating column.

The LP-5 tube potentiometer was used in the titration. The reference electrode was a calomel electrode filled with a saturated solution of KCl in methyl alcohol. The indicating electrode was a glass electrode. The potentials of the investigated system were measured after adding each quantity (0.04-0.06 ml) of the titrating solution.

We found that the higher fluoride of zirconium is insoluble in methylethyl ketone, dioxane, methyl alcohol and acetonitryl and was therefore not studied by the potentiometric method. The figure shows curves for the potentiometric titration of individual fluorides of titanium, niobium, tantalum, molybdenum and tungsten in methylethyl ketone. As can be seen, for certain ratios of sodium methylate to the fluorides there are clearly expressed discontinuities in the potentials. At different stages of titration the solutions being analyzed become turbid due to the precipitation of sodium fluoride.

In the titration of titanium tetrafluoride (curve 5) one discontinuity in potential can be observed at a ratio $\frac{CH_3ONa}{TiF_4} = 2$ corresponding to the splitting-off of two fluorine atoms as a result of the alcoholysis reaction

$$TiF_4 + 2CH_3ONa = (CH_3O)_2TiF_2 + 2NaF.$$

In the titration of niobium pentafluoride by sodium methylate (curve 1) the discontinuity in potential of the analyzed system is observed at a ratio $\frac{CH_3ONa}{NbF_5} = 2$ which corresponds to the formation of the dimethoxytrifluoride of niobium in accordance with the following equation:

$$NbF_5 + 2CH_3ONa = (CH_3O)_2NbF_3 + 2NaF.$$

The stoichiometric calculations in the titration of molybdenum hexafluoride by sodium methylate in a methylethyl ketone medium show that the first discontinuity in titration (curve 3) corresponds to the titration of two fluorine atoms, the second – a small discontinuity – coincides with the quantitative substitution of the third fluorine atom in MoF_6 by methoxy groups.

The titration of TaF_5 by sodium methylate is accompanied by a sharp drop in the potentials of the analyzed system. The character of the curve (curve 4) and the stoichiometric calculations show that the process takes place in two stages. At first, according to the equations

$$TaF_5 + CH_3ONa = CH_3OTaF_4 + NaF;$$
$$CH_3OTaF_4 + 3CH_3ONa = (CH_3O)_4TaF + 3NaF;$$

the methoxy groups substitute one and then another three fluorine atoms.

In tungsten hexafluoride (curve 2) the methoxy groups substitute five fluorine atoms according to the equation

$$WF_6 + 5CH_3ONa = (CH_3O)_5WF + 5NaF.$$

In all cases of titration the replacement of methylethyl ketone by the mixed solvent methylethyl ketone-benzene (volumetric ratio 1 : 1) only led to a decrease in the potential discontinuities, preserving their clarity and the previous stoichiometry of the process.

Experiments showed that the suggested titration can be used for the quantitative determination of these fluorides. In the quantitative determination of accurate weights of WF_6 the error is ±1.2%; NbF_5 – ± 0.6%, MoF_6, according to the first discontinuity in titration, ± 1.0%; TiF_4 – ± 2% and TaF_5 – ± 1.3%.

LITERATURE CITED

1. A. P. Kreshkov, Report to the Eighth Mendeleev Congress, Abstracts of Reports of the Analytical Chemistry Section [in Russian] 3, 34 (1958).
2. N. A. Izmailov, The Electrochemistry of Solutions [in Russian] (Kharkov, Gorkii Kharkov State University Press, 1959).

3. A. P. Kreshkov, A Manual on Acid-Base Titration in Nonaqueous Media [in Russian] (Moscow, D. I. Mendeleev Moscow Institute of Chemical Technology Press, 1958).
4. R. Shanti, Palit, Mekhr Natkh Das and G. R. Somayadzhulu, Nonaqueous Titration [in Russian] (Moscow, State Chemistry Press, 1958).
5. C. Hennart and E. Merlin, Chim. analyt. 40, 5, 167 (1958).
6. N. A. Izmailov and E. I. Bail', "Ukr. khim. zh.," 23, 5, 662 (1957).
7. R. Cundiff and P. Markunas, Analyt. Chim. Acta 21, 68 (1959).
8. O. Ruff and R. Jpsen, Ber. 36, 1777 (1903).
9. H. Priest and W. Schumb, J. Am. Chem. Soc. 70, 2232 (1948).
10. N. S. Nikolaev and Yu. A. Buslaev, "Zh. neorg. khim.," 4, 554 (1959).
11. O. Ruff and F. Eisner, Ber. 40, 2926 (1907).
12. O. Ruff, J. Zedner and E. Schiller, Ber. 42, 492 (1909).
13. N. S. Nikolaev, Yu. A. Buslaev and A. A. Opalovskii, "Zh. neorg. khim.," 3, 8, 1732 (1958).
14. Fluorine and its Compounds, Vol. 1, Edited by J. Simons [Russian translation] (Moscow Foreign Literature Press, 1956).
15. A. Weissberger et al., Organic Solvents [Russian translation] (Moscow, Foreign Literature Press, 1958).

THE THERMAL DECOMPOSITION OF URANIUM AMMONIUM PENTAFLUORIDE

N. P. Galkin, B. N. Sudarikov and V. A. Zaitsev

Translated from Atomnaya Énergiya, Vol. 11, No. 6, pp. 554-555, December, 1961
Original article submitted February 1, 1961

A number of papers [1-4] have dealt with the thermal decomposition of uranium ammonium pentafluoride. The conditions of decomposition and the composition of the resulting products have been described. It has been observed that uranium ammonium pentafluoride decomposes into uranium tetrafluoride and ammonium fluoride according to the reaction

$$NH_4UF_5 \longrightarrow UF_4 + NH_4F.$$

The present work forms a part of investigations conducted by the authors into the reaction between uranium hexafluoride and ammonia. As already mentioned [5-7], uranium hexafluoride is reduced by ammonia in the temperature range 100-200°C with the formation of uranium ammonium pentafluoride, containing about 10% free ammonium fluoride. The results of a thermal gravimetric analysis of this product are shown in the figure.

The figure shows three endothermic effects at temperatures of 220-280, 320-360 and 420-450°C. At these temperatures the specimens lose weight. At a temperature of 220-280°C the loss in weight is 9.4%, which corresponds to almost complete removal of the free ammonium fluoride. After this only uranium ammonium pentafluoride is found in the residue. Its decomposition commences at about 320°C, the reaction occurring in two stages: At temperatures of 320-360°C the loss in weight is 5.9% and at 420-450°C it is 4.2%. The product, roasted at temperatures above 450°C, is uranium tetrafluoride.

The ammonium fluoride combined with the uranium tetrafluoride therefore splits off in two stages, in approximately equal amounts. It might be assumed that this is due either to the difference in the bond strength of the separate ammonium fluoride molecules or to the difference in the bond strength of the ammonia and the fifth fluorine

Composition of Gases Obtained on Roasting Uranium Ammonium Pentafluoride and a Mixture of it With Ammonium Fluoride in a Current of Argon. Time of Roasting at Each Temperature is 2 hours.

Composition of initial products	Temp. of roasting, °C	Loss in wt. of specimen, %	Composition of gases			
			in percent		in moles per mole of ammonia	
			ammonia	fluorine	ammonia	fluorine
90.5% NH_4UF_5 + 9.5% NH_4F*	280	11.8	58.1	41.9	1.0	0.6
The same	360	4.9	82.5	17.5	1.0	0.2
» »	460	2.3	16.1	83.9	1.0	4.7
NH_4UF_5**	280	3.1	59.2	40.8	1.0	0.6
The same	360	4.6	85.1	14.9	1.0	0.2
» »	460	2.5	17.0	83.0	1.0	4.4

* A mixture of uranium ammonium pentafluoride with ammonium fluoride was obtained by the reaction of uranium hexafluoride with ammonia at 100°C.

** Uranium ammonium pentafluoride was obtained by crystallization from aqueous solutions and was dehydrated in vacuum.

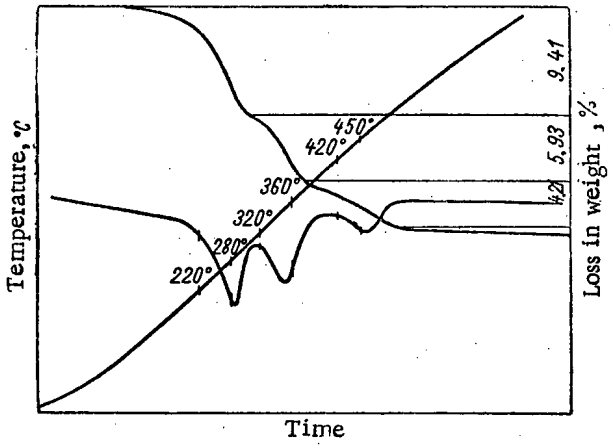

The thermal decomposition of uranium ammonium pentafluoride containing 10% free ammonium fluoride.

ion. This problem can only be resolved by a direct analysis of the gases obtained due to thermal dissociation of the uranium ammonium pentafluoride at different temperatures. These experiments were performed and the date are given in the table.

As can be seen from the table, at 280°C there is quantitative removal of free ammonium fluoride; at this temperature there is also partial decomposition of the uranium ammonium pentafluoride with the preferential splitting-off of ammonia. At 360°C the decomposition of the ammonium pentafluoride is mainly due to the removal of ammonia; the fluorine ion undergoes very little splitting-off. Finally, at 460°C mainly fluorine is removed from the remaining product.

The investigations indicate that in uranium ammonium pentafluoride the fifth fluorine ion is more firmly bound to the uranium than ammonia; in the temperature range 280-460°C the uranium fluoric acid HUF_5 is apparently stable, this acid being unknown in aqueous solutions.

LITERATURE CITED

1. J. Impe Van, Chem. Engng. Progr. 50, 5, 230 (1954).
2. H. Bernhardt et al., Nucl. Sci. Abstrs. 10, 792 (1956).
3. S. Gasco and C. Fernader, An. Real. cos. asp. fis. y chem. B54, 3, 181 (1958).
4. V. Dadape and N. Krishna Prasad, Report No. 1668 Presented by India to the Second International Conference on the Peaceful Uses of Atomic Energy (Geneva, 1958).
5. B. Ayers, Report CC-1504 (1944).
6. R. Spenceley and F. Teetrel, USAEC Report FMPC-400 National Lead Company of Ohio (May 6, 1953).
7. N. P. Galkin, B. N. Sudarikov and V. A. Zaitsev, "Atomnaya Énergiya," 8, 6, 530 (1960).

ATOMIC ENERGY AT THE SOVIET EXPOSITION IN LONDON

Translated from Atomnaya Énergiya, Vol. 11, No. 6, pp. 556-557, December, 1961

One of the divisions of the Soviet Trade and Industrial Fair last summer in London was devoted to a display of the Soviet Union's achievements in the peaceful uses of atomic energy. The exhibit presented a telling illustration of the scope of work carried out along this line in the USSR. Exhibits of nuclear reactor models and accelerator models available for export from the Soviet Union, a list of isotopes proposed for sale, and the exhibit of sophisticated equipment could not help but attract the attention of specialists and representatives of business circles in Britain.

Fig. 1. The British Prime Minister H. Macmillan and I. S. Patolichev, Minister of Foreign Trade of the USSR, viewing a model of the I. V. Kurchatov nuclear electric power station at Belyy Yar.

photo by A. Stuzhin

The most popular exhibit was again, as in other Soviet expositions abroad, the model of the atomic icecutter LENIN. The model never failed to attract a crowd of admirers. Many of the visitors expressed the view that the icecutter LENIN was an example of the most economical and best justified use of atomic power.

There was an ample supply of materials giving a rounded picture of large-scale industrial experiments underway in the Soviet Union on optimizing reliability and minimizing costs in nuclear electric power stations. The attention of visitors was drawn to excellently fabricated models of the I. V. Kurchatov nuclear power station at Belyy Yar and of a nuclear power station built around a fast-neutron reactor. The fuel reloading process and the flow of coolant through the pipes of the coolant system were clearly represented in the operating models (Fig. 1).

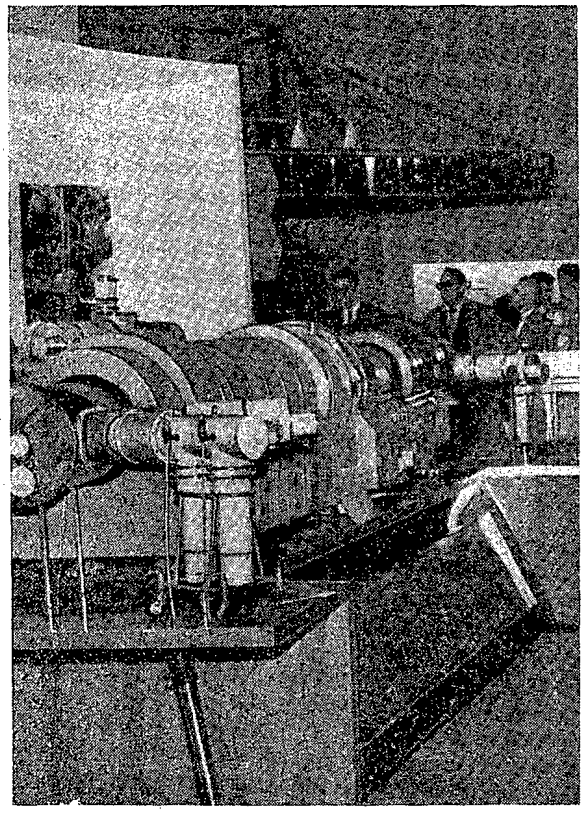

Fig. 2. The OGRA thermonuclear facility.
photo by A. Stuzhin

A 1:5 scale model of the OGRA facility highlighted the exhibit on fusion research (Fig. 2). Specialists bestowed particular attention on the UDP-1 plasma diagnostic device designed to investigate the state of the plasma at the machine output, and to monitor the energy of hard gammas and neutrons. A high-pressure gas scintillation counter with continuous circulation of make-up gas, designed for fast-neutron spectrometry, is the first of its kind in the world to find practical use. The scintillation counter can be used to determine the temperature of a deuterium plasma upward of a million degrees with high accuracy, independently of the presence of any background gammas.

A line of electronic measuring apparatus for nuclear research included pulse amplifiers, scaling circuits, pulse-height analyzers, and gamma-ray spectrometers. Among the pulse analyzers, we may note the miniature AI-50 50-channel analyzer with transistorized circuitry. The memory unit is assembled from magnetostrictive (nickel) delay lines. The AI-5 gamma-ray spectrometer is a single-channel analyzer with automatically varied discrimination level; the exposure time may be set over a 0.75-200 min. range, and resolving time is approximately 2 μsec. The AI-3 analyzer records the number of pulses received from each of 100 consecutively scanned channels on the screen of a memory tube (skiatron), and records numerical data on paper tape. Standardized components and printed circuitry are used in these analyzers.

In the section devoted to isotope applications in science and industry, a large selection of instruments and devices were on display. Some of these instruments were making their debut at international expositions. Among these were the noncontacting BTP-1 beta coating thickness gage, the ROTOP-3A radiation thickness gage for measuring depth of settled coal dust in mines, the RPSN-3 instrument for determining sulfur content in petroleum, and many others.

The health monitoring instrument which enjoyed greatest popularity among visitors was the ILK-2 designed for personnel dosimetric monitoring; an activated phosphor contained in the device scintillates upon exposure to infrared light. Specialists gave a high evaluation of the RV-3 portable aerosol radiometer, and the portable transistorized radiometric station designed for measurement of total gamma background, activation of surfaces and water, etc.

The "Atoms for Peace" section of the Soviet exhibit at London was a consistent success with visitors. There is no doubt that this section, as well as the exposition as a whole, contributed to better understanding between the peoples of the Soviet Union and Britain.

V. A.

ATOMIC ENERGY AT THE FRENCH NATIONAL EXPOSITION IN MOSCOW

(August 15 to September 15, 1961)

Translated from Atomnaya Énergiya, Vol. 11, No. 6, pp. 557-560, December, 1961

The display devoted to France's achievements in the field of nuclear power and associated applications, at the French national exposition in Moscow, was accommodated at two stands exhibiting the activities of the Commissariat de l'Energie Atomique and French "nuclear" firms.

The exhibits on display included materials used in nuclear reactor construction, and components made of those materials. High-purity magnesium and its alloys, with 0.5% zirconium, A-5 aluminum (99.0% pure), A-9 aluminum (99.99% pure), aluminum-magnesium and aluminum-iron-nickel alloys with excellent corrosion resistance in contact with hot pressurized water have made definite headway in France in fuel element cladding.

Experimental specimens of nuclear fuel made in ceramic form and fuel elements to be used in the Chinon nuclear power station now under construction, where fuel meat will be uranium with 0.5% molybdenum added, were on display.

The central point of the exhibit on the first stand was a model of the dual-purpose uranium-graphite reactor G-2, in operation since 1958 at Marcoule (Fig. 1).

The core of the G-2 reactor is a graphite stack 10 × 10 meters and weighing 1270 tons, containing 1200 channels. 28 units consisting of uranium rods enclosed in a magnesium jacketing with transverse ribs 30 cm in length are accommodated in each channel. The entire reactor contains 33,600 such units. Loading of nuclear fuel and removal of spent uranium slugs are handled by a special load transfer machine during operation of the reactor.

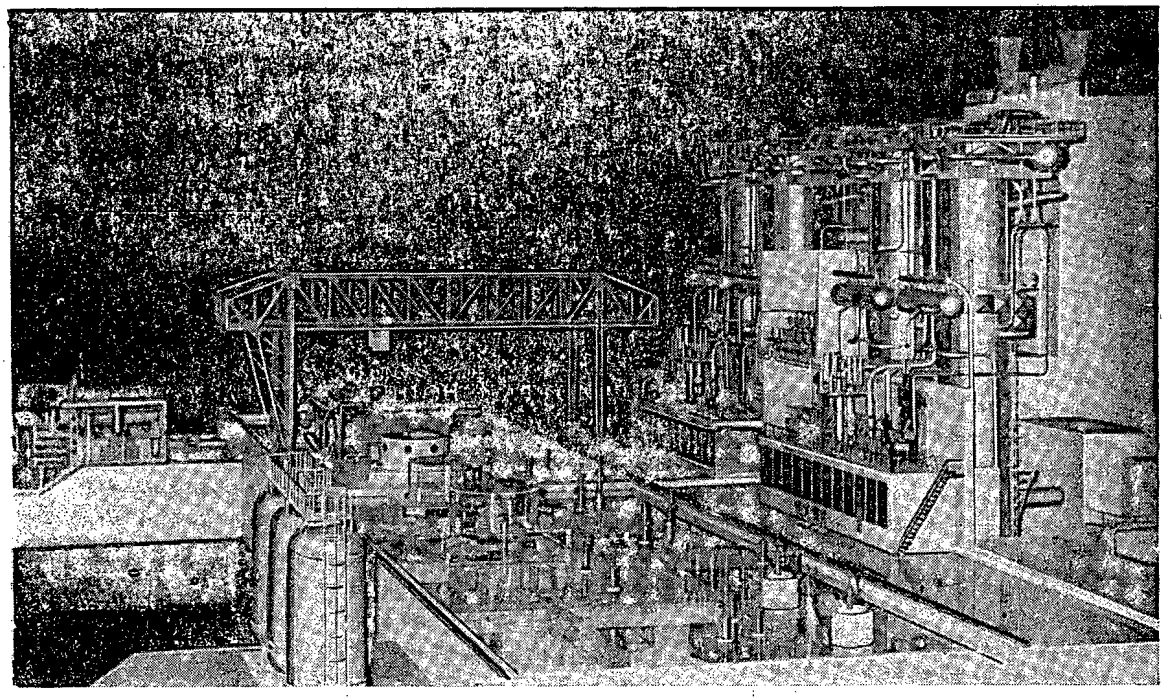

Fig. 1. Model of the G-2 reactor.

The slugs are cooled with carbon dioxide gas. The exit temperature of the coolant gas is 350°C. The thermal rating of the G-2 reactor is 200 Mw, and the electrical power rating is 30 Mw. The reactor is housed within a cylindrical hermetically-sealed horizontal containment shell of prestressed concrete.

A model of the RAPSODIE fast-neutron reactor (Fig. 2), which is slated for startup at the Cadarache nuclear research center sometime during 1963, was also operated at the exhibit. The RAPSODIE is France's first experimental breeder reactor, rated at 10 Mw, with sodium coolant. Uranium and plutonium pellets are burned as fuel, and the breeder material is a uranium-molybdenum alloy. Coolant temperature is 540°C.

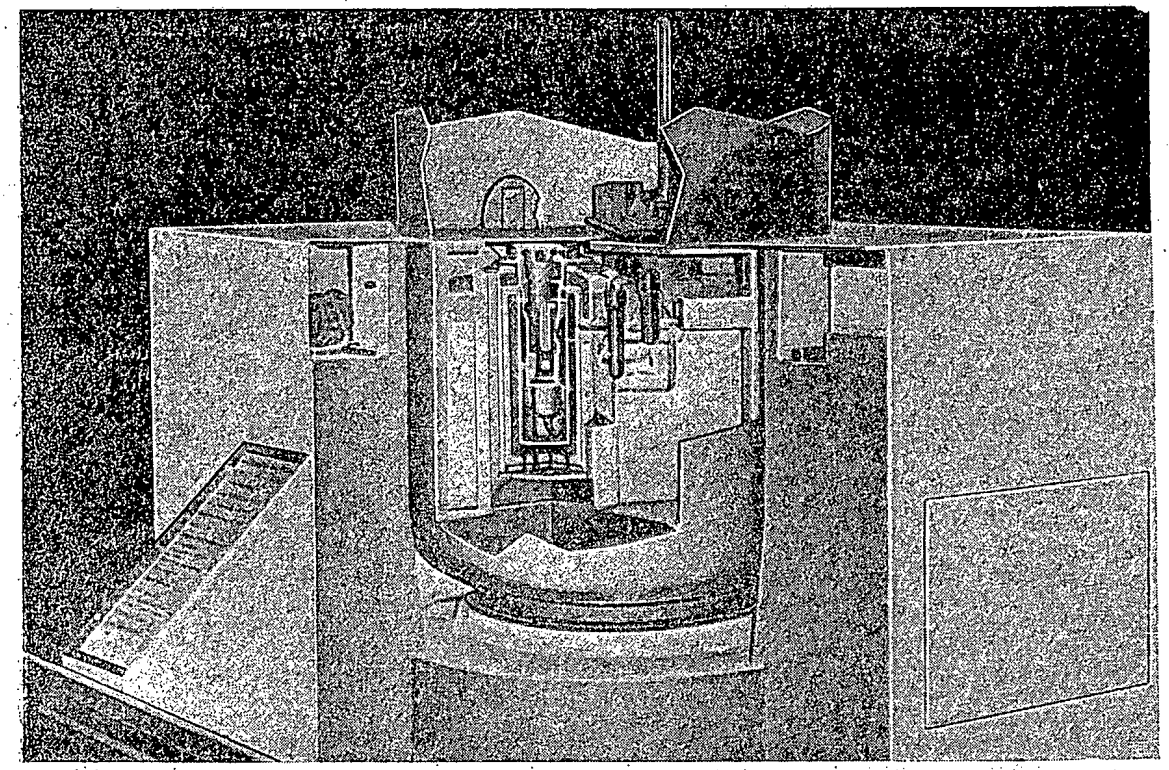

Fig. 2. Model of the RAPSODIE fast-neutron reactor.

High-energy research was represented by a model of a bubble chamber, a panel representing the SATURNE synchrotron, another representing the linear accelerator at Orsay, and some photographs showing results of interactions between high-energy particles.

An "Isotopes" stand constituted an independent feature of the exhibit. The "Isotopes" stand demonstrated equipment for isotope production and labeled-compounds synthesis, an inventory of isotope products available for delivery from the Commissariat de l'Energie Atomique, and shipping containers for isotope deliveries.

By 1960, France counted no less than 981 organizations engaged in the use of sotopes, including 93 medical institutions, 300 scientific research outfits and 588 industrial firms. The entire range of applications of radioactive elements was distributed in the following manner: level and thickness gaging: 44%; gamma radiography: 24%; applications of tracer atoms to technical research and activation analysis: 10%; batch mixing controls: 8%; petroleum lease transfer control: 3%; radiation chemistry: 30%; pharmacological research: 3%; agricultural research: 1%; miscellaneous applications: 1%.

One trend in French research is currently geared to development of techniques utilizing secondary x-rays in the analysis of the composition of substances. Two separate facilities are being assembled, one of them using spent fuel elements from the EL-3 reactor, the other using two plastic irradiators assembled from Co^{60} gamma sources with a total activity of about 160,000 gram-equivalents of radium.

A broad line of equipment for handling radioactive substances (glove boxes, manipulators, lead bricks, etc.) were displayed.

Special "Kenriman" containers of 9 liters and 500 liters volume are being used to transport high-level liquid wastes. The center of gravity is designed low and the oval shape assures high stability under any shipping conditions, avoiding any hazard of the container tipping over.

Apparatus, instrumentation, and equipment used by French industry for scientific research and isotope applications were on display at the industrial pavilion, along with individual experimental samples of electronic devices developed by the electronics department at Séclin.

Some of the instruments repeated to a certain degree the exhibits presented in 1960 at the Moscow French exhibit of electronic instruments (at the Polytechnic Museum in Moscow).

Specimens of electronic instruments developed by the electronics division of the Commissariat de l'Energie Atomique were also displayed.

One outstanding feature of the electronic and physical instrumentation exhibited was the impressive number of instruments assembled from modular components. At the present stage, the electronics division has developed and put into production over 25 functional modular components meeting various needs, including proportional and pulse amplifiers, high-speed decade scalers with a resolving time of 0.1 μsec, count-rate meters with digital readout, discrimination devices and pulse selectors for gamma-ray spectrometers, coincidence circuits, millimicrosecond pulse generators, supply packages, etc.

One example representative of this line of instruments is the SGS-1 gamma-ray spectrometer, for which errors in the size of recorded pulses as a function of energy remain within 2% of true value over the 0.02 to 3 Mev range.

French instrument designers devote close attention to the use of semiconductor ferrite components in new instruments.

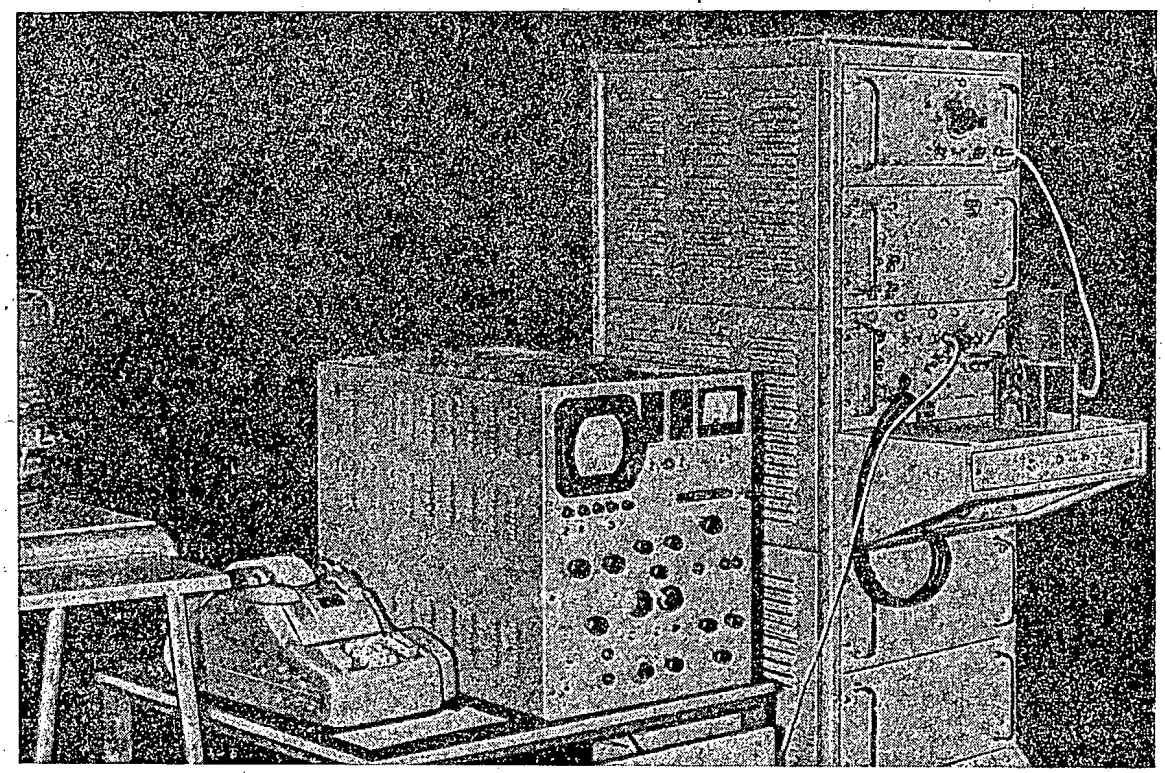

Fig. 3. 40-channel analyzer.

A 400-channel analyzer (Fig. 3) exhibited featured the following characteristics: linearity 0.5%, resolving time 12 μsec $\pm$ 0.5 μsec, maximum counting rate for a single channel $50 \cdot 10^4$ cps, channel capacity of 100,000 counts. All of the basic components are transistorized.

Also on display were electrostatic generators, and an "L" type neutron generator of 0.6 ma ion current, 10 to 200 μsec pulse width, pulse repetition rate from 500 to 1000 pulses per second. The neutron flux attains 10^7 neutrons/ /sec per microampere for the (d, t) reaction.

Equipment for quality control of reactor materials was represented by an induction vacuum melting furnace for uranium and an arrangement for testing hermetic sealing of nuclear fuel slugs loaded into the pile. The latter operates on the principle that the slugs are loaded into special casings which are then filled with pressurized helium, and the slugs are left inside for some time. The slug is then tested with a helium leak detector for the presence of leaks. If helium is detected, it is assumed that the slugs are not leakproof.

French specialists were on hand during the period from September 6 to 9 to deliver lectures of various trends in research in the field of the uses of nuclear energy.

L. P.

DIRECT-CYCLE REACTOR WITH DIPHENYL COOLANT

Translated from Atomnaya Énergiya, Vol. 11, No. 6, pp. 562-564, December, 1961

A project for a direct-cycle reactor with diphenyl coolant, DCDR, has been developed for the Marquardt firm in the course of a year (see Fig. 1). This reactor is an improved version of the OMR type reactor. The improvement consists in the use of a direct coolant cycle and graphite-clad fuel elements. The graphite makes it possible to lengthen the reactor run between loadings, improves the fuel temperature characteristics, and introduces additional moderator material into the pile core.

The use of the direct cycle and the low costs of the structural steel employed (in combination with a working fluid of low vapor pressure and low corrosive activity) opened the way for increased savings. The cost of the system turbine was appreciably lowered because of the excellent thermodynamic properties of diphenyl, use of which permits a low pressure level at the turbine entrance, low turbine runner speed, and fewer turbine stages.

Steam admitted to the turbine expands without compensation, is heated in the turbine exhaust duct and is condensed in a conventional heat exchanger where the condensate returning to the reactor is heated. The heat evolved

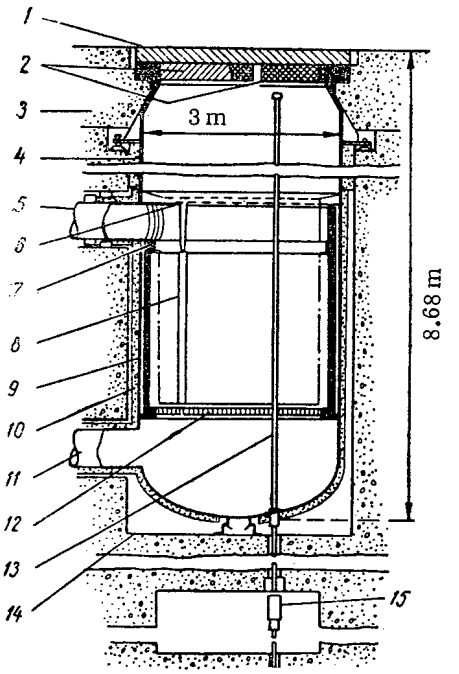

Fig. 1. A cross section through the reactor: 1) reactor vessel top; 2) rotating shielding screen for fuel-transfer control; 3) concrete biological shielding; 4) reactor vessel; 5) coolant exit; 6) thermal barrier; 7) peripheral annular support fuel-assembly grid; 8) fuel-element assembly; 9) thermal shielding; 10) lagging; 11) coolant entrance; 12) support plate; 13) control-rod thimble; 14) reactor well; 15) control rod drive.

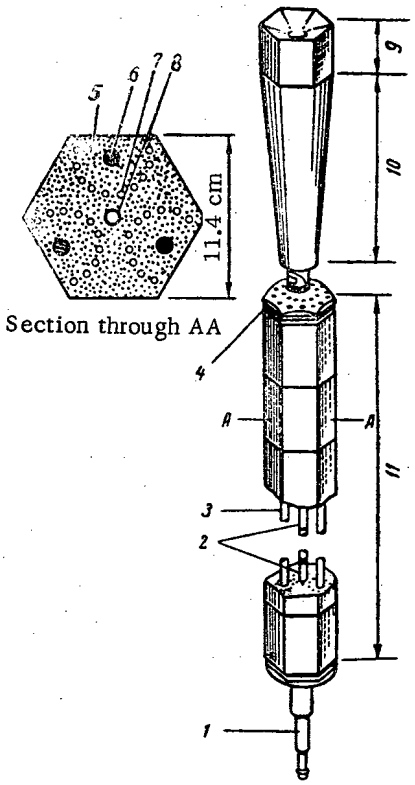

Fig. 2. DCDR reactor fuel assembly: 1) positioning rod; 2) positioning pins; 3) fuel element; 4) annular fuel assembly head; 5) graphite; 6) 12.7 mm diameter uranium carbide fuel element; 7) 5.3 mm diameter coolant channel; 8) positioning pin hole; 9) thermal barrier; 10) displacer; 11) fuel assembly sections.

as a result of the condensation of spent diphenyl vapor may be utilized for space or process heat, again opening up possibilities for further reduction in system costs. The cost of coolant makeup is further minimized as a result of the presence of graphite and the engineering of a thermal barrier in the reactor vessel, which reduces the volume of hot diphenyl above the core.

Diphenyl ($C_{12}H_{10}$), with a molecular weight of 154, belonging to the group of aromatic hydrocarbons, is the working fluid used in the pile. Diphenyl melts at 69°C, boils at 255°C. The vapor pressure of diphenyl is 23 atm at the peak surface temperature of the fuel elements. The amount of radiolysis is for diphenyl about the same as for terphenyl, but the former's thermal stability is somewhat superior to that of the latter.

The thermodynamic properties of diphenyl encourage the use of a simple turbine with a relatively reduced number of stages, since bleeding and steam preheat stages are unnecessary.

The coolant gains access to the core from below, and from there proceeds through the fuel elements between the core and thermal barrier to the plenum chamber formed by the core and thermal barrier above the core. The in-pile volume of diphenyl is successfully reduced by means of the thermal barrier with pyrolysis of the diphenyl checked at the same time. A tank filled with cold diphenyl (at a temperature of 200°C) is situated above the top thermal barrier, and functions as a biological shield. Over 15% of the volume of core diphenyl serves as a reflector. The core is surrounded by an annular steel thermal shield, a steel support structure and a steel positioning grid. Control rods not in contact with coolant channels will be placed in 19 of the core's 373 hexagonal cells. They are designed to be driven into the core from below by magnetically-actuated drive mechanisms.

Control rods may be replaced via the reactor vessel top. Coolant exits from the reactor at a temperature of 455°C and pressure of 23 atm and is led to a separator where 16% of the diphenyl is vaporized at a temperature of 443°C and pressure of 18.5 atm. This saturated vapor is then brought to the turbine where it is expanded and becomes superheated with a temperature of 350°C and pressure of 0.035 atm. The vapor is then brought to saturation once more in a regenerator unit and later condenses. The condensate is compressed to the same pressure level as obtained in the separator, and is heated to 310°C in the regenerator. The condensate is then mixed with diphenyl arriving from the separator, and this mixture is returned to the reactor at a temperature of 432°C and pressure of 25 atm.

To avoid release of fission products from the fuel elements (Fig. 2) into the coolant flow, a ternary barrier is provided for in the design. A material such as niobium, capable of resisting prolonged exposure to elevated temperatures, will be used for fuel cladding. The second, graphite, cladding will function as a barrier, blocking diffusion of fission products, and, finally, the surface of the graphite in contact with the coolant will be covered with polygraphite. Each pile fuel assembly will consist of eight hexagonal sections (30 cm high) connected to a central guide rod. Each of the three fuel elements in the assembly will be surrounded by ten channels (5.3 mm diameter) for coolant flow.

The lower values of working pressure in the coolant loop act to markedly reduce any hazard of tube and sealing failures. Thanks to the absence of water and high pressure levels, hazards associated with coolant leaks are likewise averted. Calculations show that the DCDR reactor has a negative temperature coefficient of reactivity, which is sufficiently large to assure stable reactor performance during load transfers and power transients. The basic characteristics of the DCDR reactor are the following:

Net electric power, Mw	20
Net cycle efficiency, %	31
Reactor vessel height, m	8.5
Reactor vessel diameter, m	3
Core height, m	2.44
Core diameter, m	2.44
Number fuel elements	354
Fuel element diameter, mm	12.7
Pitch of triangular lattice, cm	7.3
Uranium enrichment, %	1.55
U^{235} loading, kg	64
Initial conversion ratio	0.505

Coolant flowrate, tons/hr	2530
Pressure drop across core, atm	2
In-pile temperature rise of coolant, °C	32
Maximum fuel-element surface temperature, °C	482
Average fuel-element surface temperature, °C	455
Average coolant flowrate, m/sec	4.57
Average thermal flux, kcal/$m^2 \cdot hr$	$1.31 \cdot 10^5$
Peak thermal flux, kcal/$m^2 \cdot hr$	$3.17 \cdot 10^5$

The Marquart company reports that studies were carried out on structural materials for the DCDR reactor. An experimental loop was used to test boiling and condensation of the organic fluid.

V. B.

A NOTE ON NEUTRON IRRADIATION EFFECTS ON THE MECHANICAL PROPERTIES OF STEELS

Translated from Atomnaya Énergiya, Vol. 11, No. 6, pp. 566-570, December, 1961

The problem of embrittlement in low-carbon and low-alloy steels exposed to neutron bombardment has attracted much attention of late, since it is related to the problem of promoting maximum safety in the operation of large-scale nuclear reactors. This problem was spotlighted in the reports delivered to a symposium on reactor steels (London, December, 1960, under the auspices of the Iron and Steel Institute).

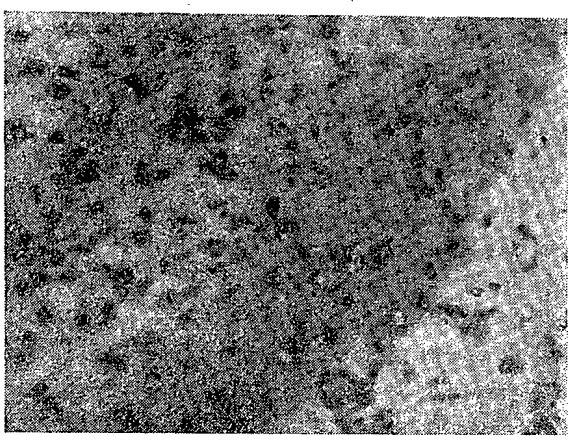

Fig. 1. Electron microphotograph of copper in a transmitted beam following irradiation by an integral flux of $1.4 \cdot 10^{20}$ neutrons/cm^2 (the loops formed by coalesced imperfections are clearly visible).

A. Cottrell considered some questions involving the nature of hardening and embrittlement of metals exposed to radiation, and expressed the view that the radiation hardening process is similar to precipitation hardening and is related to the formation of disperse clusters of defects which may take the form of loops (Fig. 1). His report discussed some possible mechanisms active in hardening; anchoring of dislocations and increase in resistance to the motion of dislocations through the crystal. On the basis of an analysis of the yield limit of irradiated steels as a function of grain size, Cottrell suggested that hardening of the steels was associated predominantly with an increase in the resistance to motion of dislocations through the crystal, while anchoring of dislocations is almost independent of radiation exposure. This view of the mechanism underlying brittle fracture provided the basis for a semi-empirical formula expressing the shift of the ductile-to-brittle transition temperature as a function of the neutron exposure dose $\Delta T = 55\ (\varphi t)^{1/3}$, where (φt) is the integral flux of neutrons having energies > 1 Mev, expressed in units of 10^{18} neutrons/cm^2.

TABLE 1. Typical Neutron Fluxes in Irradiation Facilities

Reactor and position of facility	Neutron flux, neutrons/cm^2·sec			Flux ratio, fast-neutron flux to thermal flux	Time taken to reach a dose of $5 \cdot 10^{18}$, neutrons/cm^2 (E > 1 Mev)
	thermal	fast			
		E > 1 Mev	E > 9 Mev		
Brookhaven reactor, reflector	$8 \cdot 10^{12}$	$5 \cdot 10^{11}$	$9 \cdot 10^{10}$	1/15	5 months
Oak Ridge reactor, next to core	$5 \cdot 10^{12}$	$2 \cdot 10^{12}$	$2.5 \cdot 10^{11}$	1/3	5-6 weeks
Oak Ridge reactor, core	$1 \cdot 10^{13}$	$3 \cdot 10^{12}$	$8 \cdot 10^{11}$	1/3	3 weeks
MTR reactor, next to core	$5 \cdot 10^{13}$	$1 \cdot 10^{13}$	$7 \cdot 10^{11}$	1/5	6 days

A report by F. Harris et al. cited results of a study of the shift in transition temperature as a function of the integral flux of fast neutrons (E > 2.9 Mev). The fast-neutron flux was determined with the aid of a S^{32} threshold detector having an effective threshold of 2.9 Mev. The results of tests of samples cored from various sections of welded steel plates were graphed over a range determined by the equations $\Delta T = 27.3\ \varphi_s^{1/3}$ and $\Delta T = 56.7\ \varphi_s^{1/3}$, where ΔT is the transition temperature shift, in °C; φ_s is the integral flux of neutrons of energies > 2.9 Mev in units of 10^{18} neutrons/cm^2. The shift in transition temperature is determined on standard Charpy V-notched specimens in both static and impact bending tests. The top curve, apparently representing the most cautious estimate, is in fairly satisfactory agreement with Cottrell's estimate. However, R. Berggren's data indicate that the equation $\Delta T = A\varphi^{1/3}$ will yield values slightly low of the mark at large exposure doses.

The presence of a certain correlation between the shift in transition temperature and the flux of fast neutrons (E > 1 Mev) is demonstrated in a paper by J. Hawthorne. The techniques used in recording fast-neutron flux are surveyed in a paper by L. Steel. This paper provides an analysis of applications of several detectors: Co^{59} detector in a cadmium steel shell (120 ev); S^{32} (2.9 Mev) and Ni^{58} (5 Mev). Further experiments were conducted on a preliminary determination of neutron spectra, using Pu^{239}, Np^{237} and U^{238}. Irradiation took place in reactors of various types with different flux and neutron spectrum characteristics (Table 1), enabling the researchers to compare findings obtained under different sets of exposure conditions.

TABLE 2. Chemical Analysis of Steels

Material, type	Thickness, mm	Impurity content, %							
		C	Mn	Si	P	S	Ni	Cr	other impurities
A302B hardfaced metal (argon welding)	100	0.23	1.48	0.23	0.015	0.018	0.1	0.16	0,55 1.17
A302B. hardfaced metal (argon welding)	140	0.1	1.37	0.41	0.01	0.17	0.72	0.09	0.49
A212B, hardfaced metal (argon welding)	160	0.07	0.7	0.45	0.012	0.024	0.14	0.09	0.48
Forging SA336	280	0.19	0.65	0.26	0.011	0.014	0.79	0.4	0.64 0.12
A302B, sheet steel	100	0.22	1.37	0.30	0.015	0.011	0.2	0.26	0.64
A302B, sheet steel	150	0.20	1.31	0.25	0.012	0.023	0.2	0.17	0.47
A212B, sheet steel	160	0.29	0.79	0.28	0.014	0.030	0.13	0.06	0.03
A212B, sheet steel	100	0.26	0.76	0.24	0.011	0.031	0.22	0.2	0.02
A201, sheet steel	150	0.28	0.69	0.20	0.010	0.032	0.12	0.1	0.01
A201, sheet steel	50	0.16	0.62	0.24	0.010	0.026			

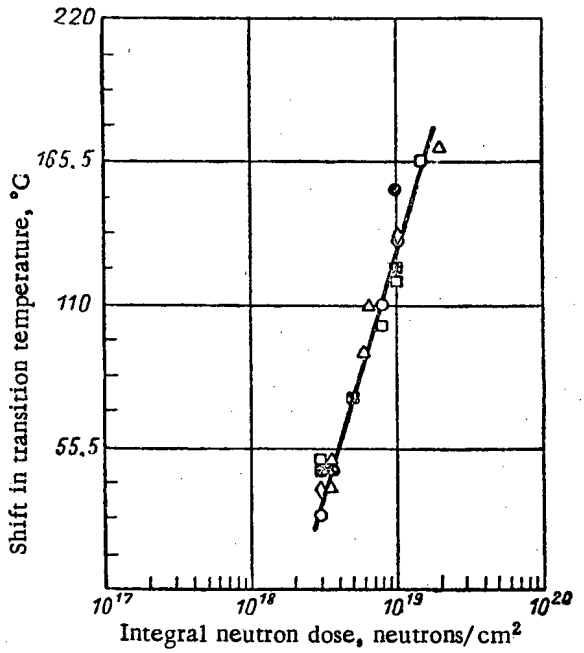

Fig. 2. Shift in transition temperature as a function of integral flux of fast neutrons of energy > 1 Mev: △) A201 steel; □) A212B steel; ○) A302B steel; ◇) SA336 steel; ■) Hardfaced metal A; ●) hardfaced metal B.

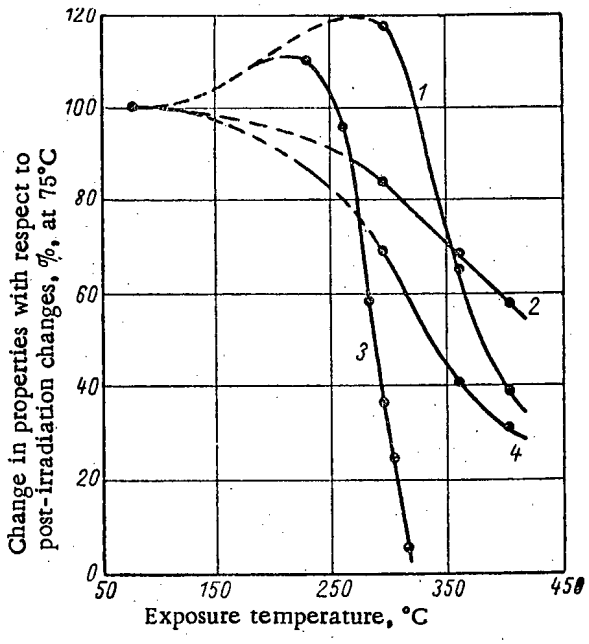

Fig. 3. Effect of irradiation temperature on impact and tensile properties of A212B steel (integral flux of neutrons $2 \cdot 10^{19}$ neutrons/cm² at E > 1 Mev); 1) tensile strength; 2) uniform extension; 3) transition temperature for notched specimens tested for impact bending; 4) yield limit.

Table 2 offers the brands and constituents of steels and hardfaced metals subjected to irradiation. The experimental values for shift in transition temperature contained in J. Hawthorne's report, obtained for fluxes with different ratios of thermal and fast neutrons, are directly proportionally to the logarithm of the integral flux of neutrons having energies > 1 Mev (Fig. 2), which attests to the restricted role of the softer portion of the neutron spectrum.

To date, it has been assumed that mechanical properties were independent of irradiation temperature in the low-temperature region, and that mechanical properties deteriorated as the irradiation temperature was raised. However, the data adduced in the papers of Berggren and Harris indicate that the effect of temperature (at least in reference to steels) is of a much more complex nature, and that there exists a temperature range (100-300°C) within which radiation effects attain their maximum effect (Fig. 3). One typical feature is that different properties vary in different ways as the temperature is changed, and that the effect of temperature is essentially dependent on the composition of the steel (Table 3).

TABLE 3. Brittle Temperature Increase for Steels Irradiated in Integral Flux $5 \cdot 10^{18}$ Neutrons/ cm^2 (E > 1 Mev) at Temperatures 80 and 315°C (V-notched Charpy specimens)

Steel	Brittleness temperature, °C			Increase, °C		$\frac{\Delta T(315^\circ C)}{\Delta T(80^\circ C)}$
	prior to irradiation	after irradiation at 80° C	after irradiation at 315° C	at 80° C	at 315 °C	
hot-rolled A212B	—57	0	—39	57	18	0.31
normalized A212B	—48	14	—33	62	15	0.25
normalized A212 (anneal 645 °C)	—34	21	4	55	38	0.70
hot-rolled A285A	0	102	46	102	46	0.45
normalized A285A	—15	60	43	75	58	0.78
cooled (in furnace, from 925 to 595° C) A301B	—9	82	27	91	36	0.39

The effects of post-exposure annealing on the properties of steels were reported in several papers. Berggren showed that recovery of the mechanical properties of A212B steel upon annealing proceeded in several distinct stages. For example, the change in the critical brittleness temperature delineated two such stages.

The recovery process proceeds under tension in a more complex manner and can be broken down into at least four distinct stages. The most characteristic phenomenon is a certain extension of tensile strength and yield point over the early stage of annealing at temperatures somewhat in excess of the irradiation temperature. A similar effect was noted in a paper by L. Trudeau who detected an increase in the critical temperature as a result of annealing A201 steel and nickel-alloyed fine-grained and coarse-grained steels at 204°C, all of which were exposed to an integral flux of $6 \cdot 10^{19}$ neutrons/cm^2 at temperatures below 100°C. Anneals at temperatures above 300°C as a rule lead to appreciable recovery from the consequences of exposure.

The results of dynamic tests carried out by J. Hawthorne demonstrated that the anneal elicited the recovery of properties of some carbon steels irradiated at 100 and 300°C. For example, an 80-hour anneal at 315°C of specimens of A212B steel irradiated at 100°C reversed the change in transition temperature by as much as 75%. The increase in exposure time to 162 hours was without effect on the transition temperature, although the energy of rupture in the ductile region attained the initial value. Raising the annealing temperature to 370°C contributes to an almost complete recovery of radiation-induced alteration of both the transition temperature and energy of rupture in the ductile region (Fig. 4). A comparison of the results of an anneal of A212B steel exposed to various integral fluxes shows that the rate of recovery speeds up as integral flux is increased. We then see that the modifications introduced by irradiation at a higher temperature are more stable, and that recovery of properties proceeds at a slower rate. However, the composition of the steel has little effect on recovery rate.

TABLE 4. Effect of Neutron Bombardment at 156°C on Critical Brittleness Temperature for Aluminum-Killed Low-Carbon Steel (0.13% C; 0.034% S; 0.034% P; 1.05% Mn; 0.1% Si)

Specimen shape and tests	Integral neutron flux, neut/cm² (at 2.9 Mev)	Critical temp. for mode of fracture (50% ductile fracture), °C		Shift in transition temp., °C
		pre-exposure	post-exposure	
Large specimens tested for static bending	$8.8 \cdot 10^{18}$	0	110	110
V-notched Charpy specimens, impact-tested	$8.1 \cdot 10^{17}$	15	90	75
	$9.4 \cdot 10^{18}$	15	90	75

L. Trudeau has studied the effect of several metallurgical factors on changes in the mechanical properties of steels following irradiation, and has shown that a decrease in impurity content and free-carbide content in steel attenuates radiation embrittlement to some degree, while the value of the transition temperature following irradiation, for an alloy of iron with 3.25% nickel, depends on grain size and on the initial transition temperature.

Some compellingly interesting static bending tests performed on large notched steel specimens (50 x 70 x 500 mm), reported upon by D. Harris, have shown that the values of the shift in transition temperature in impact tests of standard Charpy specimens came out slightly lower than the true values (Table 4). The shift in transition temperature was arrived at in terms of the nature of fracture experienced, but the values obtained were in harmony with those found from the change in energy of formation and in energy of crack propagation (Fig. 5). The latter circumstance allows us to proceed with great confidence in using the experimental findings in order to evaluate the behavior of a steel member encountered in practice.

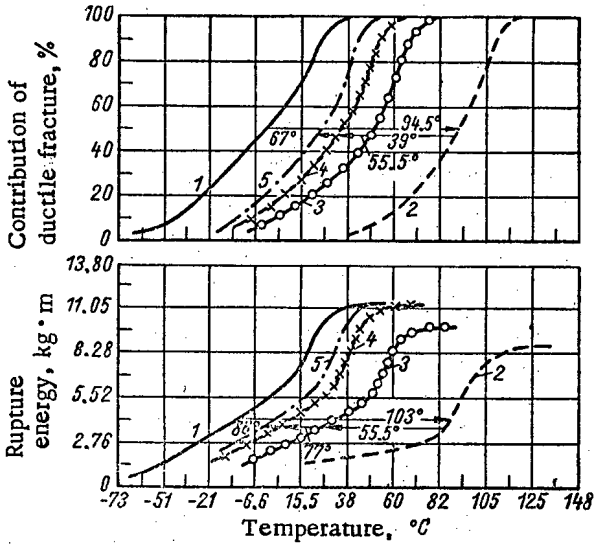

Fig. 4. Cold-shortness curves for A212B steel (100 mm sheet thickness) subsequent to exposure and reannealing: 1) prior to exposure; 2) after exposure (T > 100°C at flux of $8 \cdot 10^{18}$ neutrons/cm²; E > 1 Mev); 3 to 5) following exposure and anneal 3) at 260°C, 168 hours; 4) at 315°C, 168 hours; 5) at 370°C, 168 hours].

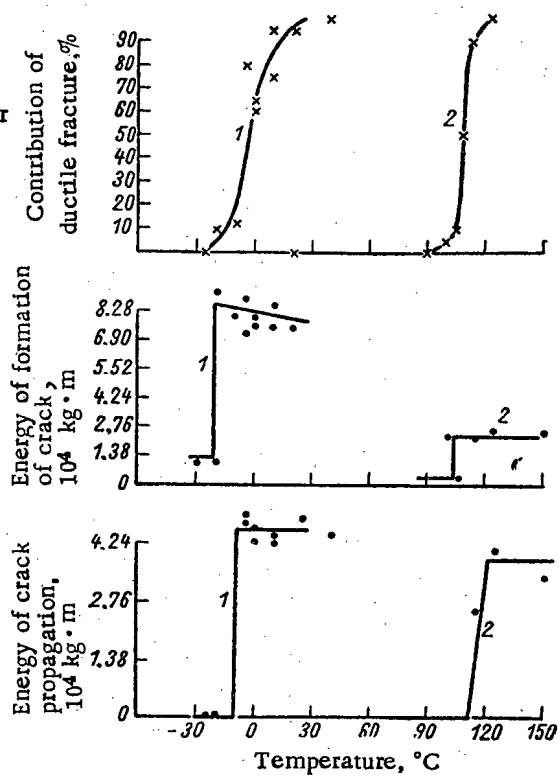

Fig. 5. Cold-shortness curves for large specimens (50 x 70 x 500 mm) of low-carbon boiler-plate steel, aluminum-filled (0.13% C, 1.03% Mn): 1) prior to irradiation; 2) subsequent to irradiation.

Considering the question of reliability of reactor pressure vessels, A. Cottrell indicated that maintaining the vessel temperature higher than some minimum value would be an effective way to enhance reliability, more so than lowering allowable stresses, since, should the vessel temperature fall below the critical mark, brittle fracture would occur in the case of large pressure vessel thickness, despite the fact that effective stresses would be much lower than the yield point. This critical temperature is most reliably arrived at via the Robertson method, which is however extremely cumbersome for irradiated specimens.

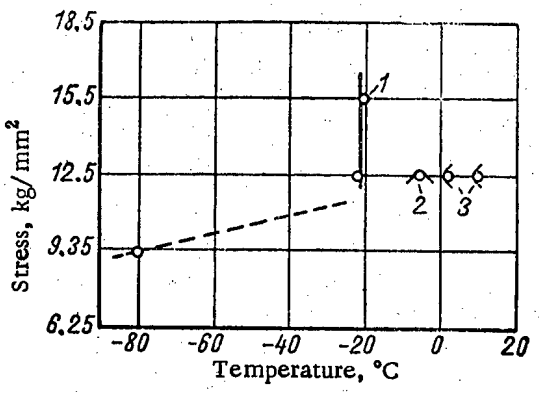

Fig. 6. Typical results of Robertson tests (isothermal and in the presence of a temperature gradient) on low-carbon boiler-plate steel, aluminum-killed (specimen thickness 50 mm, specimens prepared from sheet steel 100 mm thick): 1) tests in presence of temperature gradient; 2) isothermal testing (critical state); 3) isothermal testing (no propagation of cracks). Cracks were observed to propagate parallel to rolling direction.

D. Harris suggests pretesting of reactor pressure vessel materials by the Robertson method (Fig. 6) followed up by radiation-induced shifting of the transition temperature as a viable method for determining the minimum operating temperature (or the allowable exposure dose for a given temperature level). The transition temperature shift is measured by impact testing of Charpy specimens in this method. To arrive at preliminary data, the formula $\Delta T = 55\ \varphi_s^{1/3}$ may be used. Periodic testing of Charpy specimens placed directly in contact with the wall of the pressure vessel has been suggested as a method for monitoring changes in the properties of the reactor pressure vessel during reactor operation. Tests of such specimens irradiated for 30 months at temperatures of 140 and 300°C in a neutron flux of $1.4 \cdot 10^8$ neutrons/cm^2 and $E > 2.9$ Mev (Calder Hall and Chapel Cross reactors) failed to reveal any changes of properties in tension or shift in the ductile-to-brittle transition temperature. It is true that this shift should be one of approximately 10°C according to a tentative estimate, and this is generally speaking pretty much commensurable with the spread of testing data.

P. A. Platonov

BIBLIOGRAPHY

NEW BOOKS AND SYMPOSIA

Translated for Atomnaya Énergiya, Vol. 10, No. 2, p. 573.

Jaderna Energie 7, No. 12 (1961) a periodical issued by the Czechoslovak Atomic Energy Commission attached to the State Committee on Industrial Development

Contents:

F. Behounek: Effect of radiations from nuclear facilities on the surrounding locality.

V. Kovanicova: Dimensional stability of uranium in thermal cycling.

B. A. Ushakov: Thermionic energy converters.

J. Kubalek: Pulse generators for electronic-measurements instrumentation.

Abstracts.

Correspondence and Information.

Survey of the literature.

INDEX

THE SOVIET JOURNAL OF ATOMIC ENERGY

Volumes 10 and 11, Numbers 1-6

THE SOVIET JOURNAL OF

ATOMIC ENERGY

A translation of ATOMNAYA ÉNERGIYA,
a publication of the Academy of Sciences of the USSR

(Russian original dated January, 1961)

Vol. 10, No. 1 November, 1961

CONTENTS

Annual subscription $75.00
Single issue 20.00
Single article 12.50

CONTENTS (continued)

Note. The Table of Contents lists all materials that appears in Atomnaya Énergiya. Those items that originated in the English language are not included in the translation and are shown enclosed in brackets. Whenever possible, the English-language source containing the omitted reports will be given. Consultants Bureau Enterprises, Inc.

ERRATA

VOL. 9, NO. 2

Page		Reads	Should Read
655	First equation	$C = C_0 1 + \left[\frac{E(o) + E(d)}{2E_0}\right]$	$C = C_0 \left[1 + \frac{E(o) + E(d)}{2E_0}\right]$
620	Table 5, 1st column, 8th row	Charge in grams of elementary boron per 1 cm^2 of column cross section per 1 hr receiver	Charge in grams of elementary boron per 1 cm^2 of column cross section per 1 hr
	Table 5, 1st column, 10th row	Temperature in receiver of column, °C	Temperature at top of column, °C

THE SOVIET JOURNAL OF

ATOMIC ENERGY

A translation of ATOMNAYA ÉNERGIYA,
a publication of the Academy of Sciences of the USSR

(Russian original dated February, 1961)

Vol. 10, No. 2 November, 1961

CONTENTS

Annual subscription $75.00
Single issue 20.00
Single article 12.50

CONTENTS (continued)

NOTE

The Table of Contents lists all materials that appears in Atomnaya Énergiya. Those items that originated in the English language are not included in the translation and are shown enclosed in brackets. Whenever possible, the English-language source containing the omitted reports will be given.

Consultants Bureau Enterprises, Inc.

THE SOVIET JOURNAL OF

ATOMIC ENERGY

A translation of ATOMNAYA ÉNERGIYA,
a publication of the Academy of Sciences of the USSR

(Russian original dated March, 1961)

Vol. 10, No. 3 January, 1962

CONTENTS

Annual subscription $ 75.00
Single issue 20.00
Single article 12.50

CONTENTS (continued)

NOTE

The Table of Contents lists all materials that appear in Atomnaya Énergiya. Those items that originated in the English language are not included in the translation and are shown enclosed in brackets. Whenever possible, the English-language source containing the omitted reports will be given.

Consultants Bureau Enterprises, Inc.

THE SOVIET JOURNAL OF

ATOMIC ENERGY

A translation of ATOMNAYA ÉNERGIYA,
a publication of the Academy of Sciences of the USSR

(Russian original dated April, 1961)

Vol. 10, No. 4 January, 1962

CONTENTS

Annual subscription $ 75.00
Single issue 20.00
Single article 12.50

CONTENTS (continued)

NOTE

The Table of Contents lists all materials that appear in Atomnaya Énergiya. Those items that originated in the English language are not included in the translation and are shown enclosed in brackets. Whenever possible, the English-language source containing the omitted reports will be given.

Consultants Bureau Enterprises, Inc.

THE SOVIET JOURNAL OF

ATOMIC ENERGY

A translation of ATOMNAYA ÉNERGIYA, a publication of the Academy of Sciences of the USSR

(Russian original dated May, 1961)

Vol. 10, No. 5 March, 1962

CONTENTS

Annual subscription	$ 75.00
Single issue	20.00
Single article	12.50

CONTENTS (continued)

NOTE. The Table of Contents lists all material that appears in Atomnaya Énergiya. Those items that originated in the English language are not included in the translation and are shown enclosed in brackets. Whenever possible, the English-language source containing the omitted reports will be given.

Consultants Bureau Enterprises, Inc.

THE SOVIET JOURNAL OF

ATOMIC ENERGY

A translation of ATOMNAYA ÉNERGIYA, a publication of the Academy of Sciences of the USSR

(Russian original dated June, 1961)

Vol. 10, No. 6 March, 1962

CONTENTS

Annual subscription $75.00
Single issue 20.00
Single article 12.50

CONTENTS (continued)

Note. The Table of Contents lists all materials that appears in Atomnaya Énergiya. Those items that originated in the English language are not included in the translation and are shown enclosed in brackets. Whenever possible, the English-language source containing the omitted reports will be given. Consultants Bureau Enterprises, Inc.

THE SOVIET JOURNAL OF

ATOMIC ENERGY

A translation of ATOMNAYA ÉNERGIYA, a publication of the Academy of Sciences of the USSR

(Russian original dated July, 1961)

Vol. 11, No. 1 March, 1962

CONTENTS

Annual subscription $75.00
Single issue 20.00
Single article 12.50

CONTENTS (continued)

NOTE

The Table of Contents lists all materials that appear in Atomnaya Énergiya. Those items that originated in the English language are not included in the translation and are shown enclosed in brackets. Whenever possible, the English-language source containing the omitted reports will be given.

Consultants Bureau Enterprises, Inc.

THE SOVIET JOURNAL OF

ATOMIC ENERGY

A translation of ATOMNAYA ÉNERGIYA, a publication of the Academy of Sciences of the USSR

(Russian original dated August, 1961)

Vol. 11, No. 2 March, 1962

CONTENTS

Annual subscription $75.00
Single issue 20.00
Single article 12.50

THE SOVIET JOURNAL OF

ATOMIC ENERGY

A translation of ATOMNAYA ÉNERGIYA, a publication of the Academy of Sciences of the USSR

(Russian original dated September, 1961)

Vol. 11, No. 3 March, 1962

CONTENTS

Annual subscription $75.00
Single issue 20.00
Single article 12.50

CONTENTS (continued)

NOTE

The Table of Contents lists all materials that appear in Atomnaya Énergiya. Those items that originated in the English language are not included in the translation and are shown enclosed in brackets. Whenever possible, the English-language source containing the omitted reports will be given.

Consultants Bureau Enterprises, Inc.

THE SOVIET JOURNAL OF

ATOMIC ENERGY

A translation of ATOMNAYA ÉNERGIYA, a publication of the Academy of Sciences of the USSR

(Russian original dated October, 1961)

Vol. 11, No. 4 April, 1962

CONTENTS

Note to subscribers— The author index for volumes 10 and 11, 1961 will be published in volume 11, no. 6.

Annual subscription $ 75.00
Single issue 20.00
Single article 12.50

THE SOVIET JOURNAL OF

ATOMIC ENERGY

A translation of ATOMNAYA ÉNERGIYA, a publication of the Academy of Sciences of the USSR

(Russian original dated November, 1961)

Vol. 11, No. 5 May, 1962

CONTENTS

Annual subscription $75.00
Single issue 20.00
Single article 12.50

CONTENTS

THE SOVIET JOURNAL OF

ATOMIC ENERGY

A translation of ATOMNAYA ÉNERGIYA,
a publication of the Academy of Sciences of the USSR

(Russian Original Dated December, 1961)

Vol. 11, No. 6 May, 1962

CONTENTS

Annual subscription $ 75.00
Single issue 20.00
Single article 12.50

CONTENTS (continued)

Note. The Table of Contents lists all materials that appears in Atomnaya Energiya. Those items that originated in the English language are not included in the translation and are shown enclosed in brackets. Whenever possible, the English-language source containing the omitted reports will be given. Consultants Bureau Enterprises, Inc.

THE SOVIET JOURNAL OF ATOMIC ENERGY

Volumes 10 and 11, Numbers 1-6

(A Translation of Atomnaya Énergiya)

T

U

V

Y

Z

Soviet Journals Available in Cover-to-Cover Translation

ABBREVIATION	RUSSIAN TITLE	TITLE OF TRANSLATION	PUBLISHER	TRANSLATION BEGAN Vol.	Issue	Year
AÉ	Atomnaya énergiya	Soviet Journal of Atomic Energy	Consultants Bureau	1	1	1956
Akust. zh.	Akusticheskii zhurnal	Soviet Physics – Acoustics	American Institute of Physics	1	1	1955
	Antibiotiki	Antibiotics	Consultants Bureau	4	1	1959
Astr(on). zh(urn).	Astronomicheskii zhurnal	Soviet Astronomy–AJ	American Institute of Physics	34	1	1957
Avto(mat). svarka	Avtomaticheskaya svarka	Automatic Welding	British Welding Research Association (London)		1	1959
	Avtomatika i Telemekhanika	Automation and Remote Control	Instrument Society of America	27	1	1956
	Biofizika	Biophysics	National Institutes of Health*		1	1957
	Biokhimiya	Biochemistry	Consultants Bureau	21	1	1956
Byull. éksp(erim). biol. i med.	Byulleten' éksperimental'noi biologii i meditsiny	Bulletin of Experimental Biology and Medicine	Consultants Bureau	41	1	1959
DAN (SSSR) / Dokl(ady) AN SSSR	Doklady Akademii Nauk SSSR	The translation of this journal is published in sections, as follows:				
		Doklady Biochemistry Section	American Institute of Biological Sciences	106	1	1956
		Doklady Biological Sciences Sections (Includes: Anatomy, biophysics, cytology, ecology, embryology, endocrinology, evolutionary morphology, genetics, histology, hydrobiology microbiology, morphology, parasitology, physiology, zoology sections) — Life Sciences	American Institute of Biological Sciences	112	1	1957
		Doklady Botanical Sciences Sections (Includes: Botany, phytopathology, plant anatomy, plant ecology, plant embryology, plant physiology, plant morphology sections) — Life Sciences	American Institute of Biological Sciences	112	1	1957
		Proceedings of the Academy of Sciences of the USSR, Section: Chemical Technology — Chemical Sciences	Consultants Bureau	106	1	1956
		Proceedings of the Academy of Sciences of the USSR, Section: Chemistry — Chemical Sciences	Consultants Bureau	106	1	1956
		Proceedings of the Academy of Sciences of the USSR, Section: Physical Chemistry — Chemical Sciences	Consultants Bureau	112	1	1957
		Doklady Earth Sciences Sections (Includes: Geochemistry, geology, geophysics, hydrogeology, mineralogy, paleontology, petrography, permafrost sections) — Earth Sciences	American Geological Institute	124	1	1959
		Proceedings of the Academy of Sciences of the USSR, Section: Geochemistry — Earth Sciences	Consultants Bureau	106-123	1-6	1957-1958
		Proceedings of the Academy of Sciences of the USSR, Sections: Geology — Earth Sciences	Consultants Bureau	106-123	1-6	1957-1958
		Doklady Soviet Mathematics — Mathematics	The American Mathematics Society	131	1	1961
		Soviet Physics–Doklady (Includes: Aerodynamics, astronomy, crystallography, cybernetics and control theory, electrical engineering, energetics, fluid mechanics, heat engineering, hydraulics, mathematical physics, mechanics, physics, technical physics, theory of elasticity sections) — Physics	American Institute of Physics	106	1	1956
		Proceedings of the Academy of Sciences of the USSR, Applied Physics Sections (does not include mathematical physics or physics sections) — Physics	Consultants Bureau	106-117	1	1956-1957
Derevoobrabat. prom-st'.	Derevoobrabatyvayushchaya promyshlennost'	Wood Processing Industry	Timber Development Association (London)		9	1959
	Élecktrosvyaz	Telecommunications	Massachusetts Institute of Technology*		1	1957
Éntom(ol). oboz(renie)	Éntomologicheskoe obozrenie	Entomological Review	American Institute of Biological Sciences	38	1	1959
Farmakol. (i) toksikol(ogiya)	Farmakologiya i toksikologiya	Pharmacology and Toxicology	Consultants Bureau	20	1	1957
FMM	Fizika metallov i metallovedenie	Physics of Metals and Metallography	Acta Metallurgica*	5	1	1957
Fiziol. zhurn. SSSR (im. Sechenova)	Fiziologicheskii zhurnal im. I. M. Sechenova	Sechenov Physiological Journal USSR	National Institutes of Health*		1	1957
Fiziol(ogiya) rast.	Fiziologiya rastenii	Plant Physiology	American Institute of Biological Sciences	4	1	1957
	Geokhimiya	Geochemistry	The Geochemical Society		1	1958
FTT	Fizika tverdogo tela	Soviet Physics–Solid State	American Institute of Physics	1	1	1959
Izmerit. tekh(nika)	Izmeritel'naya tekhnika	Measurement Techniques	Instrument Society of America		1	1959
Izv. AN SSSR, O(td). Kh(im). N(auk)	Izvestiya Akademii Nauk SSSR: Otdelenie khimicheskikh nauk	Bulletin of the Academy of Sciences of the USSR: Division of Chemical Sciences	Consultants Bureau		1	1952

continued

Izv. AN SSSR, O(td). T(ekhn). N(auk): Met(all). i top.	(see Met. i top.)					
Izv. AN SSSR Ser. fiz(ich).	Izvestiya Akademii Nauk SSSR: Seriya fizicheskaya	Bulletin of the Academy of Sciences of the USSR: Physical Series	Columbia Technical Translations		1	1954
Izv. AN SSSR Ser. geofiz.	Izvestiya Akademii Nauk SSSR: Seriya geofizicheskaya	Bulletin (Izvestiya) of the Academy of Sciences USSR: Geophysics Series	American Geophysical Union		1	1954
Izv. AN SSSR Ser. geol.	Izvestiya Akademii Nauk SSSR: Seriya geologicheskaya	Izvestiya of the Academy of Sciences of the USSR: Geologic Series	American Geological Institute		1	1958
Kauch. i rez.	Kauchuk i rezina	Soviet Rubber Technology	Research Association of British Rubber Manufacturers	18	1	1959
	Kinetika i kataliz	Kinetics and Catalysis	Consultants Bureau	1	3	1960
	Koks i khimiya	Coke and Chemistry USSR	Coal Tar Research Association (Leeds, England)		1	1958
Kolloidn. zh(urn).	Kolloidnyi zhurnal	Colloid Journal	Consultants Bureau	14	1	1952
	Kristallografiya	Soviet Physics – Crystallography	American Institute of Physics	2	1	1957
Metalov. i term. obrabot. metal.	Metallovedenie i termicheskaya obrabotka metallov	Metal Science and Heat Treatment of Metals	Acta Metallurgica	6	1	1958
	Metallurg	Metallurgist	Acta Metallurgica		1	1957
Met. i top.	Metallurgiya i topliva	Russian Metallurgy and Fuels	Eagle Technical Publications		1	1960
Mikrobiol.	Mikrobiologiya	Microbiology	American Institute of Biological Sciences	26	1	1957
OS	Optika i spektroskopiya	Optics and Spectroscopy	American Institute of Physics		6	1959
	Pochvovedenie	Soviet Soil Science	American Institute of Biological Sciences		1	1958
	Priborostroenie	Instrument Construction	British Scientific Instrument Research Association		1	1959
Pribory i tekhn. éks(perimenta)	Pribory i tekhnika éksperimenta	Instruments and Experimental Techniques	Instrument Society of America		1	1957
Prikl. matem. i mekh.	Prikladnaya matematika i mekhanika	Applied Mathematics and Mechanics	American Society of Mechanical Engineers		1	1958
PTÉ	(see Pribory i tekhn. éks.)					
	Problemy Severa	Problems of the North	National Research Council of Canada			
Radiotekh.	Radiotekhnika	Radio Engineering	Massachusetts Institute of Technology*	12	1	1957
Radiotekh. i élektronika	Radiotekhnika i élektronika	Radio Engineering and Electronics	Massachusetts Institute of Technology*	2	1	1957
	Stanki i instrument	Machines and Tooling	Production Engineering Research Assoc.		1	1959
	Stal'	Stal (In English)	Iron and Steel Institute		1	1959
Stek. i keram.	Steklo i keramika	Glass and Ceramics	Consultants Bureau	13	1	1956
Svaroch. proiz-vo	Svarochnoe proizvodstvo	Welding Production	British Welding Research Association		4	1959
Teor. veroyat. i prim.	Teoriya veroyatnostei i ee primenenie	Theory of Probability and Its Applications	Society for Industrial and Applied Mathematics		1	1956
Tsvet. Metally	Tsvetnye metally	Nonferrous Metals	Primary Sources		1	1960
UFN	Uspekhi fizicheskikh Nauk	Soviet Physics – Uspekhi (partial translation)	American Institute of Physics	66	1	1958
UKh	Uspekhi khimii	Russian Chemical Reviews	The Chemical Society (London)		1	1960
UMN	Uspekhi matematicheskikh nauk	Russian Mathematical Surveys	London Mathematical Society	15	1	1960
Usp. fiz. nauk	(see UFN)					
Usp. khim(ii)	(see UKh)					
Usp. matem. nauk	(see UMN)					
Usp. sovr. biol.	Uspekhi sovremennoi biologii	Russian Review of Biology	Oliver and Boyd		48	1959
Vest. mashinostroeniya	Vestnik mashinostroeniya	Russian Engineering Journal	Production Engineering Research Assoc.		4	1959
Vop. gem. i per. krovi	Voprosy gematologii i perelivaniya krovi	Problems of Hematology and Blood Transfusion	National Institutes of Health*		1	1957
Vop. onk.	Voprosy onkologii	Problems of Oncology	National Institutes of Health*		1	1957
Vop. virusol.	Voprosy virusologii	Problems of Virology	National Institutes of Health*		1	1957
Zav(odsk). lab(oratoriya)	Zavodskaya laboratoriya	Industrial Laboratory	Instrument Society of America	25	1	1959
ZhAKh Zh. anal(it). khimii	Zhurnal analiticheskoi khimii	Journal of Analytical Chemistry USSR	Consultants Bureau	7	1	1952
ZhETF Zh. éksperim. i teor. fiz.	Zhurnal éksperimental'noi i teoreticheskoi fiziki	Soviet Physics–JETP	American Institute of Physics	28	1	1955
ZhFKh Zh. fiz. khimii	Zhurnal fizicheskoi khimii	Russian Journal of Physical Chemistry	The Chemical Society (London)		7	1959
ZhMÉI Zh(urn). mikrobiol. épidemiol. i immunobiol.	Zhurnal mikrobiologii, épidemiologii i immunobiologii	Journal of Microbiology, Epidemiology and Immunobiology	National Institutes of Health*		1	1957
ZhNKh Zh(urn). neorgan(ich). khim(ii)	Zhurnal neorganicheskoi khimii	The Russian Journal of Inorganic Chemistry	The Chemical Society (London)		1	1959
ZhOKh Zh(urn). obshch(ei) khimii	Zhurnal obshchei khimii	Journal of General Chemistry USSR	Consultants Bureau	19	1	1949
ZhPKh Zh(urn). prikl. khimii	Zhurnal prikladnoi khimli	Journal of Applied Chemistry USSR	Consultants Bureau	23	1	1950
ZhSKh Zh(urn). strukt. khimii	Zhurnal strukturnoi khimii	Journal of Structural Chemistry	Consultants Bureau	1	1	1960
ZhTF Zh(urn). tekhn. fiz.	Zhurnal teknicheskoi fiziki	Soviet Physics–Technical Physics	American Institute of Physics	26	1	1956
Zh(urn). vyssh. nervn. deyat. (im. Pavlova)	Zhurnal vysshei nervnoi deyatel'nosti (im. I. P. Pavlova)	Pavlov Journal of Higher Nervous Activity	National Institutes of Health*		1	1958

*Sponsoring organization. Translation through 1960 issues is a publication of Pergamon Press.

SOVIET

research in

ANALYTICAL CHEMISTRY

OF URANIUM

A collection of ten papers from the Consultants Bureau translations of the Soviet Journal of Analytical Chemistry and the famous "Doklady" of the Academy of Sciences (1949-58)... This collection will acquaint the analytical chemist working in this field with Soviet techniques for the determination of uranium in solutions, in ores and the products of their treatments, and in accessory minerals, plus methods for the determination of impurities in uranium.

heavy paper covers | illustrated | $10.00

CONTENTS

c/b CONSULTANTS BUREAU
227 WEST 17TH STREET, NEW YORK 11, N. Y.

RESEARCH BY SOVIET EXPERTS

Translated by Western Scientists

RADIATION CHEMISTRY
PROCEEDINGS OF THE FIRST ALL-UNION CONFERENCE
MOSCOW 1957

More than 700 of the Soviet Union's outstanding research scientists participated in this conference sponsored by the Academy of Sciences and the Ministry of the Chemical Industry. Each of the 56 reports read in the various sessions covers either the theoretical or practical aspects of radiation chemistry, and special attention is given to radiation sources used in radiation-chemical investigations. The general discussions which followed each report and reflected various points of view on the problem under analysis are also included.

PRIMARY ACTS IN RADIATION CHEMICAL PROCESSES	**$25.00**
RADIATION CHEMISTRY OF AQUEOUS SOLUTIONS (Inorganic and Organic Systems)	**$50.00**
RADIATION ELECTROCHEMICAL PROCESSES	**$15.00**
THE EFFECT OF RADIATION ON MATERIALS INVOLVED IN BIOCHEMICAL PROCESSES	**$12.00**
RADIATION CHEMISTRY OF SIMPLE ORGANIC SYSTEMS	**$30.00**
THE EFFECT OF RADIATION ON POLYMERS	**$25.00**
RADIATION SOURCES	**$10.00**

Individual volumes may be purchased separately

Special price for the 7-volume set **$125.00**

Tables of contents upon request.

CONTEMPORARY EQUIPMENT
FOR WORK WITH RADIOACTIVE ISOTOPES

Of the 110 isotopes produced in the USSR during 1958, 92 were obtained by neutron irradiation. The methods and technological procedures used in the production of isotopes and the preparation of labeled compounds from them are reviewed in detail. Shielding and manipulative devices for work with radioactive isotopes are illustrated as well as described fully. These collected reports are of interest to all scientits and technologists concerned with radioactive isotopes.

Tables of contents upon request.

Durable paper covers 66 pp. illus. $15.00

PRODUCTION OF ISOTOPES

The eighteen papers which comprise this volume were originally read at the All-Union Scientific and Technical Conference on the Application of Radioactive Isotopes, Moscow, 1957. The reports consider the problems and achievements of Soviet scientists in the production of radioactive isotopes by irradiation of targets in Soviet reactors and cyclotrons. Not only is this work of significance to producers of isotopes, but many of the papers will prove useful to isotope users as well.

Tables of contents upon request.

Durable paper covers 136 pp. illus. $50.00

Payment in sterling may be made to Barclay's Bank in London, England.

CONSULTANTS BUREAU

227 West 17th Street • New York 11, N.Y. • U.S.A.